EXPERIMENTAL AND THEORETICAL STUDIES OF THE ELECTROTHERMAL INSTABILITY IN A NONEQUILIBRIUM PLASMA

Thesis by

Robert Ridgeway Gilpin

In Partial Fulfillment of the Requirements

For the Degree of

Doctor of Philosophy

California Institute of Technology

Pasadena, California

1968

(Submitted May 15, 1968)

ACKNOWLEDGMENTS

This work has been made possible by the assistance of a number of people, each of which I would like to express my appreciation to at this time. Certainly, however, I have obtained the most assistance from my thesis advisor, Professor E. E. Zukoski. His guidance, criticism, and encouragement are most appreciated.

Each of my fellow students I must also thank for many long hours of discussion, during which many ideas were formulated. Also, I thank Dr. A. C. Pinchak and Dr. T. A. Cool for their work on this experimental apparatus before my work, during which time they developed many of the techniques and obtained many results that I used. Thanks are also due to Mr. F. T. Linton for his excellent mechanical ability in maintaining the experiment and building new equipment. Special thanks go to Mrs. Roberta Duffy for her excellent assistance in preparing this manuscript.

I would like to thank the Daniel and Florence Guggenheim Foundation and the California Institute of Technology for my financial support while at the Institute. The research activity described in this thesis was supported by the Air Force Office of Scientific Research under Contract No. AF 49(638)-1285.

ABSTRACT

Experimental and theoretical studies have been made of the electrothermal waves occurring in a nonequilibrium MHD plasma. These waves are caused by an instability that occurs when a plasma having a dependence of conductivity on current density is subjected to crossed electric and magnetic fields. Theoretically, these waves were studied by developing and solving the equations of a steady, one-dimensional nonuniformity in electron density. From these nonlinear equations, predictions of the maximum amplitude and of the half width of steady waves could be obtained. Experimentally, the waves were studied in a nonequilibrium discharge produced in a potassium-seeded argon plasma at 2000°K and 1 atm. pressure. The behavior of such a discharge with four different configurations of electrodes was determined from photographs, photomultiplier measurements, and voltage probes. These four configurations were chosen to produce steady waves, to check the stability of steady waves, and to observe the manifestation of the waves in a MHD generator or accelerator configuration.

Steady, one-dimensional waves were found to exist in a number of situations, and where they existed, their characteristics agreed with the predictions of the steady theory. Some extensions of this theory were necessary, however, to describe the transient phenomena occurring in the inlet region of a discharge transverse to the gas flow. It was also found that in a discharge away from the stabilizing effect of the electrodes, steady waves became unstable for large Hall parameters. Methods of prediction of the effective elec-

trical conductivity and Hall parameter of a plasma with nonuniformities caused by the electrothermal waves were also studied. Using these methods and the values of amplitude predicted by the steady theory, it was found that the measured decrease in transverse conductivity of a MHD device, 50 per cent at a Hall parameter of 5 , could be accounted for in terms of the electrothermal instability.

TABLE OF CONTENTS

1. INTRODUCTION

Previous work has verified the possibility of obtaining non-equilibrium ionization in a magnetohydrodynamic (MHD) plasma, and a theory has been developed which accurately predicts the conductivity of such a plasma under a wide range of conditions[1, 2, 5]. In the measurement of conductivity in these experiments, an electric field was applied to the plasma and the resulting current measured. However, for such a plasma to be utilized in a generator or accelerator, it must also be subjected to magnetic fields.

When such experiments[3, 4, 9-11] were tried either in order to measure the Hall parameter, that is, the tangent of the angle between current and electric field, or in order to produce ionization by U×B induction, serious discrepancies between theory and experiment occurred for Hall parameters greater than two. As the magnetic field was increased above the critical value, fluctuations appeared in the electric field, the effective conductivity of the plasma decreased, and the average Hall parameter reached a maximum of about two independent of the applied magnetic field.

The cause of these fluctuations and the resulting changes in plasma parameters was suggested by Velikhov[3] to be an ionization instability. Also, Kerrebrock[2] and Nedospasov[5] found that perturbations to the equations of the uniform state had a growth rate of 10^{+5} sec^{-1} and a velocity of approximately 10 m/sec under conditions when the instability occurred. The waves resulting from this instability are called 'electrothermal waves.'

This instability results from the coupling between electrical

conductivity and Joule heating which occurs in the nonequilibrium plasma. That is, an increase in conductivity causes an increase in Joule heating greater than the increase in energy losses, thus causing greater increases in electron density and conductivity. Unlike the ordinary ionization instability, however, this instability occurs only when an adequately large magnetic field is applied to the plasma, and then it occurs only for disturbances having a certain range of angles relative to the current and field vectors.

Velikhov[3] and also Solbes[6] did more extensive work on the waves to estimate the amplitude to which they would grow. Instead of treating the growth of waves from the uniform state, the approach used in this thesis will be to assume that steady, one-dimensional waves result from the instability. Then, setting the time derivatives in the energy equation equal to zero, obtain a set of solutions which are the steady, one-dimensional waves. From this analysis, the characteristic width and the maximum amplitude of steady waves can be determined. The stability of such steady waves, that is, whether or not they actually exist, was not studied analytically. Instead, an experiment was designed in which the choice of electrode configuration would naturally stabilize such waves. Steady waves were observed in this experiment, and their amplitude and half width agreed well with that predicted for the steady waves.

Next, an experiment will be described in which the electrodes were placed well outside the magnetic field so they would not affect the current pattern in the test section. Under these conditions, waves of the same characteristics were observed for Hall parameters in the

range of two to three; however, this current pattern became unstable as the Hall parameter was increased above three.

Experiments will then be discussed in which the arrangement of electrodes was similar to that occurring in a MHD generator or accelerator. That is, the electrical discharge, magnetic field, and gas flow were mutually perpendicular. In order to explain the phenomenon observed in the inlet region to such a discharge, it was necessary to take into account ionization rate effects in the theory; however, after a transverse discharge was established, one-dimensional steady waves were again observed. Now, however, they were transverse to the gas flow and transported downstream at the gas velocity.

Also, several methods of calculating the effective conductivity of a plasma with such nonuniformities were explored and the predictions compared with measured values in several of the experimental configurations.

2. THEORY OF THE NONEQUILIBRIUM PLASMA

In this section, the theory of a nonequilibrium plasma will be discussed. First, the basic equations will be presented, and then their application to determining the uniform state of the plasma and to determination of the ionization rate will be considered. With this background theory established, the electrothermal instability will be discussed, first by developing the equation of a one-dimensional disturbance, and then perturbing this equation. Finally, large amplitude steady solutions of the one-dimensional equation will be obtained and the properties of these solutions relevant to predictions of plasma behavior will be discussed.

2.1 Basic Equations

The plasma discussed here has been found[1, 2, 4] to be adequately described by a two-temperature model in which the ions and neutrals are assumed to be in equilibrium at the neutral temperature, and the electrons and excited states are in equilibrium at a higher temperature, the electron temperature.

This assumption, along with the basic assumptions of magnetohydrodynamics, that is, that the induced magnetic fields and the ionization fraction are small, gives the following basic equations for the plasma:

$$\text{continuity:} \qquad \nabla \cdot \underline{J} = 0 \tag{1}$$

$$\text{irrotational fields:} \qquad \nabla \times \underline{E} = 0 \ . \tag{2}$$

General Ohm's Law

$$\underline{J} = \sigma \underline{\underline{\mu}} \left(\underline{E} + \frac{2}{3} \frac{\varepsilon_e}{e} \frac{\nabla n_e}{n_e} \right) \tag{3}$$

where $\underline{E}$ is the electric field measured in the gas frame of reference and is equal to $(\underline{E}' + \underline{U} \times \underline{B})$ in a frame in which the gas is moving at velocity $\underline{U}$.

For $\underline{B}$ in the z-direction, the conductivity tensor is:

$$\underline{\underline{\mu}} = \frac{1}{1+\beta^2} \begin{pmatrix} 1 & -\beta & 0 \\ \beta & 1 & 0 \\ 0 & 0 & 1+\beta^2 \end{pmatrix} \tag{4}$$

where the Hall parameter $\beta = \frac{eB}{m_e \nu} = \frac{B\sigma}{en_e}$. In addition, it is assumed that:

$$\frac{1}{\sigma} = \frac{1}{\sigma_s} + \frac{1}{\sigma_c} \quad . \tag{5}$$

Here, σ_c is the conductivity based only on close encounters, and

$$\sigma_c = \frac{8}{3\pi} \frac{e^2}{m_e} \frac{n_e}{c \sum_n n_n Q_n} \quad ; \tag{6}$$

and σ_s is the Spitzer conductivity,

$$\sigma_s = \frac{8\sqrt{2}}{\pi^{3/2}} \frac{(kT_e)^{\frac{3}{2}} \gamma_E}{\sqrt{m_e}\, e^2 \ell n \Lambda^2} \quad ; \quad \Lambda^2 = \frac{9(kT_e)^3}{8\pi n_e e^6} \quad . \tag{7}$$

The above approximation to β is not quite correct due to changes in collision frequency occurring at higher magnetic fields. Feneberg[7] calculated that as β goes to infinity the error causes a 10 to 25 per cent reduction in the transverse component of σ. However, it will be shown that the plasma becomes unstable for $\beta > 2$ and thus this error in calculating β is masked by the effect of the non-uniformities resulting from the instability.

Also, the method of addition of σ_c and σ_s in eq. (5) to give the resultant σ, although widely used[1, 2], is based only on intuitive arguments. It gives values for σ within 20 per cent of more elabo-

rate techniques which are based on cross section data which have uncertainties of more than 20 per cent. Hence, this simple form of eq. (5) is justified by uncertainty in basic cross section data.

Energy Equation. The energy balance equation for the electrons is:

$$\frac{\partial}{\partial t}\left[(\varepsilon_e + I_i)n_e\right] - \frac{5}{3}\frac{\underline{J}\cdot\nabla\varepsilon_e}{e} = \underline{J}\cdot\underline{E} - \dot{R} - \dot{\Omega} + \nabla\cdot(\kappa_e \underline{\underline{\mu}}\nabla\varepsilon_e) . \qquad (8)$$

Here, the first term on the left hand side is the energy input into ionization and the second term is the energy convected by the current. The first term on the right is the Joule heating term; the second term is the radiative energy transport which, in the form used by Lutz[8], is:

$$\dot{R}(x) = \frac{14}{3}\pi\Delta\nu m_o B_o(x) - \pi\Delta\nu\sqrt{m_o}\int_0^{m_o}\frac{\sqrt{m}}{\sqrt{1-\frac{m}{m_o}}}\,dm\int_1^{\infty}\frac{dz}{z}\int_{-\infty}^{\infty}B_o(y)e^{-mz|y-x|}dy . \qquad (9)$$

The third term is the energy loss from the electrons in elastic collisions:

$$\dot{\Omega} = \frac{8}{3}\frac{m_e}{m_a} n_e \sum_m \bar{\nu}_m(\varepsilon_e - \varepsilon_a) \qquad (10)$$

where $\bar{\nu}_m$, as used by Cool[1], is the averaged collision frequency for energy transfer. The final term on the right hand side is the energy transfer by conduction in the electron gas, and κ_e, the conduction coefficient, is $(n_e\varepsilon_e)/(m_e\nu)$.

Finally, the ionization rate equation for the plasma out of equilibrium is approximately:

$$\frac{\partial n_e}{\partial t} = k_b n_{eq}^2 n_e\left(1 - \left(\frac{n_e}{n_{eq}}\right)^2\right) , \qquad (11)$$

where n_{eq} is given by the Saha equation:

$$n_{eq}^2 = n_a \left(\frac{4\pi m_e}{3k^2}\right)^{\frac{3}{2}} \epsilon_e^{\frac{3}{2}} \exp[-\frac{3}{2}\frac{I_i}{\epsilon_e}] \ . \qquad (12)$$

2.2 The Uniform Steady State

In the case when all time and space derivatives are zero, Ohm's law gives

$$\underline{J} = \sigma \underline{\underline{\mu}} \underline{E} \ ;$$

the energy equation gives

$$\underline{J} \cdot \underline{E} = \dot{R}_{ex} + \dot{\Omega}$$

where R_{ex} is the amount of radiation escaping from the plasma; and Saha's equation gives

$$n_e = n_{eq}(\epsilon_e) \ .$$

In the coordinate system with $\underline{B}$ along the z-axis, the Ohm's law becomes:

$$J_x = \frac{\sigma}{1+\beta^2}(E_x - \beta E_y) \ ,$$

$$J_y = \frac{\sigma}{1+\beta^2}(\beta E_x + E_y) \ .$$

If, in addition, $\underline{J}$ is along the x-axis, that is, $J_y = 0$, then

$$\beta = -E_y/E_x \ , \qquad (13)$$

$$J_x = \sigma E_x \ , \qquad (14)$$

and

$$\frac{J_x^2}{\sigma} = \dot{R}_{ex} + \dot{\Omega} \ . \qquad (15)$$

For use later, define J_L as the value of current, J_x, which is the solution of these equations; E_{L_o} as the value of E along J_L, that is, E_x; and E_L as the total field, $(E_x^2+E_y^2)^{\frac{1}{2}}$. Therefore, the

tangent of the angle between E_{L_o} and E_L is β and

$$\frac{J_L^2}{\sigma} = \sigma E_{L_o}^2 = \dot{R}_{ex} + \dot{\Omega} \ .$$

The procedure for calculating conductivity as a function of current is first to calculate conductivity as a function of electron energy using the Saha equation (12) and the equations of conductivity, (6) and (7). Then using the energy equation (15), calculate the current required to obtain a given electron energy. This calculation is relatively straightforward except for the calculation of R_{ex}. Cool approximated R_{ex} by calculating the amount of radiation leaving a uniform plasma on a beam of a certain length and then by choosing an average beam length, obtained an average energy loss. Using this method, a curve of σ versus J of the type shown in Figure 1 can be obtained. This figure, taken from Ref. 1, shows the good agreement between theory and experiment when no magnetic field is applied.

For analytical purposes, this curve can be characterized for relatively large ranges of σ by $\sigma = \sigma_o(J/J_L)^n$ where J_L is the total current for $\sigma = \sigma_o$.

2.3 Ionization Relaxation

Because $\epsilon_e << I_i$ and $n_e(dI_i/dt) << I_i(dn_e/dt)$ (see Cool[1]), the time-dependent energy equation for a uniform plasma is, to a good approximation,

$$I_i \frac{dn_e}{dt} = \sigma E^2 - \dot{R}_{ex} - \dot{\Omega} \ .$$

Here, E is the total electric field if no magnetic field is present, or if there is a magnetic field, it is the electric field along the current

vector. Also, if σ is proportional to n_e, then

$$\frac{1}{n_e}\frac{dn_e}{dt} = \frac{\sigma_o E^2}{n_{e_o} I_i}\left(1 - \frac{n_{e_o} I_i}{\sigma_o E^2}(\dot{R}_{ex} + \dot{\Omega})\right) . \qquad (16)$$

Cool found that when an electric field of 2 or more volts/cm was suddenly applied to the plasma, Saha equilibrium did not hold. Thus, the rate of increase of n_e could not be calculated directly from eqn. (16) but rather depended on the rate equation (11). He found, however, that the ionization rate $(dn_e/dt)/n_e$ was still roughly linearly dependent on the parameter $(\sigma_o E^2)/(n_{e_o} I_i)$. That is, the fraction of the Joule heating going into ionization was roughly a constant and equal to about 0.5. Thus, eqn. (16), using the assumption that n_e is proportional to σ, gives:

$$\frac{d\tilde{\sigma}}{dt} = 0.5\,\frac{\tilde{\sigma}}{n_{e_o} I_i} E^2 \qquad (17)$$

where $\tilde{\sigma} = \sigma/\sigma_o$.

2.4 The Electrothermal Instability

Velikhov[3] has shown that the solution for the uniform state of the plasma is unstable for Hall parameters greater than about 2. Kerrebrock[2] and also Nedospasov[5] have determined the growth rate and phase velocity of small one-dimensional disturbances by perturbing the basic equations about the uniform state.

Stability will be studied here by first deriving the energy balance for a one-dimensional disturbance. For such a disturbance, where variables are functions of x alone (Figure 2), eqn. (1) gives J_x = constant (J_o) and eqn. (2) gives E_y = constant (E_o). Equation (3)

then gives the other two components:

$$J_y = \sigma E_o + \beta J_o ,$$
$$E_x = \beta E_o + \frac{1+\beta^2}{\sigma} J_o - \frac{2}{3} \frac{\varepsilon_e}{en_e} \frac{\partial n_e}{\partial x} . \qquad (18)$$

Using equation (18), the Joule heating term

$$\underline{J} \cdot \underline{E} = \sigma E_o^2 + 2\beta J_o E_o + \frac{1+\beta^2}{\sigma} J_o^2 - \frac{2}{3} \frac{\varepsilon_e}{en_e} J_o \frac{\partial n_e}{\partial x} .$$

Also, assuming Saha equilibrium holds locally:

$$\frac{1}{n_e} dn_e = \frac{3}{4} \left(1 + \frac{I_i}{\varepsilon_e}\right) \frac{d\varepsilon_e}{\varepsilon_e} .$$

Thus, the energy equation (8) can be written in terms of n_e. Again using the fact that $\varepsilon_e << I_i$, eqn. (8) gives:

$$I_i \frac{\partial n_e}{\partial t} - \frac{2}{3} \frac{J_o \varepsilon_e}{en_e} \frac{\partial n_e}{\partial x} - \frac{4}{3m_e(1+\beta^2)I_i} \frac{\partial}{\partial x} \left(\frac{\varepsilon_e^3}{\bar{\nu}} \frac{\partial n_e}{\partial x} \right) =$$
$$\sigma E_o^2 + 2\beta J_o E_o + \frac{1+\beta^2}{\sigma} J_o^2 - \dot{\Omega} - \dot{R} . \qquad (19)$$

Using the solution for the uniform case, eqn. (15) with $\sigma = \sigma_o (J/J_L)^n$ gives:

$$\dot{\Omega} + \dot{R}_{ex} = \frac{J_L^2}{\sigma_o} \left(\frac{\sigma}{\sigma_o}\right)^{2/n - 1} . \qquad (20)$$

Substituting this into (19), the right hand side becomes

$$\sigma E_o^2 + 2\beta J_o E_o + \frac{1+\beta^2}{\sigma} J_o^2 - \frac{J_L^2}{\sigma_o} \left(\frac{\sigma}{\sigma_o}\right)^{2/n - 1} - (\dot{R} - \dot{R}_{ex}) . \qquad (21)$$

Normalized by $\sigma_o E_{L_o}^2$, the Joule heating in the uniform solution, the first four terms of (21) give the net electronic heating term, $\tilde{\Omega}$.

$$\tilde{\Omega} = \frac{\Omega}{\sigma_o E_{L_o}^2} = \tilde{\sigma} \left(\frac{E_o}{E_{L_o}}\right)^2 + 2\beta \frac{J_o}{\sigma_o E_{L_o}} \left(\frac{E_o}{E_{L_o}}\right) + \frac{1+\beta^2}{\tilde{\sigma}} \left(\frac{J_o}{\sigma_o E_{L_o}}\right)^2 - \tilde{\sigma}^{2/n - 1} . \qquad (22)$$

Since Q must be zero for the uniform case, $\sigma = \sigma_o$, substituting $\tilde{\sigma} = 1$ and setting Q equal to zero gives:

$$\frac{J_o}{\sigma_o E_{L_o}} = \frac{-\beta \pm \left[(1+\beta^2)\left(\frac{E_{L_o}}{E_o}\right)^2 - 1\right]^{\frac{1}{2}}}{1+\beta^2} \left(\frac{E_o}{E_{L_o}}\right) \quad . \tag{23}$$

Thus, the heating term, Q, is expressed as a function of the parameters $\tilde{\sigma}$, E_o/E_{L_o}, and β. The parameter E_o/E_{L_o} is related to the angle of the disturbance to the uniform current by $E_o/E_{L_o} = \cos\phi + \beta \sin\phi$. The vectors E_o and E_{L_o} are shown in Figure 2.

The additional approximation that β is independent of $\tilde{\sigma}$ will be made. This is equivalent to assuming the collision frequency, $\bar{\nu}$, is independent of electron temperatures, which is approximately true when the effect of the charged particles on the collision frequency is small.

$R-R_{ex}$ is the radiative heat transfer term which will be called 'H'. Then eqn. (19) will be written:

$$I_i \frac{\partial n_e}{\partial t} - \frac{2}{3}\frac{J_o}{e n_e}\varepsilon_e \frac{\partial n_e}{\partial x} - \frac{4}{3 m_e (1+\beta^2) I_i}\frac{\partial}{\partial x}\left(\frac{\varepsilon_e^3}{\bar{\nu}}\frac{\partial n_e}{\partial x}\right) + H = Q \quad , \tag{24}$$

which, along with eqns. (22) and (23), forms the energy balance equation for one-dimensional disturbances.

(a) Small Disturbances. - To linearize eqn. (24) about the uniform solution, $n_e = n_{e_o}$ and $\varepsilon_e = \varepsilon_{e_o}$, define:

$$n_e = n_{e_o}(1+\tilde{n})$$

and

$$\varepsilon_e = \varepsilon_{e_o}(1+\tilde{\varepsilon}) \quad .$$

From Saha's equation for small $\tilde{\varepsilon}$ and $\tilde{n}$ and for $\varepsilon_{e_o} \ll I_i$: $\tilde{n} = 3/4\ (I_i/\varepsilon_{e_o})\tilde{\varepsilon}$. Also, assume that σ and n_e are related through a formula $\sigma = \sigma_o(n_e/n_{e_o})^p$. Then, inserting these equations into eqn. (24) and taking only first order terms,

$$n_{e_o} I_i \frac{\partial \tilde{n}}{\partial t} - \frac{2}{3}\frac{J_o}{e}\varepsilon_{e_o}\frac{\partial \tilde{n}}{\partial x} - \frac{4}{3}\frac{\varepsilon_{e_o}^3 n_{e_o}}{m_e(1+\beta^2)\bar{\nu} I_i}\frac{\partial^2 \tilde{n}}{\partial x^2} + H =$$

$$\sigma_o E_{L_o}^2 \left[\left(\frac{E_o}{E_{L_o}}\right)^2 - (1+\beta^2)\left(\frac{J_o}{\sigma_o E_{L_o}}\right)^2 - \left(\frac{2}{n} - 1\right)\right] p\tilde{n} . \qquad (25)$$

Inserting $\tilde{n} = n_o e^{i(\omega t + kx)}$; $k = 2\pi/\lambda$ into (25), the growth rate, $-\mathcal{I}m(\omega)$, and phase velocity, $Re(\omega)\lambda/2\pi$, of this wave can be found. This is possible because e^{ikx} is an eigenfunction[8] of the radiation term, H , and for $\lambda > \frac{2\pi}{0.1\, m_o} = 6 \times 10^{-3}$ cm,

$$H = \frac{16}{9}\left[\frac{1.24 \times 10^4}{I_i \lambda_o}\right]\pi^{5/2}\Delta\nu\frac{\sqrt{m_o}}{\sqrt{\lambda}} B_{oo} e^{i(\omega t + kx)} , \qquad (26)$$

where λ_o is the wavelength in Angstroms of light at the resonant line.

Therefore, defining

$$\omega_e = \frac{4}{3}\frac{\varepsilon_{e_o}^3 n_{e_o} (2\pi/\lambda)^2}{m_e(1+\beta^2)\bar{\nu} I_i \sigma_o E_{L_o}^2} , \qquad (27)$$

$$\omega_R = \frac{8}{9}\sqrt{2}\,\frac{1.6}{I_i}\frac{\pi^2 \Delta\nu \sqrt{m_o}}{\sigma_o E_{L_o}^2}\sqrt{2\pi/\lambda}\, B_{oo} , \qquad (28)$$

and

$$\left.\frac{dQ}{dn_e}\right|_{n_{e_o}} = p\left[\left(\frac{E_o}{E_{L_o}}\right)^2 - (1+\beta^2)\left(\frac{J_o}{\sigma_o E_{L_o}}\right)^2 - \left(\frac{2}{n} - 1\right)\right] \qquad (29)$$

equation (25) gives:

$$-\mathcal{I}m(\omega) = \frac{\sigma_o E_{L_o}^2}{n_{e_o} I_i}\left[\left.\frac{dQ}{dn_e}\right|_{n_{e_o}} - \omega_e - \omega_R\right] \tag{30}$$

and

$$Re(\omega) = \frac{2}{3}\frac{J_o}{e}\frac{\varepsilon_{e_o}}{I_i n_{e_o}}\left(\frac{2\pi}{\lambda}\right) . \tag{31}$$

When the growth rate, $-\mathcal{I}m(\omega)$, is positive, perturbations to the uniform solution grow; and since both ω_e and ω_R decrease with increased λ, for large enough λ, the growth rate is positive when $dQ/dn_e|_{n_{e_o}}$ is positive. This condition occurs in the regime of β and E_o/E_{L_o} indicated in Figure 3. The minimum value of β at which instability occurs depends on n, the exponent in the relation between σ and J. For the potassium and argon gas used in the experiments that follow, n was between 0.6 and 0.8; thus, onset of instability should occur between $\beta = 1.3$ and 2. The value of the parameter E_{L_o}/E_o is related to the angle of a disturbance to the electric field, E_L, in the uniform solution and can vary from a minimum of $1/\sqrt{1+\beta^2}$ when the disturbance lies along E_L to a maximum of ∞ when it is perpendicular to E_L. Note that for each value of E_{L_o}/E_o the angle has two values corresponding to the plus and minus signs in eqn. (23). Instability, however, occurs only for the positive sign in eqn. (23), which corresponds to disturbances which lie between the electric field and the current vectors of the uniform solution. The value of the growth rate in this instability regime is of the order of $(\sigma_o E_{L_o}^2)/(n_{e_o} I_i)$, which is approximately 10^{+5} sec^{-1}.

Steady waves are obtained, however, when their wavelength is such that the damping terms, ω_e and ω_R, just cancel the source

term, dQ/dn_e . In Figure 4 are plotted the values of ω_e for $\beta = 0$ and of ω_R . Comparing these with the value of the slope, Figure 5, for E_{L_o}/E_o between 0.5 and 0.3, the range in which steady waves were observed, gives a value of λ of the order of one cm. Figure 4 shows that for $\beta = 0$, damping of the perturbations is either by electronic heat transfer, ω_e , or by radiative transfer, ω_R , depending on the value of the electron temperature. However, the coefficient of electronic heat transfer decreases as $1/(1+\beta^2)$, which means that in the instability regime, $\beta > 2$, radiative damping is the most important.

The velocity of the waves determined from the linear analysis is $(2/3)(J_o/e)(\varepsilon_{e_o}/I_i n_{e_o})$, which is of the order of 10 m/sec. Therefore, in the rise time of 10^{-5} sec, the wave has moved only 10^{-2} cm. Thus, the waves can be considered essentially as stationary, and the $\partial n_e/\partial x$ term which gives rise to the wave velocity in eqn. (24) can be neglected.

Thus, from the linear theory of waves, the instability regime can be determined. Also, the wavelength of steady waves and the fact that the main damping mechanism is radiative transfer were determined. This, along with the fact that the velocity of the steady waves is negligible, makes it possible to simplify eqn. (24) for steady waves to:

$$H = Q \quad . \tag{32}$$

(b) Large Amplitude Disturbances. - In the treatment of small disturbances, the electronic heating term, Q, was linearized about σ_o. From this analysis, the amplitude of the disturbances cannot be

determined because it is the shape of Q that fixes this amplitude.

In Figure 6, Q is plotted as a function of σ for various β and E_{L_o}/E_o. For $\beta < \beta_{crit}$, Figure 6a, the slope of Q at σ_o is negative; however, the absolute value of the minimum slope at $\beta = 1$ is less than that at $\beta = 0$. This means that disturbances to the uniform solution at σ_o take longer to disperse as β is increased. For $\beta > \beta_{crit}$, Figure 6b, the slope of Q at σ_o is positive for a certain range of E_{L_o}/E_o, indicating that disturbances about σ_o will now grow. However, zeros do occur on either side of σ_o at which $dQ/d\sigma$ is negative. Call the upper and lower zeros σ_u and σ_L, respectively. If there is no heat transfer, that is, $H = 0$, these zeros determine the amplitude to which disturbances about σ_o will grow. That is, for the equation $I_i (dn_e/dt) = Q$, σ_u, σ_o, and σ_L are the only steady solutions. Of these, only σ_u and σ_L are stable; therefore, all points perturbed about σ_o go to either σ_u or σ_L, depending on where the perturbation conductivity is below or above σ_o.

When the heat transfer term is included, other steady solutions are possible, e.g., solutions of eqn. (32). The term H, which equals $R-R_{ex}$ in this equation, represents radiative transport of heat, 75 per cent of which occurs in the potassium resonant lines[1]. The mean free path of photons in these lines varies from 10^{-4} cm at the line centers to infinity on either side of the lines. An approximation to R was made by breaking the integral over mean free path, $1/m$ in eqn. (9), into three parts. Call R_1 the integral of m from 0 to $1/L$, R_2 the integral from $1/L$ to $1/\alpha\lambda$, and R_3 the integral from $1/\alpha\lambda$ to m_o, where L is the characteristic dimension of the plasma volume,

λ is the wavelength calculated for small disturbances, and α is a number not as yet defined. The first integral then represents photons with mean free paths larger than the plasma volume and is assumed to be the same as the radiation escaping from the plasma with uniform σ. Thus, R_1 just cancels R_{ex}. The second term, R_2, represents heat transfer occurring over distances larger than the size of the disturbances, and therefore cannot be approximated in terms of the local value or derivatives of the value of any plasma parameter. The third term, however, can be approximated, and using the diffusion approximation gives:

$$R_3 = -\frac{2}{3}\pi^2\Delta\nu\sqrt{m_o}\,\alpha^{3/2}(2\pi)^{3/2}\sqrt{\frac{2\pi}{\lambda}}\,\frac{d^2B_o}{d\zeta^2}, \tag{33}$$

where $\zeta = (2\pi x)/\lambda$. This expression is obtained by expanding the blackbody intensity, B_o, about its value at x in a Taylor series

$$B_o(y) = B_o(x) + \left.\frac{dB_o}{dx}\right|_x (y-x) + \left.\frac{d^2B_o}{dx^2}\right|_x \frac{(y-x)^2}{2} \cdots$$

and carrying out the integrals in eqn. (9). The second derivative is the first term in the expansion to give a contribution and is the only one that is kept. Note that a sine wave was an eigenfunction of the exact radiation term and gives, eqn. (26), the same dependence on wavelength as the approximation in eqn. (33). Also, if α is chosen to be $1/(4\pi)^{1/3}$, R_3 also gives the same value of the damping coefficient as the exact expression.

As an approximation to the nonlinear problem, solutions neglecting the integral part, R_2, of the radiative transfer were calculated. That is, solutions of

$$-\varkappa_R \frac{d^2(B_o/B_{oo})}{d\zeta^2} = Q \tag{34}$$

where

$$\varkappa_R = \frac{2}{3}\sqrt{2}\,\pi^2 \Delta\nu \sqrt{m_o}\,\sqrt{2\pi/\lambda}\; B_{oo} \; . \tag{35}$$

Using Planck's equation and the Saha equation gives the approximate relationship

$$B_o/B_{oo} = (n_e/n_{e_o})^s \; , \tag{36}$$

where

$$s = \frac{4}{3}\,\frac{1.24 \times 10^4}{I_i \lambda_o} \; . \tag{37}$$

λ_o is the wavelength of the resonant line in $\mathring{A}$.

For potassium, $I_i = 4.3$ and $\lambda_o = 7690\ \mathring{A}$, which gives $s = \frac{1}{2}$. Substituting this into (34) gives

$$-\varkappa_R \frac{d}{d\zeta}\left[\frac{1}{2}\left(\frac{n_e}{n_{e_o}}\right)^{\frac{1}{2}} \frac{dn_e}{d\zeta}\right] = Q(n_e) \; . \tag{38}$$

This equation can be integrated twice to give:

$$\frac{x}{\lambda} = \frac{\sqrt{\varkappa_R}}{2\pi} \int \frac{dn_e}{\sqrt{-4\,\frac{n_e}{n_{e_o}} \int \frac{Q(n_e)}{\sqrt{n_e/n_{e_o}}}\, dn_e + C}} \; . \tag{39}$$

Carrying out the integral for various constants, C gives the change in wave shape for increasing amplitude. The results were calculated for a particular Q, shown in Figure 7. The behavior is similar to that of the doubly periodic elliptic function, in that at small amplitude the waves are sinusoidal, curve A in Figure 8. However, as their amplitude increases, the ratio of the width of the high n_e part to the low n_e part becomes different from one, curve B. In this case,

since the lower zero of Q was closer to σ_o than the upper zero, the trough of the wave becomes wider than the crest. As the value of σ in the trough approaches σ_L, a solitary wave solution, curve C, is obtained. Amplitudes greater than that of the solitary wave require that n_e and thus σ drop off as in curve D ; however, since this cannot occur inside the plasma, the maximum amplitude of a steady wave if that of the solitary wave.

A check of the diffusion approximation was made by comparing the results from it with a computer calculation of the actual radiation term. For the computer calculation, the summation representation derived by Lutz[8] for the radiation integral (9) was used. However, this allows calculation of the radiation for a given wave shape but not the calculation of a wave shape from a known Q. Therefore, the following calculation procedure was used. First, a wave shape similar to one of those obtained by the diffusion approximation, Figure 8, was chosen. Then, using the computer, the actual amount of radiative heat transfer was calculated at each point in the wave. This radiative heat loss was then equated to Q, and from eqn. (39) the wave shape for the diffusion approximation was calculated.

In this way, the wave shapes which were solutions of $H = Q$ for a given $Q(n_e)$, with and without the diffusion approximation, could be compared. As would be expected, the results with and without the diffusion approximation were the same for a sinusoidal wave and the Q for such a wave was linear. However, for a solitary wave, Q is nonlinear, Figure 9a, and the resulting wave shapes, shown in Figure 9b, were appreciably different. Although the width of the solitary

wave is about the same in both cases, the amplitude of the wave calculated by the diffusion approximation was a factor of 2 too small.

Thus, going from the sinusoidal waves to the solitary wave, the diffusion approximation becomes worse and could produce as much as a factor of 2 error in the calculation of the amplitude of the solitary wave.

2.5 Calculation of Amplitude of Conductivity Variations

In the previous calculations a number of steady wave shapes were obtained as a function of two parameters, the amplitude and the angle, E_{L_o}/E_o, of the waves. A detailed stability analysis of the steady waves would be required to determine which, if any, of these waves actually exist in a plasma. However, just from the steady wave shapes of Figure 8 a few elementary conclusions can be made. First, for a given angle, that is E_{L_o}/E_o, there is a maximum amplitude at which periodic waves exist. This amplitude is fixed by the zero of Q nearest to the value σ_o for the uniform solution. Also, the peak-to-peak amplitude is approximately twice the difference between σ_o and the conductivity at the nearest zero. This last approximation will not be good for the solitary waves, as shown in the check of the diffusion approximation; however, it will be used for the closely packed waves, and there it is much more accurate. Using this criterion, we can then determine the amplitude of the waves as a function of E_{L_o}/E_o from a plot of the zeros of Q as shown in Figure 10. This plot was obtained by numerically solving for the zeros of eqn. (22). In Figure 10 we see that in the region from $E_{L_o}/E_o = 0.52$ to 0.2 the lower zero fixes the amplitude, and from $E_{L_o}/E_o = 0.61$ to 0.52 the

upper zero does. Since the maximum possible variation occurs when the two zeros are equidistant, it follows that if E_{L_o}/E_o is allowed to vary, the true maximum peak-to-peak amplitude is the difference in conductivity between the upper and lower zeros occurring when $E_{L_o}/E_o = 0.52$. For this case, $\Delta\sigma/\sigma_o = 1.2$. This criterion was used to obtain the solid curves in Figure 11.

This analysis then gives a maximum possible conductivity variation ; however, it does not in any way take into account stability. One simple approach to stability is to test the stability of a plasma with the uniform set of waves previously described when it is perturbed by disturbances of a wavelength much larger than that of the steady waves. In this case, the plasma with waves can be considered as a new uniform plasma with properties obtained by averaging over the waves. In Appendix C it is shown that the averaged energy equation can be put in the same form as the original energy equation for the plasma with constant conductivity. Thus, perturbing $\langle\sigma\rangle$ of this new plasma, we see that it, too, will be unstable if β_{eff} is greater than β_{crit}. Therefore, we conclude that the β_{eff} of the plasma with waves must always be less than the original β_{crit} for the plasma to be stable. The effective values of β and σ for a plasma with a set of plane waves is calculated in Appendix B as a function of the amplitude and angle of the waves. Using these expressions, the relationship between E_{L_o}/E_o and ϕ, and the curves of the type shown in Figure 10 to relate E_{L_o}/E_o to amplitude, Table I, was prepared. It shows β_{eff} as a function of E_{L_o}/E_o for a given theoretical Hall parameter. For both β_{th} of 3 and 5, the minimum β_{eff} occurs for a

TABLE I. Minimum β_{eff}

Angle (ϕ)	E_{L_o}/E_o	$\Delta\sigma/\langle\sigma\rangle$	s	β_{eff}	
$\beta_{th} = 3$					
12^o	.63	.00	.000	3.0	
15^o	.58	.20	.005	2.9	
20^o	.51	1.04	.135	2.1	minimum
30^o	.42	.60	.045	2.5	
40^o	.37	.36	.016	2.7	
$\beta_{th} = 5$					
10^o	.60	.00	.000	5.0	
12^o	.50	1.10	.150	3.6	
15^o	.45	1.04	.135	3.3	
20^o	.37	.80	.080	3.2	minimum
30^o	.30	.30	.045	3.5	
40^o	.25	.20	.020	3.9	

wave at 20^o to the average current. The minimum β_{eff} for β_{th} of 3 approximately equals β_{crit}, which was 2 in this case. However, β_{eff} exceeds β_{crit} for β_{th} of 5. This implies that the uniform set of waves predicted by the steady theory would not produce a stable plasma for theoretical values of Hall parameter much greater than 3. Also note that the value of E_{L_o}/E_o at which the minimum β_{eff} occurs is less than the value at which the maximum amplitude waves occur. The amplitude of the waves for minimum β_{eff} is shown by the dashed line in Figure 11.

3. APPARATUS

A schematic of the apparatus is shown in Figure 12. This apparatus was discussed in detail in Reference 12, and only some of the important features will be discussed here. The main flow of argon, 5.0 gm/sec, is heated by an arc jet which was operated at 90 volts and 70 amps for a gas temperature of 2000°K in the test section. Both the cathode and anode were water-cooled and were made of tungsten and copper, respectively. No sputtering of either material was observed.

A secondary flow of 0.17 gm/sec of argon was bubbled through a potassium bath at 790°K and injected into the main flow just after the arc jet. This stream carried the equilibrium vapor pressure of potassium at the bath temperature.

The two streams were allowed to come to equilibrium in a mixing section which consisted of a 2.2 cm I.D. by 20 cm long alumina tube. This tube was contained in a stainless steel jacket and was purged with argon to prevent any oxygen from leaking into the system.

Test sections were made of boron nitride pieces held together by a stainless steel enclosure. The test sections generally had a 1 cm by 2 cm cross section, which was smoothly shaped into the 2.2 cm mixing tube. This converging section was only 4 to 5 cm upstream of the test area; therefore, we would expect a very flat velocity profile in the duct. The configuration of electrodes and voltage probes varied from experiment to experiment; however, electrodes and probes were consistently made from tungsten wire 0.075 cm and 0.050 cm in diameter, respectively. The actual configurations will

be described in the section on the experiments.

The discharge circuits, in general, consisted of a bank of 12-volt wet cells connected in series with a 100-ohm variable resistance, an ammeter, and a pair of duct electrodes. In several experiments, a number of parallel discharges were required. In this case, several discharge circuits were used and allowed to come to a floating potential independent of each other.

The magnetic field was supplied by a variable gap electromagnet with tapered, 10-cm diameter pole pieces. At a gap of 5 cm, this magnet could produce a maximum of 10 Kg. A 1.27-cm diameter hole was bored in the pole piece, through which light intensity measurements were made. However, the field in the gap was not noticeably changed by this hole and was measured to be uniform to 5 per cent over a 9-cm diameter area.

The gas velocity in the test section was 100 m/sec, which gives a maximum UB field of about 1 V/cm. The measured electric fields were corrected for the UB term, and the actual E values recorded were $(\underline{E} - \underline{U} \times \underline{B})$.

3.1 Measurement Techniques

Several standard techniques were used to monitor the condition of the gas. The gas temperature was obtained by measuring the temperature of a 0.012-cm diameter tungsten wire with a pyrometer and then correcting as in Cool[12] for heat transfer to obtain the gas temperature.

The potassium concentration was checked by passing the

secondary flow through a cooled tube, 70 cm long and 5 cm in diameter, for a measured length of time. The amount of potassium condensed in the tube agreed to within 10 to 20 per cent of the value predicted on the basis of the vapor pressure of potassium at the potassium bath temperature.

Electric field measurements were made by measuring voltage differences between floating probes. These were measured with a high impedance circuit, 1 megohm, and recorded as oscillograms. Floating probes will give the correct electric field measurement only if they are in regions of the same electron density. This was often not the case in the experiments described; however, the error introduced by these differences in electron density is of the order of the differences in electron energy, or 0.1 to 0.2 volts. Since the voltage difference between probes was usually greater than 2 volts, differences in electron energy would introduce a maximum error of 10 per cent.

Photographs of the discharge were taken in order to obtain the spatial variation of radiation emitted. From these photographs, the distribution of electron temperature, thus electron density, and to some extent, current density could be inferred. Only time-averaged distribution could be obtained, however, since the growth rate of disturbances in the plasma, $\sim 10^{+5}$ sec^{-1}, was fast compared to the exposure time of 1/400 sec. In the normal photographic arrangement, two 45^{o} mirrors were used to obtain a view of the duct parallel to the magnetic field. A quartz window in the duct allowed viewing of the discharge. This window was not very satisfactory for quantitative

measurements in that since it was cooler than the main gas flow, impurities in the gas tended to condense on the window, fogging it. Also, the potassium, along with the high temperature, caused vitrification of the quartz, so that the window had to be replaced after each run. For these reasons, the windows were used only for qualitative determination of the discharge pattern. To obtain quantitative data, photographs were taken through narrow slits in the boron nitride wall of the test section. These slits were purged with argon to eliminate absorption of the light by cold potassium vapors in the slits or near the duct wall. Quantitative interpretation of the photographs is discussed in Appendix A.

In order to obtain higher time resolution, the light intensity was also observed with photomultiplier tubes. The apparatus used for these measurements is shown in Figure 13. Here, two 0.16-cm diameter holes were made in the boron nitride walls and again were purged with argon. The light emitted from these holes, after passing through the hole bored in the magnet pole piece, was focused on an aperture screen by a 50-cm focal length lens placed 67 cm from the test section. The screen had two 0.15-cm diameter apertures which could be positioned so that each was covered by the image of one of the holes in the test section wall. The magnification of optical system was three, giving a resolution of 0.05 cm in the duct for the 0.15 cm apertures. Behind each aperture was a 0.3-cm diameter plastic light pipe that conducted the light to an interference filter placed in front of a photomultiplier tube. The interference filters passed light to the phototubes only at the wavelength of the potassium

line doublet of 7690 Å. The output of each photomultiplier was read on an oscilloscope which gave an overall time response of 1 μs. The quantitative interpretation of these readings is discussed in Appendix A.

4. EXPERIMENTS AND COMPARISON WITH THEORY

In this section, the experiments will be described and the results will be compared with the predictions of the theory. In the first experiments described, the discharge is parallel to the gas flow. These experiments were designed primarily to determine the validity of the steady, one-dimensional theory of the preceding section.

Next, experiments of more practical importance, where the discharge was transverse to the gas flow, will be discussed. Here, extensions of the theory had to be made to take account of the ionization transient in the inlet region of the duct. However, in regions of the plasma following this transient region, the steady theory of the preceding section was again applied.

4.1 Discharge Parallel to Gas Flow

Two experiments were conducted with the discharge applied parallel to the gas flow. In the first, the electrodes were placed inside the magnetic field in such a way that they stabilized a steady current streamer pattern. In this way, the predictions of the steady theory could be compared with the observed current pattern. In the second experiment, the discharging electrodes were moved outside the magnetic field so they would not influence the current pattern. This experiment was used to determine the influence of the electrodes on the current pattern of the first experiment.

(a) Steady streamers parallel to gas flow. - The purpose of this experiment, as previously stated, was to obtain steady, one-dimensional streamers that could be compared with the theory. The

configuration of electrodes used is shown in Figure 14. Here, three separate circuits discharge parallel to the gas flow to supply the axial component of current. In addition, U-shaped tungsten wires connecting the top and bottom of the duct allow a perpendicular component of current, J_o of the theory, to circulate. The anticipated current pattern is illustrated in Figure 15, which shows that for the center streamer this configuration is equivalent to an infinite wave train.

Experimentally, it was observed that when the magnetic field was zero, nonuniformities caused by current concentrations at the upstream electrodes rapidly dispersed and the discharge was uniform, as seen in Figure 16a. However, as predicted by the theory, when the magnetic field was increased from zero, but still for β less than that at which instability occurs, the nonuniformities took longer to die out. For β greater than the critical value, the nonuniformities spread the entire length of the test section to form the current streamers in Figure 16b.

The streamers appeared stationary in the laboratory frame in this experiment because their small velocity, 10 to 20 m/sec, was cancelled by the component of gas velocity perpendicular to them.

Quantitative information about the amplitude of the conductivity variations across the streamer was obtained by photographing the discharge through vertical slits in the test section wall. The photographs were reduced as described in Appendix A. In Figure 17 are plotted the measured values of the difference between the maximum and minimum conductivity, $\Delta\sigma$, in a streamer over the mean conductivity, $\langle\sigma\rangle$. These measurements lie below the maximum possible amplitude

predicted by the theory and are close to the amplitude predicted for minimum β_{eff}.

Also to check the theory, the electric field along the streamer was measured as the magnetic field was increased. Keeping the average current density constant, the ratio of this field with zero magnetic field, E_{L_o}, to the value with magnetic field, E_o, forms the parameter E_{L_o}/E_o of the theory. Theoretically, it was found that the instability occurred only for certain ranges of this parameter, and in Figure 18 it is shown that in fact when current streamers do occur, the measured values of E_{L_o}/E_o do lie inside the instability regime. Also note that the values lie slightly below the value for maximum amplitude waves and close to the theoretical curve for minimum β_{eff}. This, along with the measured amplitude of the waves, suggests that waves producing minimum β_{eff} are indeed preferred.

The predicted values of the parameters $\Delta\sigma/\langle\sigma\rangle$ and E_{L_o}/E_o depend only on the heating term Q of eqn. (24), and are independent of the size or type of heat transfer term. The heat transfer term, however, determines the streamer width. Since E_{L_o}/E_o is less than that at which the maximum amplitude occurs, the streamers are limited by the lower zero of Q (see Figure 10). Thus, we have the condition indicated in Figure 8 where, as the amplitude of the wave increases, the width of the high conductivity region stays constant as the distance between streamers increases toward the solitary streamer case. The width of the central streamer in Figure 16 is 0.3 cm, which suggests a total wavelength of 0.6 cm for the sinusoidal waves. For comparison, the theoretical value for the conditions of this ex-

periment, $\epsilon_e = 0.24$, $\beta = 4.0$, and $E_{L_o}/E_o = 0.45$, can be obtained from Figures 4 and 5. Figure 5 gives $d\Omega/dn_e = 1.1$. Using this value in Figure 4 and remembering that ω_e would be decreased by a factor of 1/17 at $\beta = 4$, it can be seen that the main heat transfer mechanism would be radiation, ω_R, and the predicted wavelength for steady, sinusoidal waves would be 0.8 cm. This is in good agreement with the observed value.

In this experiment, the spacing of the upstream electrodes was chosen by trial and error to give the most stable streamer configuration and did not by itself determine the streamer spacing. This was best illustrated by an experiment in which the electrodes were placed well outside the magnetic field. The results of this experiment will be described in the next section.

(b) Long test section. - The purpose of this experiment was to determine what influence the electrodes of the previous experiment had on the streamer spacing. The test section for this experiment was 20 cm long so that the discharge electrodes could be placed 2.5 cm outside the magnetic field. In this way, the nonuniformities introduced by electrodes could disperse before the discharge entered the magnetic field region. To study the streamers, two light probes were used. These were first placed parallel, then perpendicular, to the flow. With the probes parallel to the flow, the velocity at which the streamers were transported down the duct was determined. To the accuracy of the measurement, this was the gas velocity of 100 m/sec. From the light output with the probes perpendicular to the flow, Fig-

ure 19, the angle of the streamers to the axis of the duct and the streamer width could be determined.

For β less than three but greater than the critical value, the streamers appeared at the expected angle of 20° to the axis of the duct and were essentially one-dimensional. Correcting for the angle of the streamers, their width perpendicular to the wave was 0.35 cm and their spacing was about 1.0 cm. As would be expected, the streamer width was the same as in the previous experiment; however, the streamer spacing was also about the same. This indicates that the streamer configuration studied in the previous experiment was indeed the naturally occurring stable configuration and that the electrodes did not produce it artificially.

One difference in the observed streamers between this and the previous experiment that may be due to the lack of stabilizing electrodes here is that for $\beta > 3$ the streamers started becoming unstable, and for $\beta > 5$ steady, one-dimensional streamers did not exist.

A similar phenomenon, formation of one-dimensional streamers at low β which broke up into secondary streamers at higher β, was observed by Velikhov[3] when studying the instability in a pulsed discharge tube.

The effect that the breakup of the one-dimensional streamers had on the measured values of σ_{eff} and β_{eff} is shown in Figures 20 and 21. The dashed curve in each figure indicates the effective values calculated from eqns. B-8 and B-9 of Appendix B that would result from waves of the measured amplitude at 20° to the average current. The measured values of σ_{eff} lie considerably below this dashed

curve for $\beta > 3$, and in fact for large β approach the theoretical value calculated in Appendix B for a two-dimensional, isotropic distribution of waves. The measurement of β_{eff} also agrees with the calculated value for a two-dimensional, isotropic distribution. Note in particular that the measured values of β_{eff} rise with β_{th} until at $\beta_{th} \approx 3$, when $\beta_{eff} = 2$, the measured β_{eff} levels off and in fact decreases slightly with further increases in β_{th}. This behavior is consistent with the theoretical observation that β_{eff} cannot exceed β_{crit}. This condition is fulfulled here by the one-dimensional streamers breaking up into secondary streamers, thus effectively increasing the average angle between the streamers and current and decreasing the effective Hall parameter of the plasma.

Measurements in other experiments[4, 9] showed similar reductions in the effective values of conductivity and Hall parameter. However, in those cases, the amplitude of conductivity fluctuations was not measured; thus, the cause of the reduction could not definitely be related to the electrothermal instability.

4.2 Discharges Transverse to the Gas Flow

As opposed to the experiments in the previous section, in MHD generators or accelerators, the discharge, gas velocity, and magnetic field are mutually perpendicular. In the experiments described in this section, the phenomenological behavior of such a discharge will be observed, and application of the theory of steady, one-dimensional waves will be made where possible. Some extensions to this theory will be necessary to explain the transient behavior in the inlet region.

(a) Inlet. - In these experiments, the pairs of electrodes discharge across the gas flow. Photographs of the inlet of such a duct are shown in Figures 22 and 23. In Figure 22, the effect of increasing the magnetic field while keeping the external resistance constant is shown. As the magnetic field is increased, the bright region of the discharge (and hence the regions of large conductivity and current density) move farther downstream in the duct. Since this increases the current path length, the resistance of the duct goes up and the current decreases. Also, it was observed that luminous layers extended back from the electrodes along the electrode walls. For high β (Figure 22c), the light from the center of the duct decreased until only the glow from these wall layers is seen. Alternatively, if the applied voltage was increased for a constant β (Figure 23), the transverse part of the discharge moved closer to the upstream electrode pair until it appeared between them. This last condition could also be produced by adding a pre-ionizing discharge upstream of the test area.

Thus, there were three modes of operation that could be distinguished on the basis of the length of duct required for the ionization transient. In the first mode, where light is emitted only from the gas along the electrode walls, the transient length is larger than the test section length, and the entire duct operates in the shorted mode, as described by Kerrebrock[13]. In the second mode, light appears in the center of the duct, but considerably downstream of the first electrode pair. This mode will be called the 'transition mode.' In the third mode, the ionization length is short, and light is emitted the full length of the test section. This mode will be called the 'normal mode;' how-

ever, from photomultiplier observations, it will be shown that this mode differs from that described by Kerrebrock in that the current is carried across the duct in a series of transverse streamers.

Qualitatively, the same modes of behavior occurred with a single transverse discharge: therefore, further study of the inlet problem was carried out with a single electrode pair. In Figure 24 are shown recordings of the electric field normal to the gas flow, $V_\perp$, and the light output from a point on the centerline of the duct 1 cm downstream of the electrode pair. For $\beta = 0$, the light intensities and voltages were constant; however, as β increased, first closely-packed streamers appeared, $\beta = 2.0$. This pattern could be produced at higher values of β by increasing the electric field or by pre-ionization, and is typical of the 'normal' mode of operation. At higher β, $\beta = 3$ and 4 in this case, a regular saw-tooth pattern appeared in the normal component of electric field, and each sharp drop in this field was followed by the passage of a solitary streamer. This behavior is typical of the transition mode. At Hall parameters larger than 4, the period of the streamer formation became very irregular, with some long periods where no transverse streamers occurred; that is, the duct was operating in the shorted mode.

Since the shorted and normal modes are then limits of the behavior observed in the transition mode, it was the transition mode that was studied in most detail.

(a-1) A single transverse discharge operating in the transition mode. - In Figure 25 are shown voltage drops normal, $V_\perp$, and parallel, $V_\parallel$, to the gas flow and the light intensities L_1, L_2, and

L_3, from three points along the centerline of a duct operating in the transition mode. The light intensities as functions of time in Figure 25 have been converted into light intensities as functions of distance at given instants of time in Figure 26. From the two figures, it can be seen that each sharp drop in the $V_\perp$ voltage is correlated with a sharp increase in radiant energy about 0.5 cm downstream of the electrodes. This has been interpreted as the formation of a new streamer between the electrodes. As this streamer is swept downstream, a gradual increase in $V_\perp$ occurs. Also note that the Hall voltage $V_\parallel$ is very small during the gradual rise of the applied field (the amplification of $V_\parallel$ is twice that of $V_\perp$) and does not begin to rise until just before the formation of a new streamer. Measurements of the time required for the streamers to be swept from one light probe to the next showed that, to the precision of the measurements, the streamers were being carried with the gas at the gas velocity.

The behavior just described for the discharge in a magnetic field is very similar to that occurring for an ordinary arc with no magnetic field discharging across a gas stream. This is not surprising because the basic cause of the behavior in both cases is a highly nonlinear shape to the heating term, Q. In particular, Q must be zero at least at two values of the temperature and be negative in the region between them.

From the previous measurement, it is possible to construct a more detailed qualitative explanation for the inlet phenomenon in this discharge. As β is increased from zero, nonuniformities caused by

the electrodes take longer to disperse, and thus high conductivity paths are formed along the electrode walls. These streamer-like paths tend to short out the Hall field which, if entirely shorted out, would decrease the electronic heating rate for a given transverse field by a factor $1/(1+\beta^2)$. This decrease in the electronic heating lengthens the ionization transient, thus shifting the discharge farther downstream. For $\beta > \beta_{crit}$, the transverse part of the discharge forms into a solitary streamer of the type described in the theory. On either side of the streamer, the conductivity is at the lowest zero of Q ; thus, there is no net electronic heating there. This means that the streamer does not tend to spread out, but its width will stay constant as it is swept downstream with the gas. However, as it is carried downstream, the electric field between the electrodes rises, and thus causes the electronic heating to again become positive there. This causes an increase in the ionization rate which, if large enough, causes the conductivity between the electrodes to increase above the value it had on either side of the old streamer. When this conductivity has increased to approximately the mean value it had in the old streamer, an increase in Hall field must follow in order to maintain the continuity of current along the duct. This is because there are now two roughly one-dimensional regions of different conductivity adjacent to each other; the newly formed high conductivity region between the electrodes, and the old region of low conductivity adjacent to the streamer. Since current density perpendicular to the interface between the regions must be the same, the Hall field in the higher conductivity region must be larger than that in the low conductivity re-

gion. This increase in the Hall field also causes an increase in the electronic heating: thus, a feedback loop is formed which causes the final, rapid rise of conductivity to form a new streamer.

The mechanism just described for formation of new streamers is essentially the mechanism of the electrothermal instability with the additional complication that the conductivity of the gas must first be raised from the very low value of conductivity in the entering gas before the instability can take over. The time required for the conductivity to be increased from the value entering the test section to the value at which the Hall field increases is the critical time, since it varies greatly with conditions in the duct. It also determines in which mode the duct will operate.

(a-2) Calculation of the inlet relaxation length. - The time required for the first phase of the stream production process can be calculated. Since the electric field parallel to the gas flow during this phase is zero, the field along the current is $E/\sqrt{1+\beta^2}$, where E is the field across the duct. Thus, eqn. (17) gives

$$\frac{d\tilde{\sigma}}{dt} = 0.5 \frac{\sigma_o}{n_{e_o} I_i} \frac{\tilde{\sigma} E^2}{1+\beta^2} \quad . \tag{40}$$

In this equation, the effect of the magnetic field is to reduce the Joule heating rate by a factor $1/(1+\beta^2)$, as expected.

The electric field, E, is calculated for the idealized circuit shown in Figure 27. Here, the old streamer is considered simply as a conducting path of constant resistance, r, per unit length, giving:

$$E = E_{o_i} \frac{1 + 2\frac{x}{w}}{1 + \frac{2}{w} \alpha (v_g t + x)} \quad , \tag{41}$$

where

$$\alpha = \frac{r(w + 2v_g t_o)}{R + r(w + 2v_g t_o)} \tag{42}$$

and E_{o_i} is the field along the streamer when it first forms. Since α is also the ratio of the minimum voltage across the duct to the source voltage, it is approximately equal to the expected loading factor for a generator. Using (40) in (41) and integrating from the time a given slug of gas enters the electric field (which is assumed to start on a line between the electrodes) until it is at a point $v_g(\tau+t_o)-x$ behind the electrodes, gives:

$$\ell n \frac{\tilde{\sigma}}{\tilde{\sigma}_i} = \frac{0.5\sigma_o E_{o_i}^2}{n_{e_o} I_i(1+\beta^2)} \frac{(1+2\frac{x}{w})^2}{\frac{2}{w}\alpha v_g} \left[\frac{1}{1+\frac{2}{w}\alpha(x-v_g t_o)} - \frac{1}{1+\frac{2}{w}\alpha v_g \tau} \right] . \tag{43}$$

This expression, plotted in Figure 28, gives σ as a function of x at a given time, τ, since the formation of the last streamer. Note that, as expected from qualitative arguments, a maximum does occur in $\sigma(x)$ between the electrodes and the old streamer. The value of τ at which this maximum reaches σ_o is taken as the time, τ_s, for the smooth rise in voltage, that is, the time for the first phase in the streamer production process. Because of the E^2 dependence of the Joule heating term, the conductivity is rising rapidly when it crosses the value σ_o; thus, τ_s is not strongly dependent on the value of σ chosen.

The parameter that determines how the electric field increases as the old streamer is blown downstream is the distance it has been blown, $v_g\tau_s$, normalized by the duct width, w. This parameter is plotted in Figure 29 as a function of the reciprocal of the reduced

Joule heating, $E_{o_i}^2/(1+\beta^2)$, for several values of α. Note that as α is increased, that is, as the ratio of the electrical resistance of the duct to the external resistance is increased, the time τ_s increases. This is because the electric field between the electrodes rises less rapidly as the old streamer is swept downstream. Also note that τ_s increases when the magnetic field is increased or the applied electric field decreased, that is, when the parameter $(1+\beta^2)/E_{o_i}^2$ is increased. The theoretical curves show good agreement with the observed length of the smooth voltage rise measured on the voltage traces, $V_\perp$, such as those in Figure 24. In Figure 29b, the measured total period of the streamers is plotted and compared to the theoretical values of $v_g\tau_s$. The difference between the two represents the time, in this case 50 to 100 μs, required for the final growth of the new streamer and the associated drop of the duct voltage due to its shorting of the old streamer. Since this time depends on the growth rate of the electrothermal instability in the gas used, it would not depend on v_g or w. Thus, at higher gas velocities, the distance $v_g\tau$ over which the final phase of the streamer production occurs may become long enough that the two phases cannot be separated. However, in the case where they can be separated, the length of τ_s will determine the mode in which the duct will operate.

(a-3) Prediction of the mode of operation. - In Figure 29a, note that as $(v_g\tau_s)/w$ approaches $1/(2\alpha)$, τ starts increasing rapidly. This is because the voltage between the duct electrodes is approaching its maximum, which is the source voltage, V. As this limit is reached, the field along the old streamer must decrease, which may

cause it to extinguish before a new streamer is formed. Experimentally, it was observed that for $(v_g\tau_s)/w > 0.25/\alpha$, the period of streamer formation became very erratic, and occasionally long periods occurred when the Hall field stayed near zero and no streamers appeared. That is, the duct was in the shorted mode.

In the other limit, when the distance $v_g\tau_s$ is less than the wavelength of steady disturbances, λ, the model again breaks down. Here, the distance between streamers is determined by the steady state equation for the streamers, and the duct is then operating in the 'normal' mode.

The condition for the existence of transverse streamers, $(v_g\tau_s)/w < 0.25/\alpha$, means that the circuit must be operating nearly as a constant current source. In the case $\alpha = 0$, that is, a constant current, an explicit expression can be obtained for the position of the maximum conductivity in eqn. (43). Putting this expression back into (43) and solving for the value of $(v_g\tau_s)/w$ at which $\tilde{\sigma} = \sigma_o$ gives:

$$\frac{v_g\tau_s}{w} = \frac{1}{2}\left\{\left[27\left(\ell n \frac{\sigma_o}{\sigma_i}\right)\frac{v_g\tau_o}{w}(1+\beta^2)\right]^{\frac{1}{3}} - 1\right\} \qquad (44)$$

where τ_o, the ionization parameter for $\beta = 0$, equals $(I_i n_{e_o})/(\sigma_o E_{o_i}^2)$.

This value of $(v_g\tau_s)/w$ can then be used to predict the mode of operation of a discharge. That is:

if $(v_g\tau_s)/w > 0.25/\alpha$, the duct is shorted;

if $\lambda/w < (v_g\tau_s)/w < 0.25/\alpha$, the duct is in the transition mode and the length of the ionization region is $v_g\tau_s$; and

if $(v_g\tau_s)/w < \lambda/w$, the duct is in the normal mode.

(b) Preionized discharge. - One way of decreasing $v_g \tau_s$ and thus producing the normal mode is to increase the initial value of the conductivity, σ_i, in eqn. (44). This was accomplished by applying a pre-ionizing discharge upstream of the test section. The pre-ionizing discharge consisted either of a pair of electrodes discharging parallel to the magnetic field or of a device similar to that used by Evans[14]. The latter consisted of a 0.16-cm diameter ceramic tube, spanning the 2-cm dimension of the duct and located just upstream of a regular electrode pair.

As would be expected, the effect appeared to be independent of the type of preionizer used. The effect of the latter type of preionizer is shown in the photographs of Figure 30. Figures 30 b, c, both with magnetic field, show the marked effect that the pre-ionizing discharge has on the visual appearance of the downstream discharge. It appears to have changed from operation in the transition mode with an ionization transient of several duct widths, Figure 30b, to the normal mode, Figure 30c, which visually appears very nearly the same as the discharge without magnetic field in Figure 30a.

In Figure 31, the effect of pre-ionization on the photomultiplier and voltage measurements is shown. Here, the preionizer was placed two duct widths upstream, so that the fields from it would cause a minimum of disturbance to the test discharge. As the pre-ionizing current, I_{pre}, is increased, the time for the gradual rise of the voltage decreases, thus decreasing the voltage fluctuation. A limit is reached at which further increases in the pre-ionizing discharge do not change the test discharge. At this point, the streamers in the test discharge

are closely packed and the voltage, $V_\perp$, is essentially constant. This set of streamers now looks much like those predicted by the periodic solution obtained in the theory, where the distance between the streamers depends on their amplitude, and their maximum amplitude is fixed by the lowest zero of Q. A duct with such a set of transverse streamers has been defined as operating in the normal mode.

The light intensity and voltage seen at the test section when only the preionizer was on is shown at the bottom of Figure 31. From these measurements, σ_i with pre-ionization was estimated to be 0.1 to 0.2 of σ_o, which was 1.5 mho/cm. However, this is an increase of about a factor of 10 over the σ_i without pre-ionization, which is the equilibrium value of 0.03 mho/cm for this plasma. In Figure 29, the calculated effect on $v_g\tau_s$ of a factor 10 increase in σ_i is shown and is consistent with the observed shorting of the ionization transient.

(c) Multiple transverse discharges. - The normal mode of operation was studied in a duct with a series of circuits discharging in parallel across the test section. The visual appearance of such a discharge for several values of β is shown in Figure 32. Here, four pairs of electrodes spaced 1 cm apart can be seen. Gas flow is from left to right. The first electrode pair on the left with the ceramic tube placed immediately in front acts as the preionizer. The main change that can be seen as β is increased is that an asymmetry develops in the bright regions around the electrodes. The bright regions at the anodes, upper electrodes, shifts downstream and the bright region at the cathodes, lower electrodes, shifts upstream. These photographs were made for the magnetic field pointing into the plane of the paper;

therefore, since the $\underline{J} \times \underline{B}$ force is in the direction of the gas flow, this is an accelerator configuration. Reversing the magnetic field reverses the asymmetry of these bright regions. This is consistent with the idea that there are certain ranges of angles relative to the current and field vectors at which perturbations are unstable; however, the important point is that there are high conductivity regions extending parallel to the electrode walls.

A test section with electrodes spaced every $\frac{1}{2}$ cm, which is less than the streamer spacing of 1 cm, was used for photomultiplier and voltage measurements in the normal mode. The development of the transverse streamer pattern is shown in Figure 33 as a function of β. When β was increased from zero to 1.4, which is still below the value at which the instability develops, the electric field increased and the light intensities decreased. This is due to the high conductivity zones along the electrode walls previously mentioned.

As β is increased above the critical value of about 2, a set of regular streamers appeared. These streamers have the same size and spacing as those seen with a single pre-ionized discharge, Figure 31. The similarity of the two situations indicates that the upstream discharges act mainly as preionizers for the following ones.

A regular pattern of transverse streamers was also observed by Zauderer[11] in high-speed photographs of a magnetohydrodynamic generator with a similar electrode configuration, but with xenon gas as the working fluid.

A detailed study of the streamers was made. In Figure 34 is shown a comparison of the light traces at the centerline of the duct

and at various points toward each wall. From these measurements, it was found that streamers were distinguishable and essentially one-dimensional to within 2 mm of the discharge electrodes. Also, signals shown in Figure 35 from light probes placed 1 cm apart along the centerline of the duct were compared. These signals are displaced 100 μs relative to each other in Figure 35 to correct for the time required for the gas to transverse the distance between the probes. Note that occasionally a streamer will split into two; however, the streamers in general do not change much in this 100 μs. This time is long compared to the instability growth time of 10 μs ; thus, the streamers can be considered as steady.

Therefore, since the streamers in the center of the duct are steady and one-dimensional, the conductivity and field variations should be predicted by the theory. In Figure 36, these variations, measured in the transverse streamers of a case for $\beta = 5$, are shown on a $\sigma/\langle\sigma\rangle$ versus E_{L_o}/E_o plot to lie within the calculated instability regime. Note that,as in the previously mentioned experiments, the streamers again are found at a value of E_{L_o}/E_o somewhat smaller than the one at which the maximum amplitude occurs, 0.52 in this case, and thus their amplitude is limited by the lowest zero of Q.

Also as shown in Figure 37, the values of E_{L_o}/E_o measured lie close to the predicted value for minimum effective Hall parameter. This is consistent with the fact that the measured values of conductivity variations again fall below the maximum possible value in the range close to the value for minimum β_{eff}. It will be re-

membered, however, that the minimum β_{eff} calculated for one-dimensional waves was not small enough to produce a plasma that was stable with respect to large amplitude disturbances. That is, stable, one-dimensional waves were not expected to occur for $\beta_{th} > 3$; however, they were observed to the maximum β_{th} we could produce,which was 7.3. One possible explanation is that since the distance between electrodes was only about two wavelengths, the electrodes may have had a strong stabilizing effect on the waves. A fluctuation in $V_{\perp}$, shown in Figure 33, occurred as each streamer passed an electrode pair. This field, for a truly one-dimensional set of streamers, should be constant,and its fluctuation may be related to the mechanism by which the electrodes stabilize the transverse streamers. For these reasons, the streamer pattern in a larger device may be considerably different than it is here.

No significant aerodynamic effects were observed when the direction of the $\underline{J} \times \underline{B}$ force was reversed. Data are shown for the $\underline{J} \times \underline{B}$ force parallel and anti-parallel to the gas velocity, indicated by 'brake' and 'accel.', respectively. Also, the measurements when normalized were the same for currents from 2 to 6 amps/cm^2. Since the shape of the curves of the electronic heating term is independent of the average current, the only effect that changing the average current should have is in the change in the exponent n of the σ versus J formula. The change of this exponent between J = 2 and 6, however, was too small to have an effect distinguishable from the normal scatter in the data. Note, however, that significantly different results would be expected in other gases, where the n may be

considerably different.

(c-1) Effective conductivity in the normal mode. - In these experiments, the transverse current was held constant as β was increased; therefore, E_{L_o}/E_o is equal to the ratio of the effective conductivity, σ_{eff}, to the conductivity, σ_o, with $\beta = 0$. To show that the measured σ_{eff} is consistent with the observed amplitude and pattern of conductivity fluctuations, a calculation of the effective conductivity was made for a duct with hot boundary regions on either side of a region with transverse conducting paths. This was done by calculating average fields and currents in each region from an analysis similar to Rosa's[15] and matching them across the division between the two regions (Appendix B). This analysis gave eqn. (B-8) for the relationship between σ_{eff} and $\langle\sigma\rangle$. Using eqn. (B.43) to correct this expression for the change in $\langle\sigma\rangle$ gives:

$$\frac{\sigma_{eff}}{\sigma_o} = \left[\frac{\gamma + 1/(1 - \langle\sigma\rangle/\sigma_{BL})\, S\, \beta^2}{(\gamma + \beta^2)(1 + S)^{1/2}}\right]^{2/3}, \qquad (45)$$

where γ specifies the effective boundary region and is equal to

$$\gamma = 1 + \frac{w}{\delta}\,\frac{1}{(\sigma_{BL}/\langle\sigma\rangle - 1)} \quad .$$

Here, w is the width of the duct, δ is the width of the hot boundary region, and σ_{BL} is the average conductivity of the boundary. S is the mean square deviation for a sine wave of the normalized peak-to-peak amplitude plotted in Figure 38. With no transverse streamers, that is, with $\Delta\sigma/\langle\sigma\rangle = 0$, the σ_{eff} would decrease along the curve marked 1-D in Figure 39. This curve gives the effective conductivity for one-dimensional nonuniformities parallel to the flow and the magnetic field.

The actual data lie considerably above this curve, due to the beneficial effect of the transverse streamers. The solid curves in Figure 39 show the σ_{eff} calculated from eqn. (45) with S = 0. 125, that is, for $\Delta\sigma/\langle\sigma\rangle$ = 1. 0 and for γ = 3. 0 and 5. 0. Most of the data are contained in this range of γ, which corresponds to two boundary regions, each of thickness 0. 5 cm and having a conductivity 1. 5 to 2. 0 times that in the main stream. These values are consistent with estimates that could be made from photographs of the duct. However, γ cannot in general be calculated with any degree of accuracy, and therefore only S is known.

Louis[16] has suggested that even though the actual conductivity nonuniformities may display distinct regularity, the effective conductivity might adequately be predicted by assuming an isotropic distribution of these nonuniformities. A calculation of σ_{eff} was made following the suggestion of Louis (Appendix B). However, the calculation procedure of Yoshikawa and Rose[17] was modified by using the assumption that the collision frequency was constant rather than the assumption used earlier that it was dominated by Coulomb collisions. Although this assumption is closer to the condition of this experiment, it does not change the result significantly. From this calculation, again correcting for the change of $\langle\sigma\rangle$,

$$\frac{\sigma_{eff}}{\sigma_o} = \left[\frac{1 + (SI)^2 - \frac{2SI}{\beta} + \left(\frac{SI}{\beta}\right)^2}{\left(1 - \frac{1}{\beta} SI + \beta SI\right)(1+S)^{1/2}} \right]^{2/3} , \qquad (46)$$

where I as defined in eqn. (B.37) goes to $\pi/4$ for large β and S is the mean square deviation of the conductivity. Equation (46) gives

the curve marked 3-D in Figure 39, where S = 0.125. This curve was too high; however, when the above calculation is reformulated such that only isotropic conductivity fluctuations in the two dimensions perpendicular to the magnetic field are allowed, better agreement was obtained. Here, the equation for σ_{eff} is:

$$\frac{\sigma_{eff}}{\sigma_o} = \left[\frac{1 - S + \frac{S^2}{4}\beta^2}{(1 - \frac{S}{2} + \frac{S}{2}\beta^2)(1 + S)^{1/2}} \right]^{2/3} . \qquad (47)$$

This result, marked 2-D in Figure 39, agrees with the data at the higher values of β. It should be noted that the duct used in these experiments was only 1 cm wide in the direction of the magnetic field, and thus would tend to stabilize the plasma against nonuniformities in this dimension. However, no mechanism can be seen which would tend to produce nonuniformities along the magnetic field even in a larger duct, and in fact Zauderer has observed a similar two-dimensional conductivity pattern in a duct 5 cm wide.

5. SUMMARY AND CONCLUSIONS

In a nonequilibrium plasma, the constant electron density solution to the energy equation is unstable for Hall parameters greater than about two. This instability is due to the strong coupling between the electrical conductivity and the heating of the electron gas. However, a wave can be chosen with a wavelength such that the energy input due to this coupling is just canceled by the damping effect of radiative diffusion of energy. This wave is then a steady solution. Using the diffusion approximation to the radiative transport term in the energy equation, a set of these steady solutions was calculated. In these solutions, the non-linearity in the electron heating term produced a dependence of wave shape on wave amplitude and as a result gave a limit on the amplitude of periodic solutions. This limit gave a prediction of a maximum peak-to-peak amplitude, $\Delta\sigma/\langle\sigma\rangle$ of about one. Also, the wavelength of steady waves was found to be on the order of one cm.

If steady waves exist in practice, these are the characteristics expected; however, whether the waves actually exist or not depends on their stability with respect to an arbitrary disturbance, and this was not determined analytically. It was found that a plasma with a set of steady waves would be unstable when perturbed by a disturbance of a wavelength much larger than that of the steady waves, if the effective Hall parameter of the plasma with waves exceeded the original critical Hall parameter of the plasma. This occurred for $\beta_{th} > 3$, and implies that the steady, one-dimensional waves would not be stable

for larger Hall parameters.

To check the predictions for the steady waves, an experimental configuration was designed in which the electrode geometry would naturally tend to stabilize the steady waves. In this experiment, steady waves were observed, and their amplitude and wavelength agreed with predicted values.

Next, the waves were studied in an experiment where the electrodes were outside the test section and could not stabilize the waves. Here, steady waves with the same characteristics as before were observed at Hall parameters slightly above the critical value. However, for values higher than about three, the one-dimensional waves became unstable and broke up into secondary waves.

With the basic predictions of the theory of the electrothermal waves verified, the manifestation of this instability in a generator or accelerator configuration was next studied. The main difference between this and the two previous configurations is that the electrical discharges here are transverse to the gas flow. The most noticeable effect of this change occurred in the inlet to the discharge region. Three different modes of operation of the inlet were observed, depending on the applied magnetic and electric field strengths, gas velocity, and initial degree of ionization. These were: first, a shorted mode in which high conductivity regions extended along the electrode walls and conductivity in the center of the duct was very low; second, a transition mode in which solitary current streamers were successively formed in the inlet, blown downstream, and extinguished; and finally, a normal mode in which closely-packed transverse streamers

existed the entire length of the duct. The behavior of the duct in the transition mode was studied analytically, and it was found that the main effect on the behavior of the inlet was the high conductivity regions formed along the electrode walls. These regions, which were caused by the instability amplifying the local heating at the electrodes, shorted out the Hall field in the center of the duct and decreased the Joule heating there by a factor $1/(1+\beta^2)$. Also, from this analysis, it was shown that one way to produce the normal mode and thus increase the transverse conductivity was to pre-ionize the gas entering the duct. The effect of pre-ionization was verified experimentally.

The normal mode was studied in a duct with a number of parallel transverse discharges. The characteristics of the streamers here were shown to agree with those predicted by the steady, one-dimensional theory. Also, several methods were explored for calculating the transverse conductivity of the duct. Experimentally, it was observed that this conductivity at $\beta_{th} = 5$ was about 40 per cent of the theoretical value for a uniform plasma with no waves. This value was found to correspond to a distribution of nonuniformities of the measured amplitude in planes parallel to the magnetic field, that is, in the planes in which they were observed experimentally.

In conclusion, much of the anomalous behavior of a non-equilibrium plasma when it is subjected to crossed electric and magnetic fields can be explained in terms of the electrothermal instability. Useful quantitative estimates of effective plasma parameters can be made using the predictions of the steady, one-dimensional theory for the electrothermal waves.

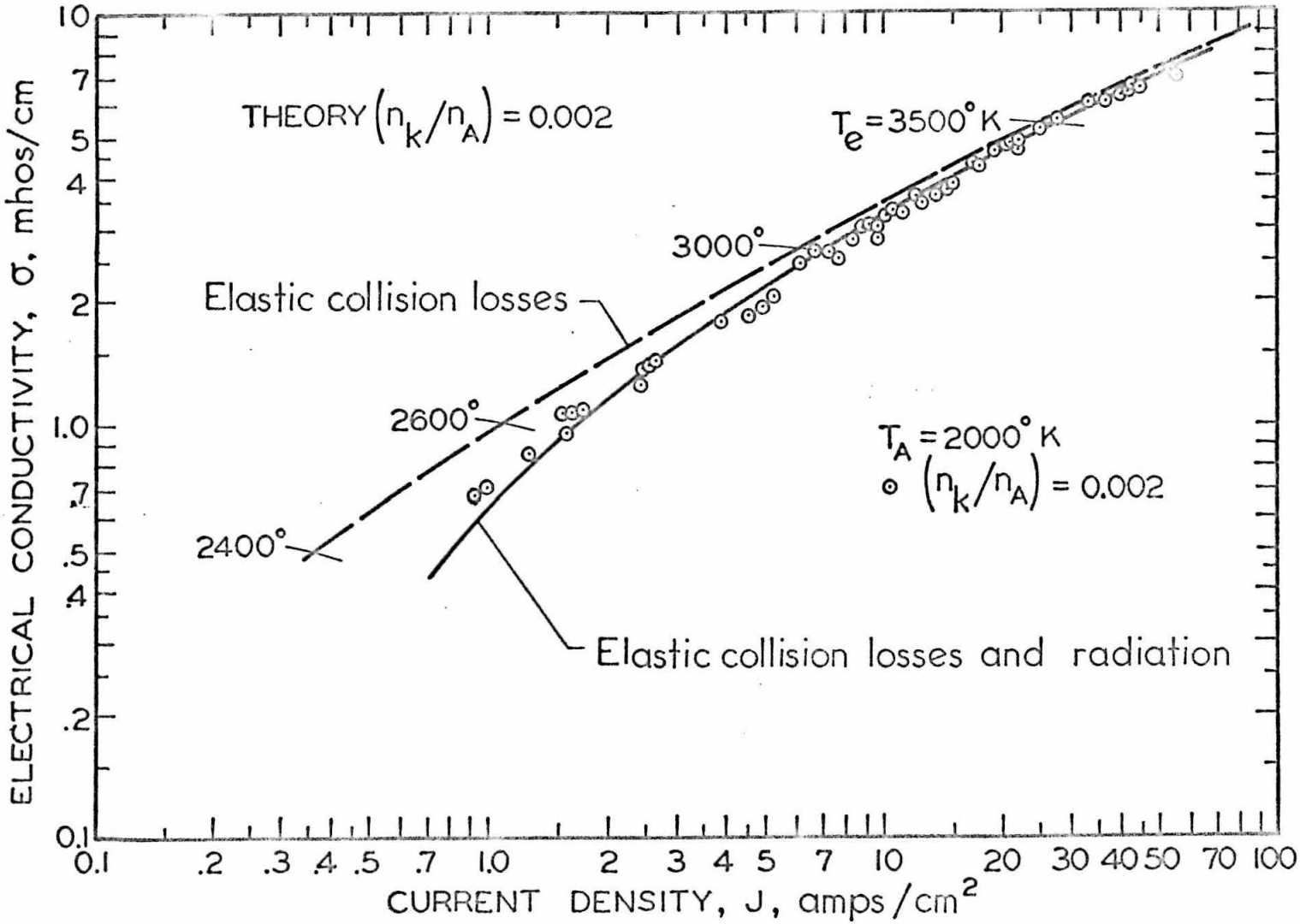

FIG. 1 STEADY STATE CONDUCTIVITY

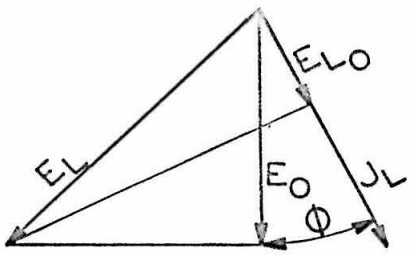

VECTORS OF THE UNIFORM STATE

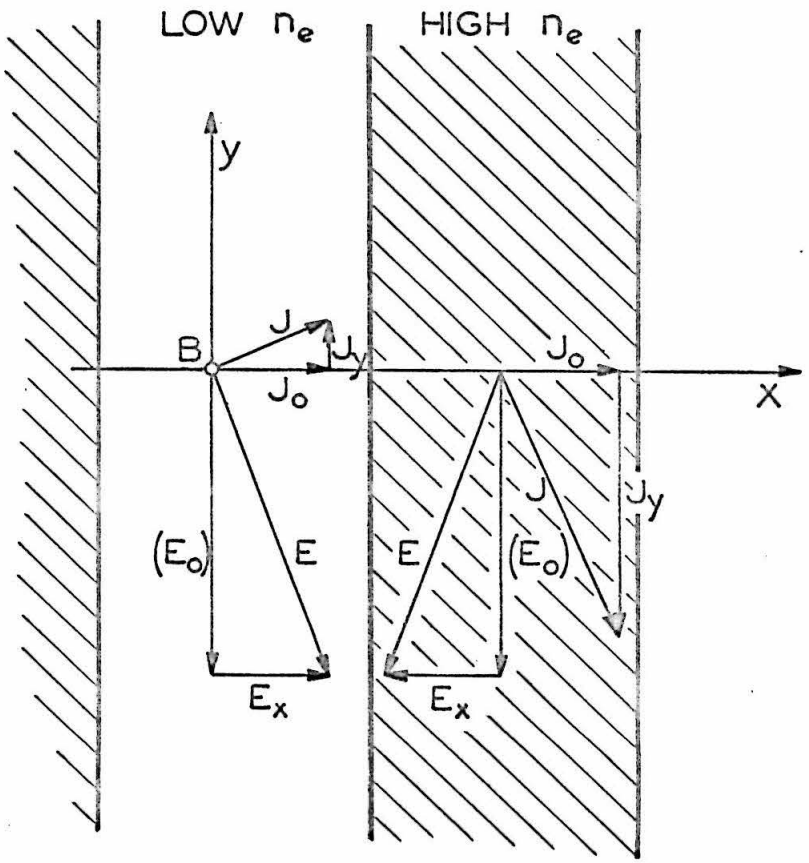

FIG. 2 COORDINATE SYSTEM FOR 1-D PROBLEM

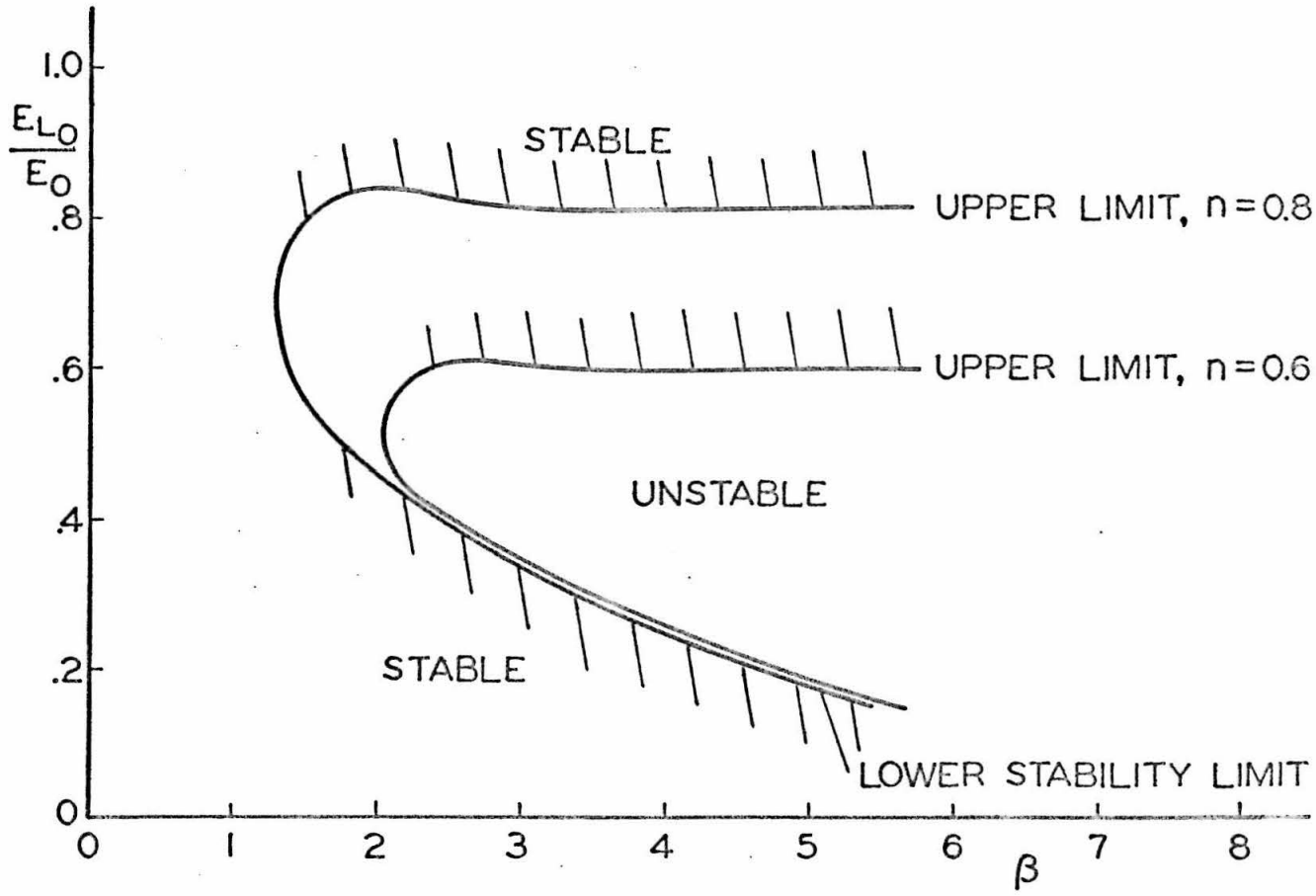

FIG. 3 INSTABILITY REGIME FOR ELECTROTHERMAL WAVES

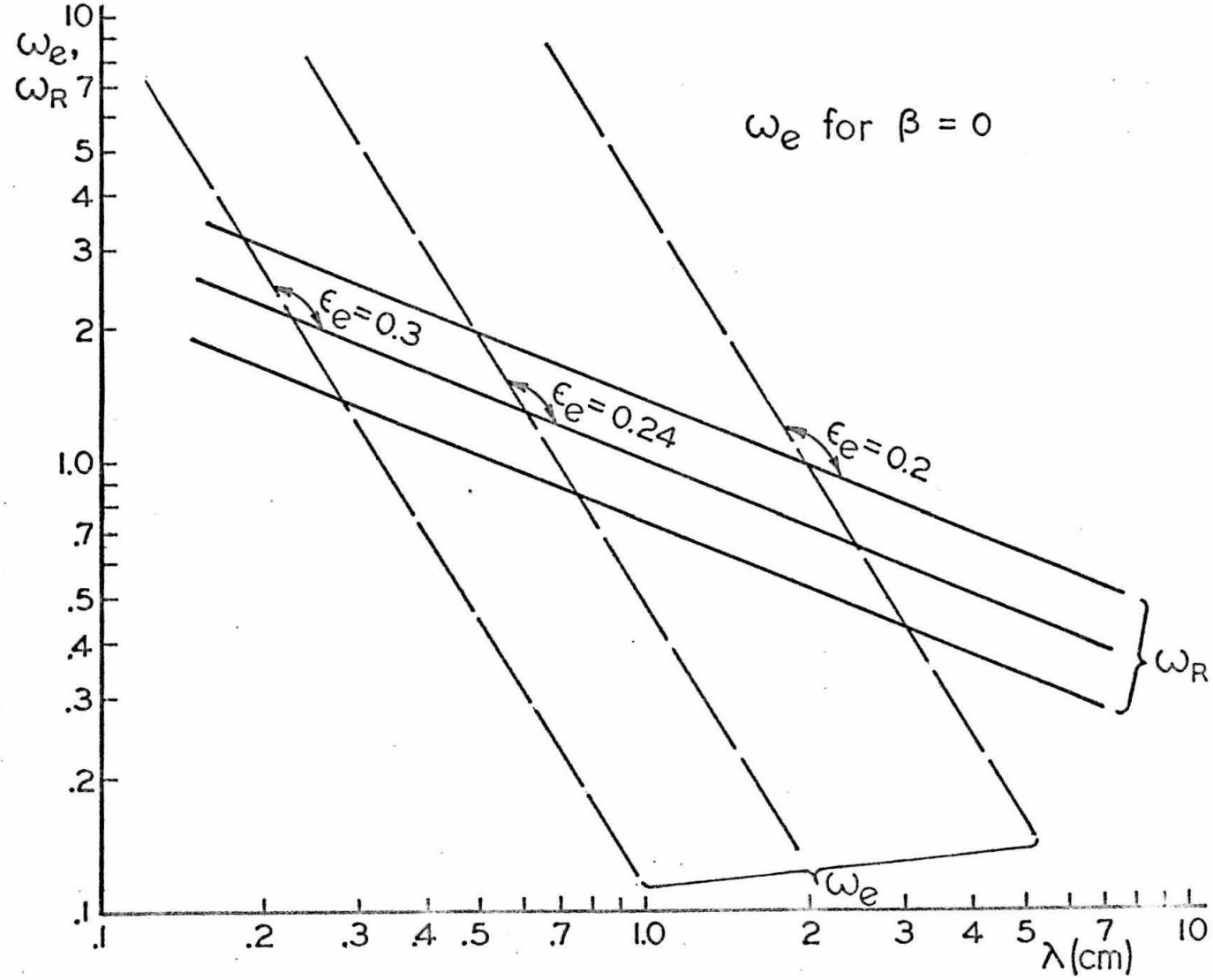

FIG. 4 RADIATIVE AND ELECTRONIC HEAT TRANSFER

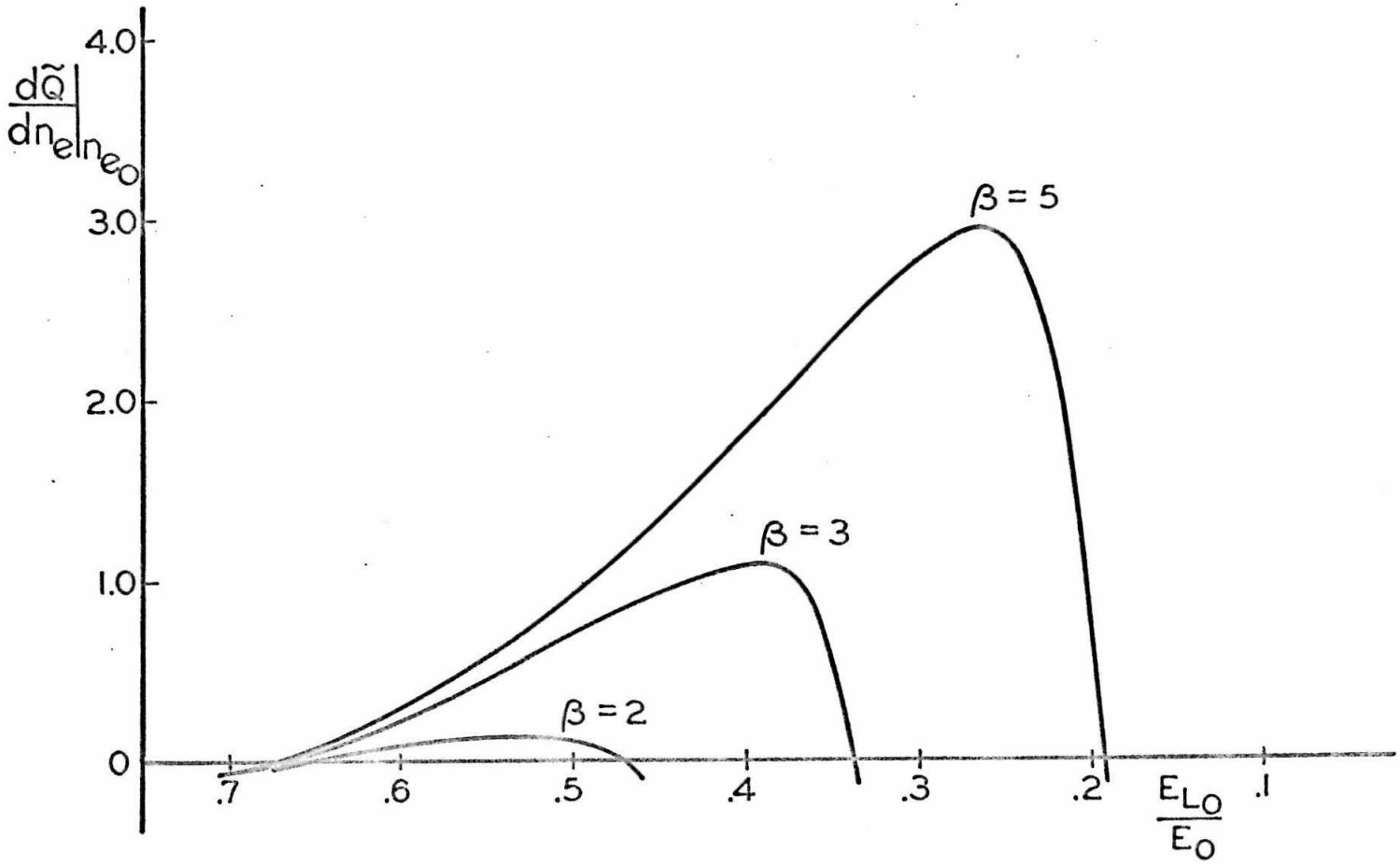

FIG. 5 SLOPE OF Q AT UNIFORM SOLUTION

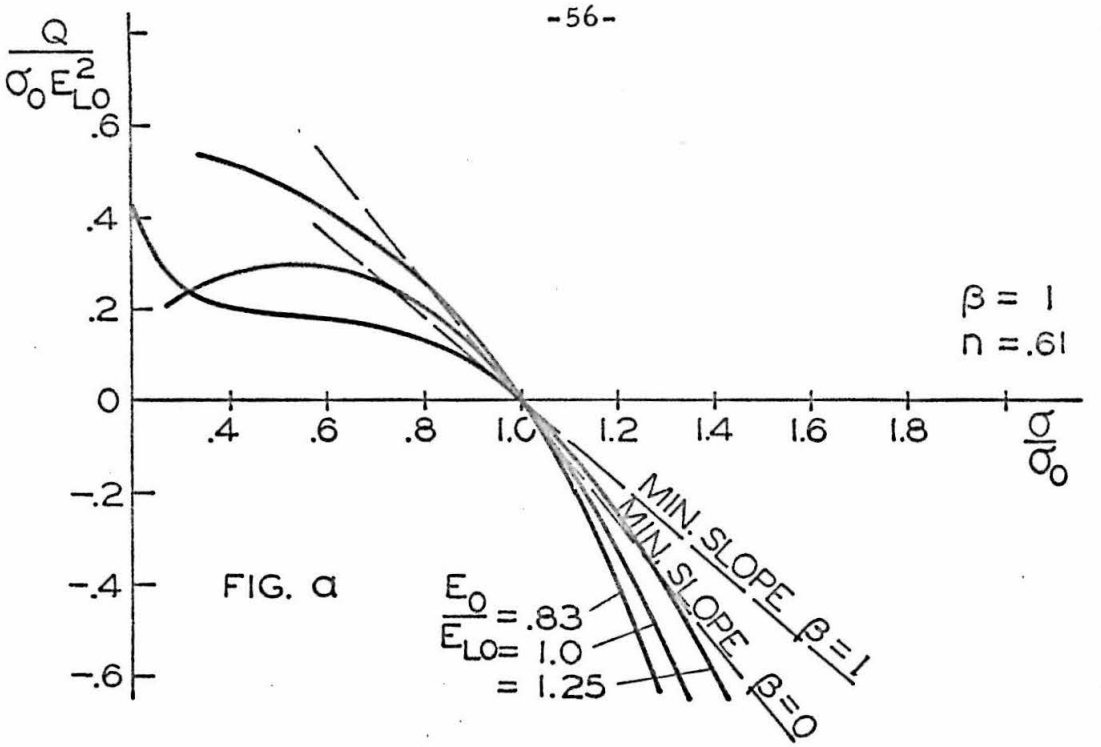

FIG. a

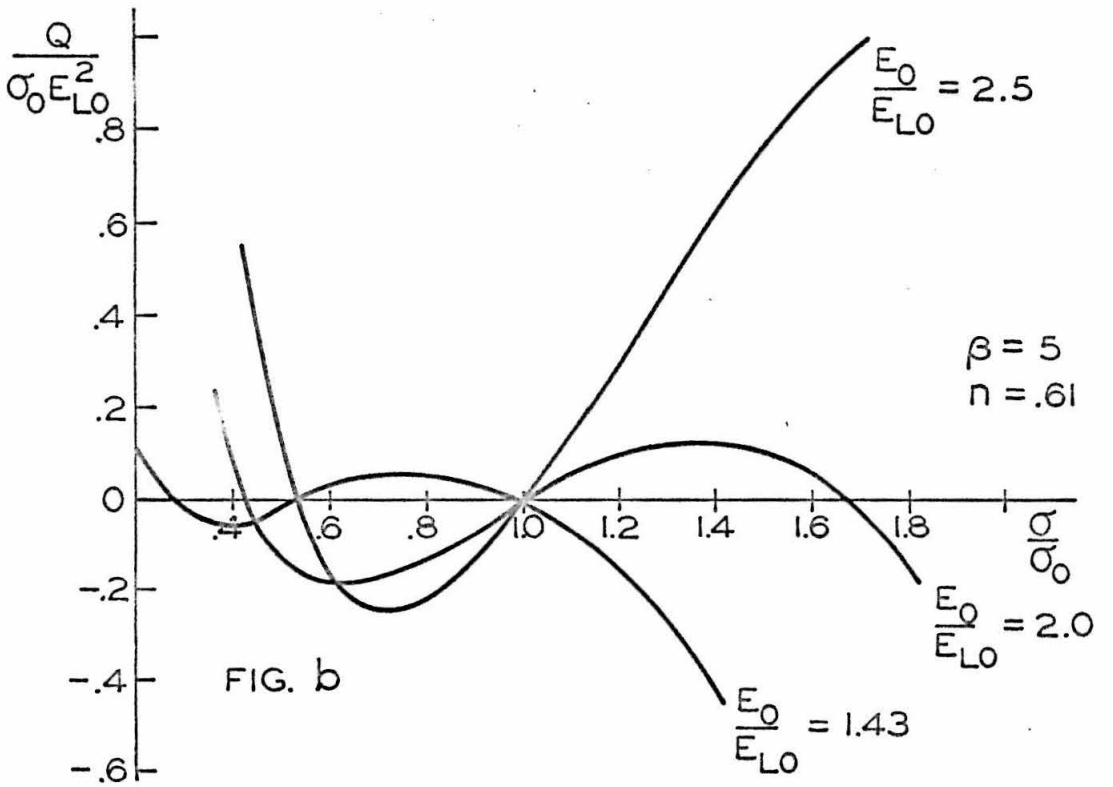

FIG. b

FIG. 6 a & b THE ELECTRONIC HEATING TERM

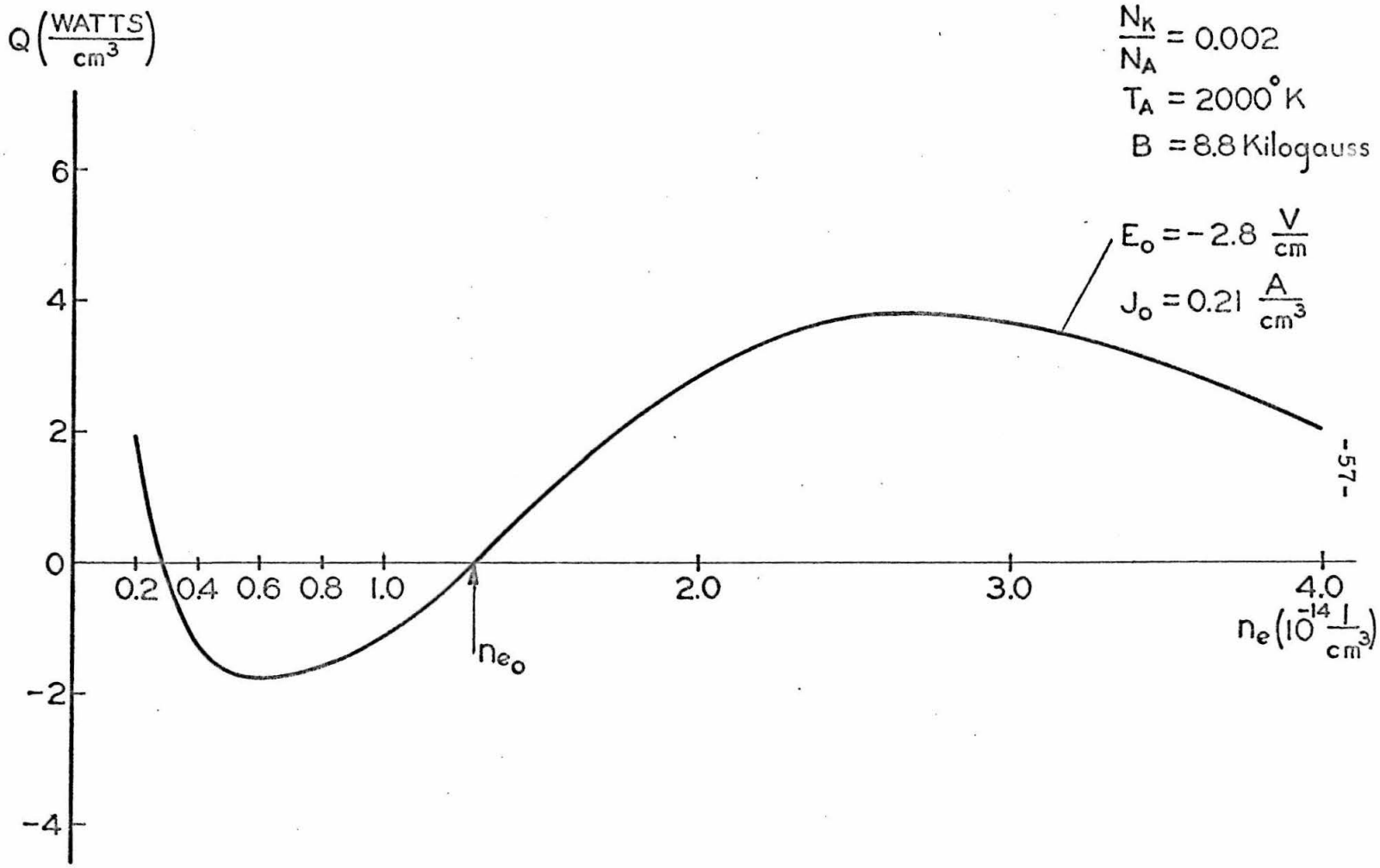

FIG. 7 ELECTRONIC HEATING TERM $(Q(n_e))$

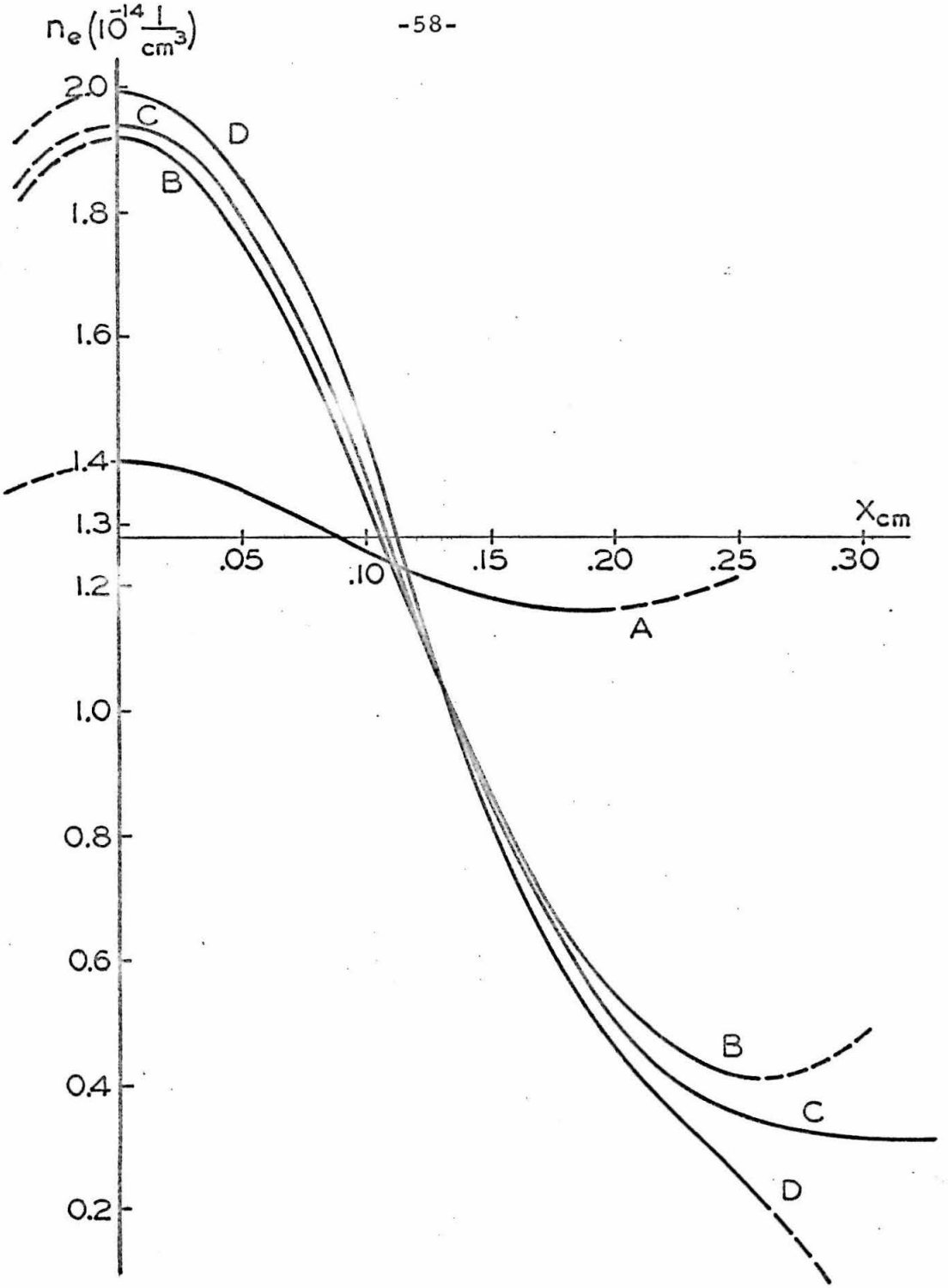

FIG. 8 WAVE SHAPE AT VARIOUS AMPLITUDES FOR $Q(n_e)$ IN FIGURE 7

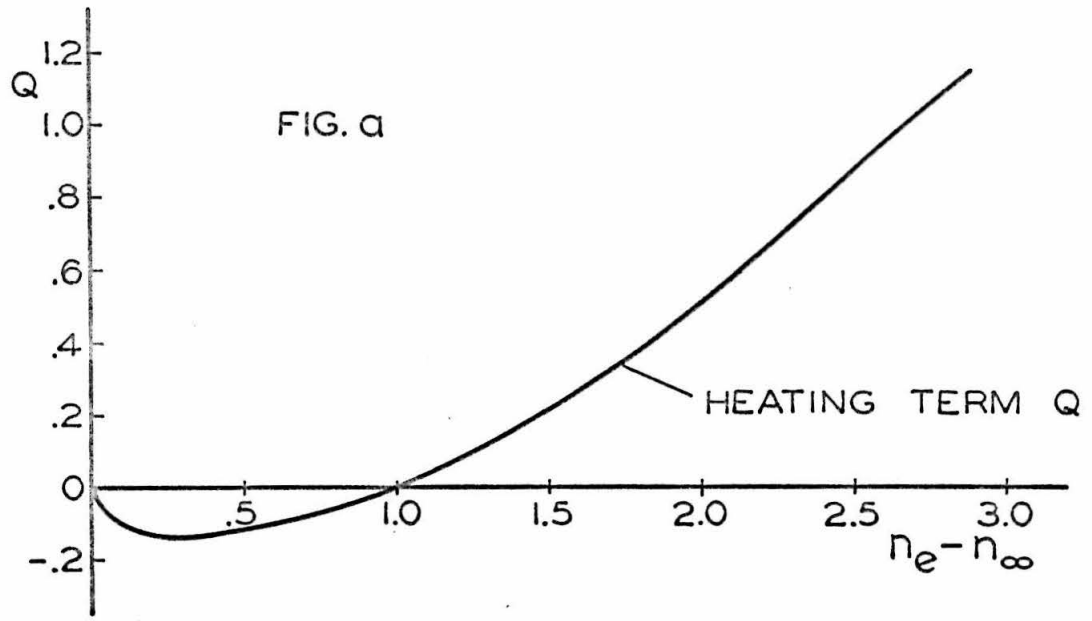

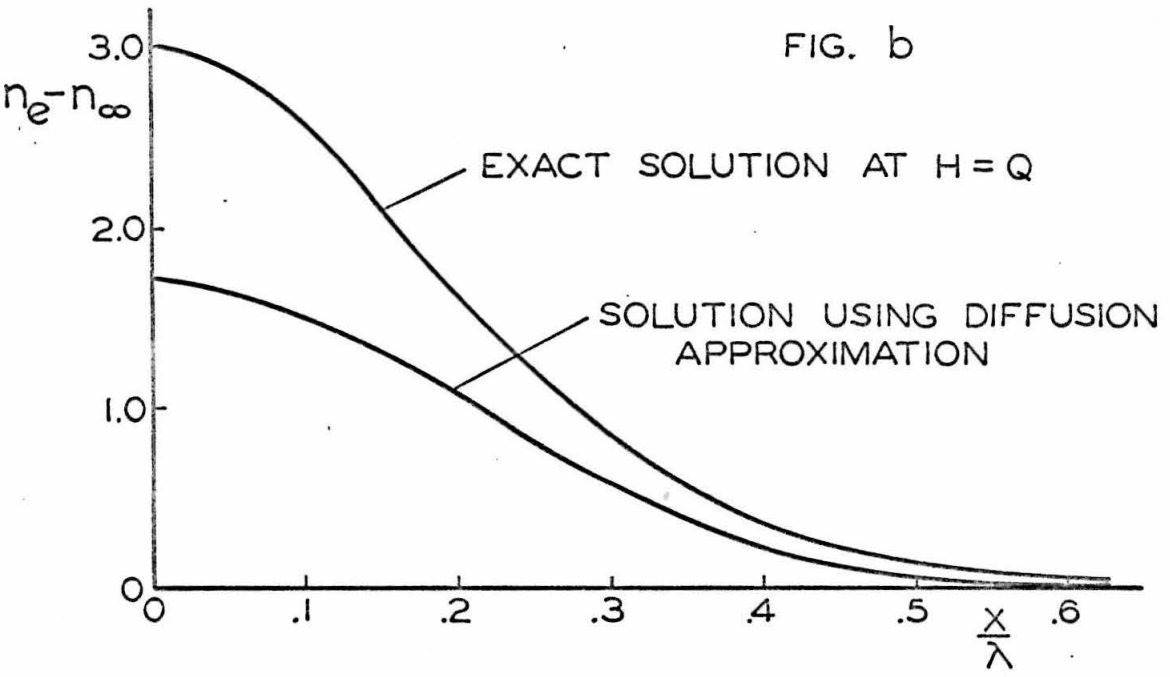

FIG. 9a & b CHECK OF THE DIFFUSION APPROXIMATION

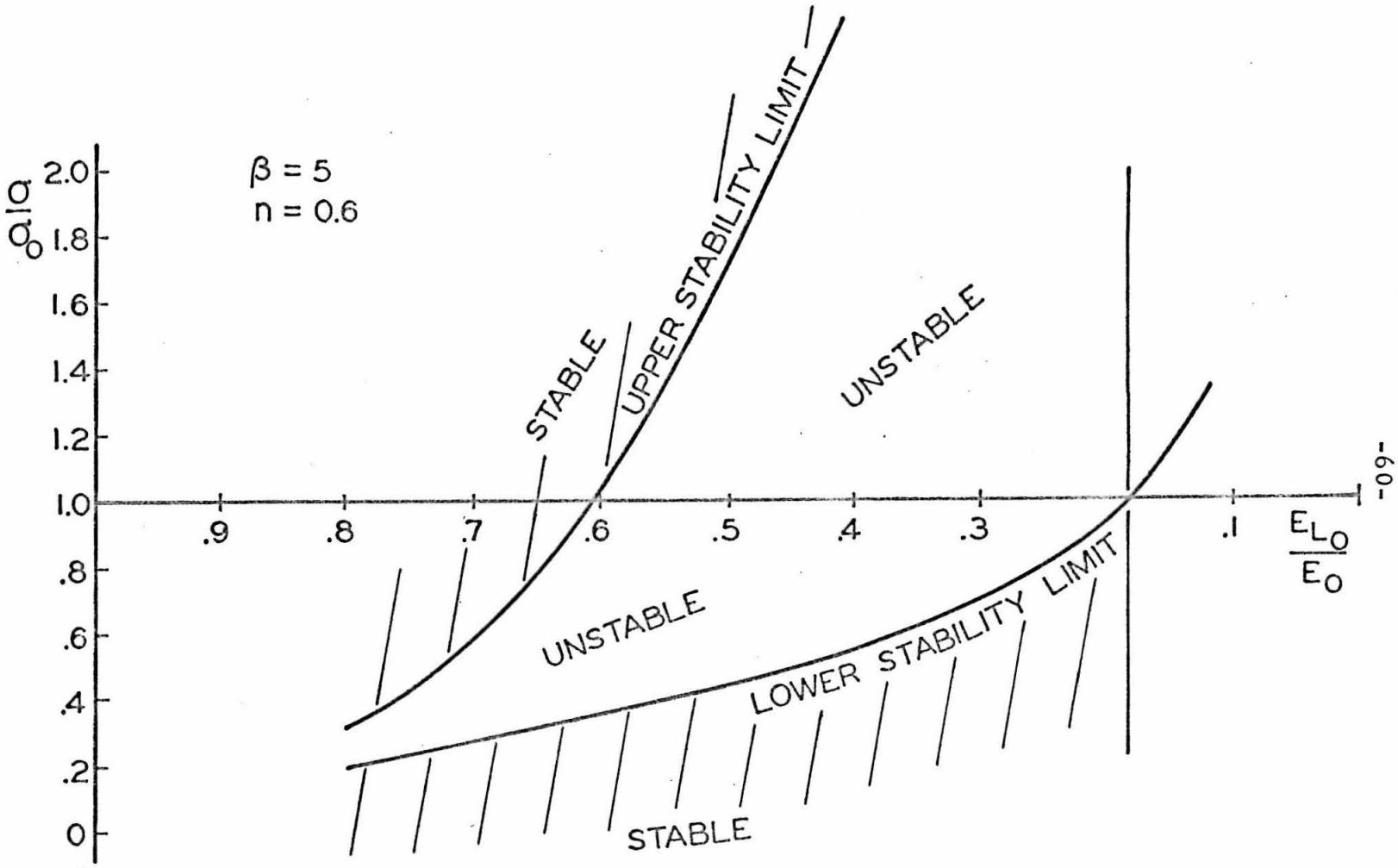

FIG. 10 STABILITY LIMITS FOR CONDUCTIVITY VARIATIONS

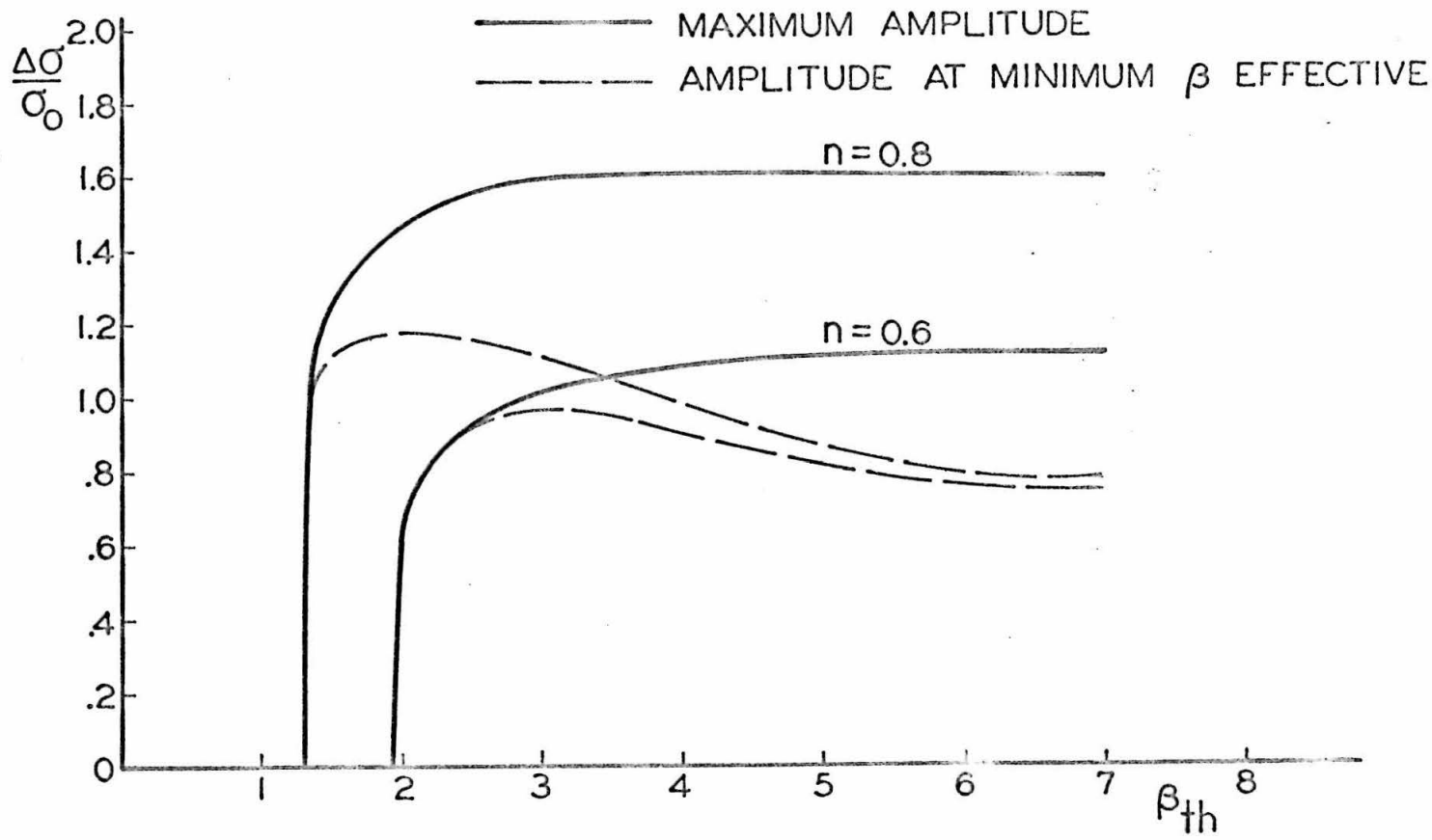

FIG. 11 AMPLITUDE OF CONDUCTIVITY VARIATION

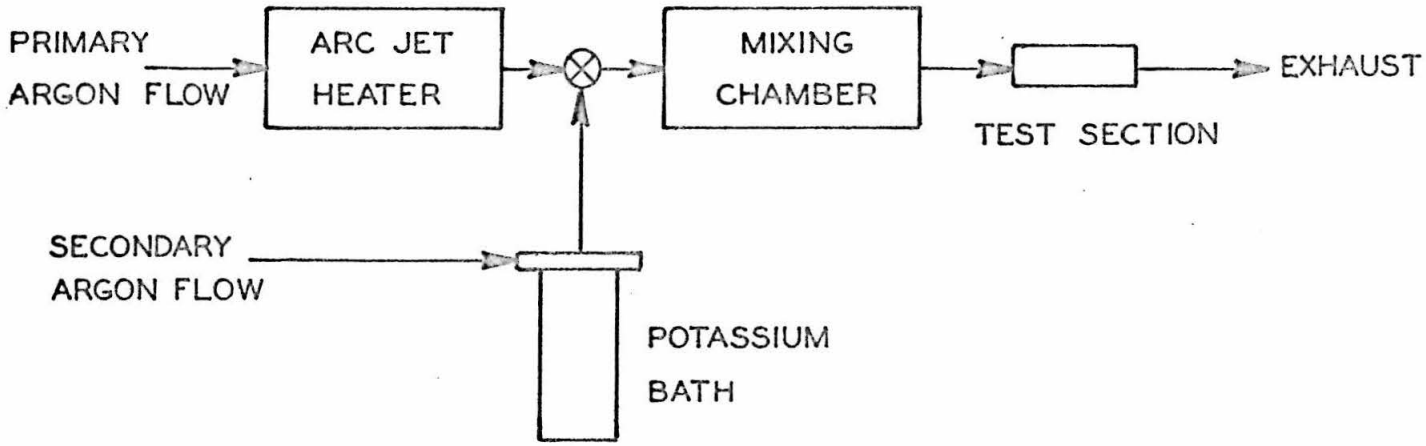

FIG. 12 SCHEMATIC DIAGRAM OF FLOW SYSTEMS

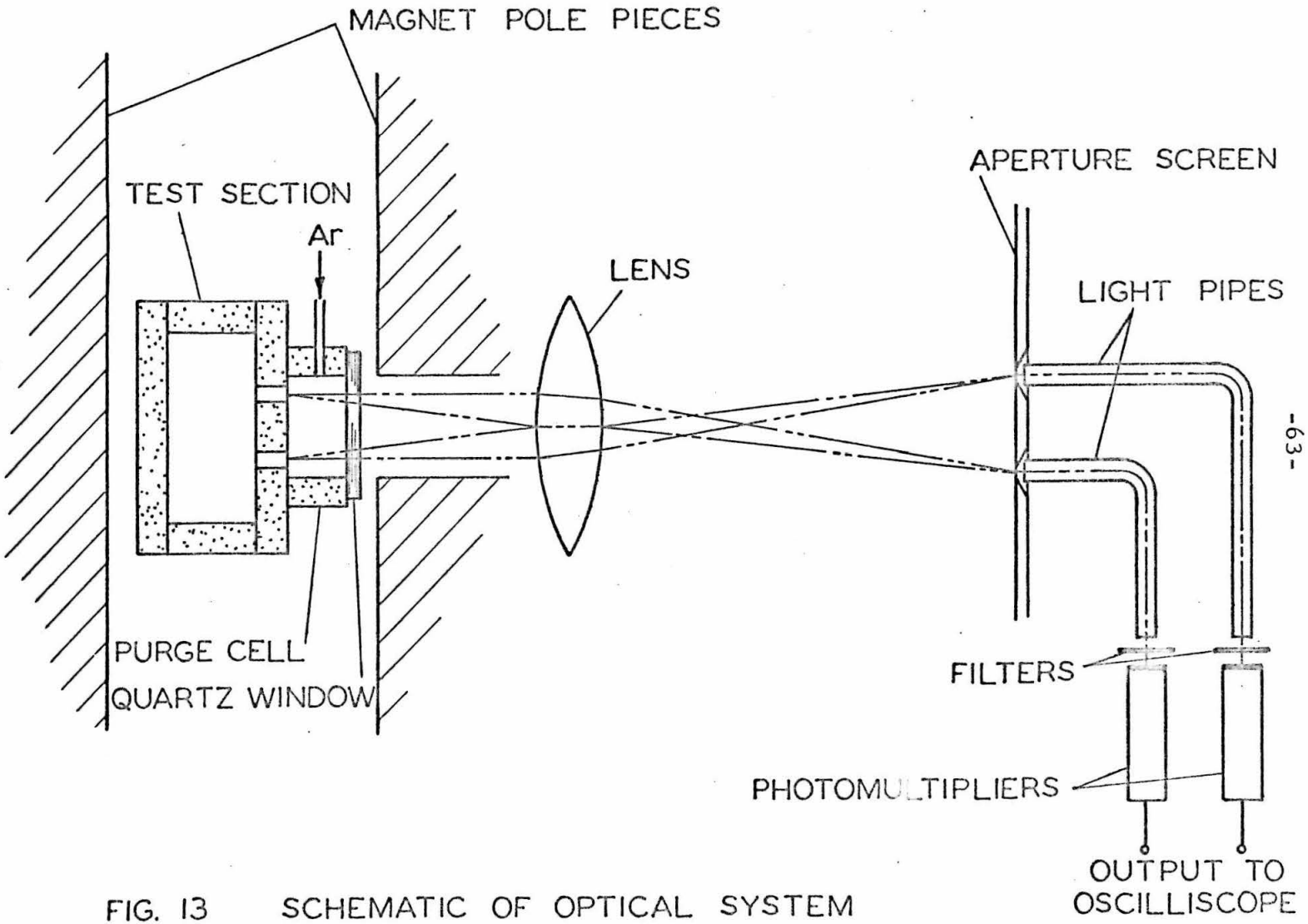

FIG. 13 SCHEMATIC OF OPTICAL SYSTEM

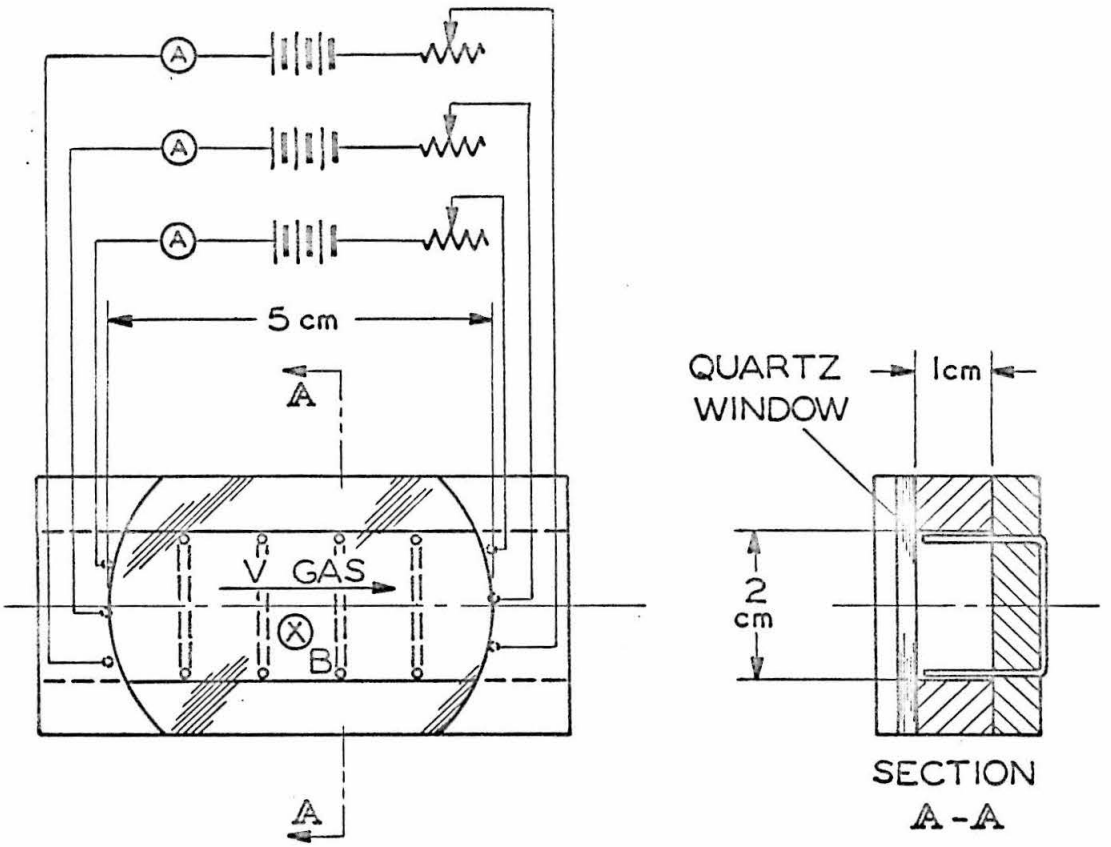

FIG. 14 TEST SECTION FOR THREE STREAMER CONFIGURATION

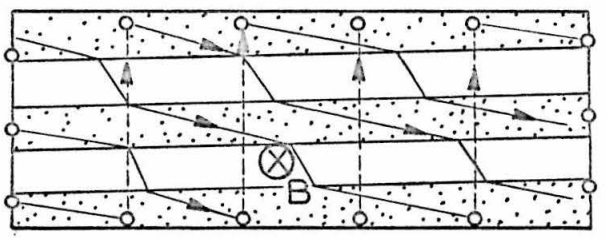

FIG. 15 SCHEMATIC CURRENT PATTERN WHICH PRODUCES CURRENT STREAMERS IN FIGURE 16

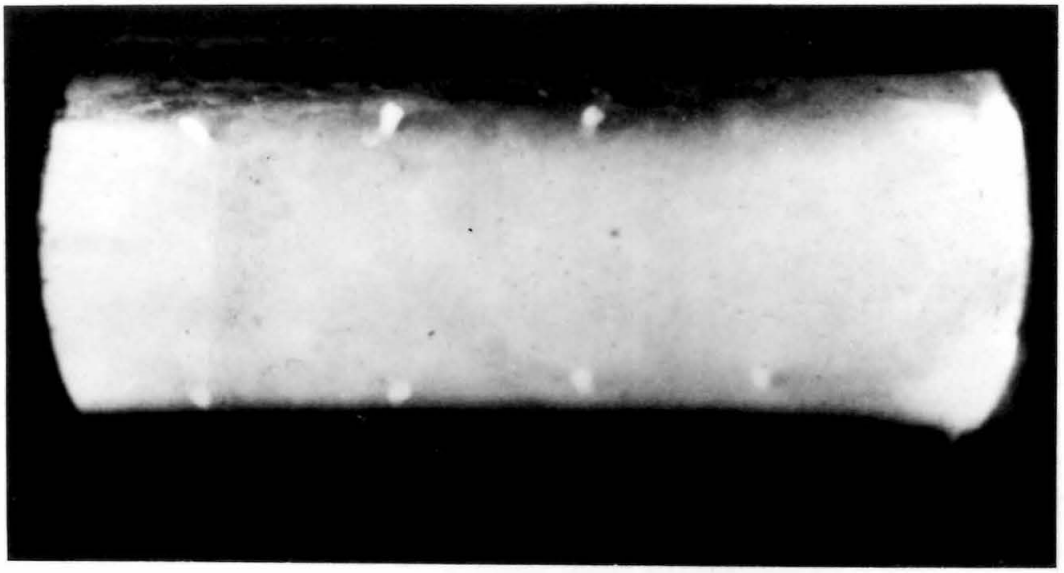

(a)

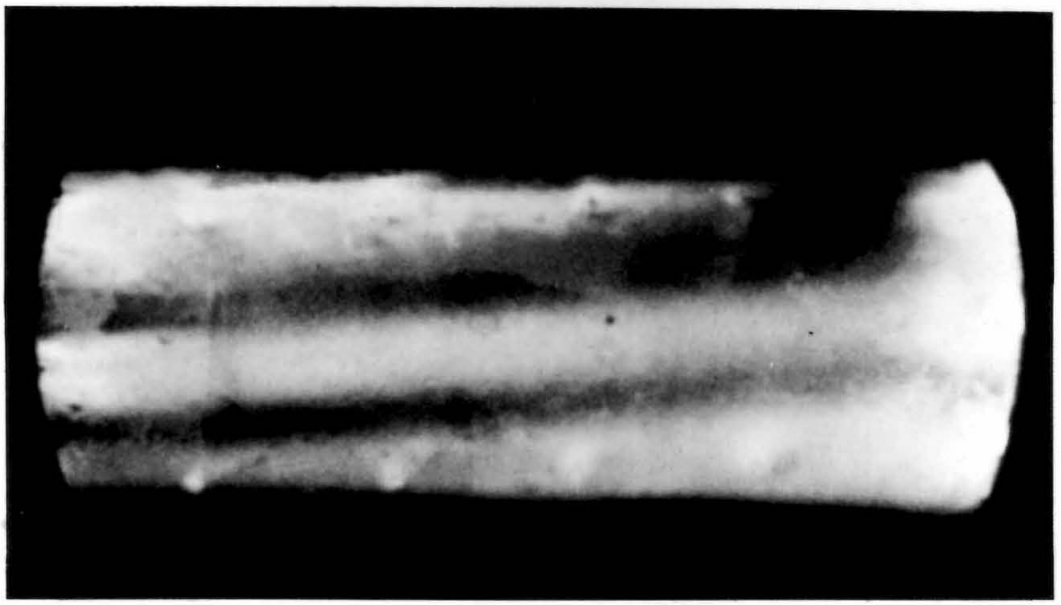

(b)

Fig. 16 Pictures taken though window in test section wall
(a) Uniform luminousity produced when only an electric was applied.
(b) Current streamer pattern that appeared when a magnetic field was added.

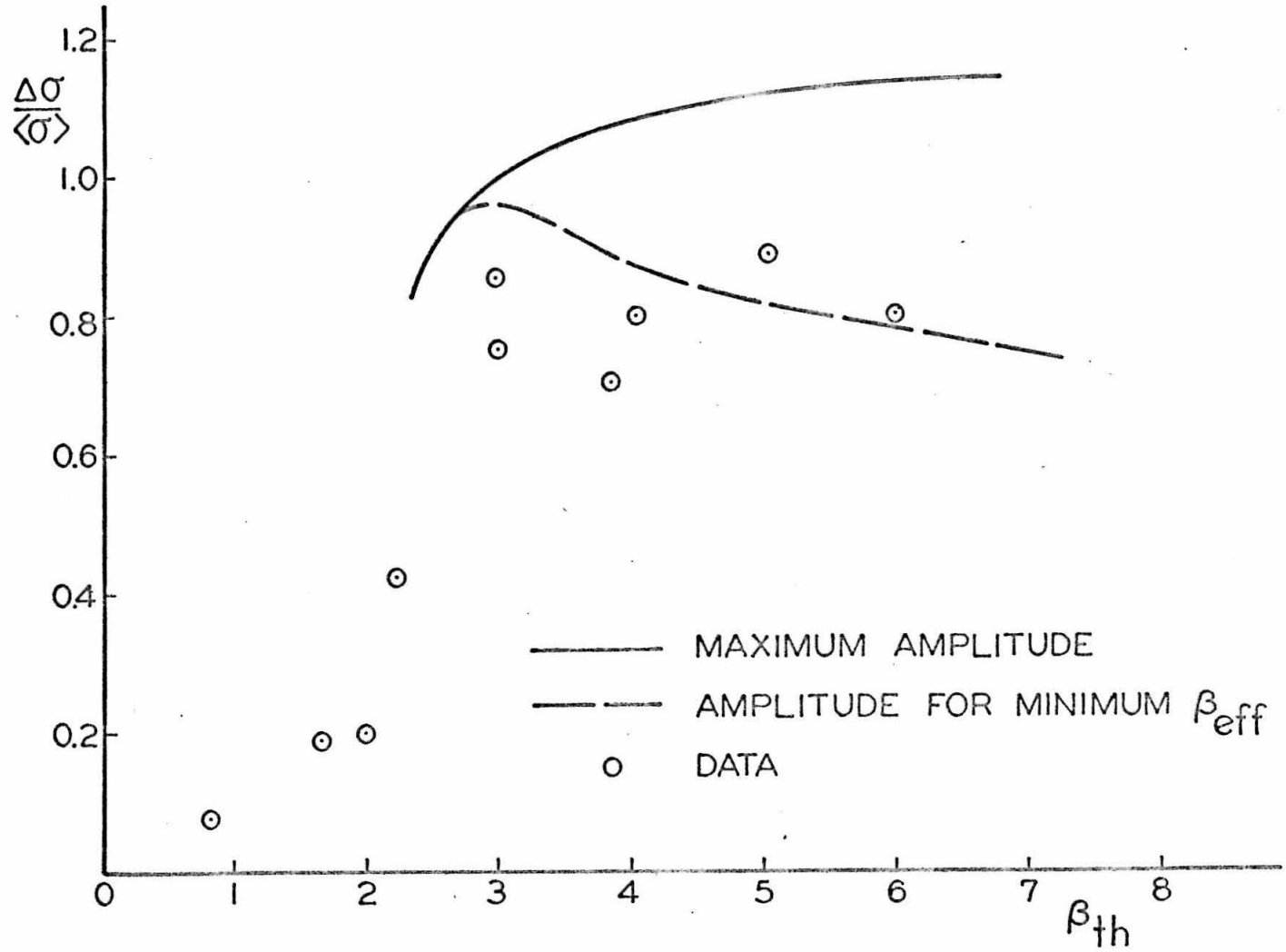

FIG. 17 PEAK TO PEAK AMPLITUDE OF STEADY STREAMERS

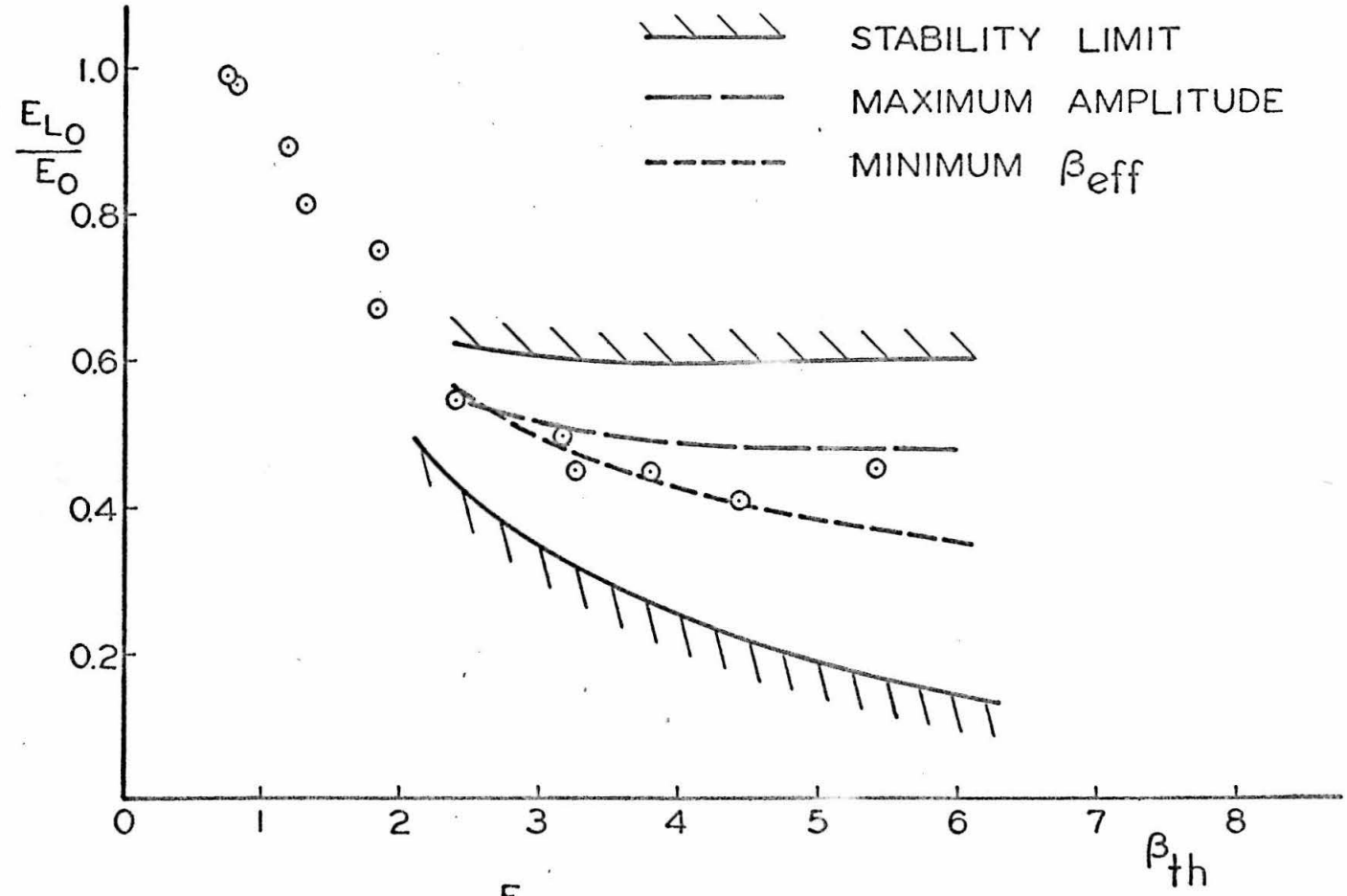

FIG. 18 $\frac{E_{L_0}}{E_0}$ OF STEADY STREAMERS

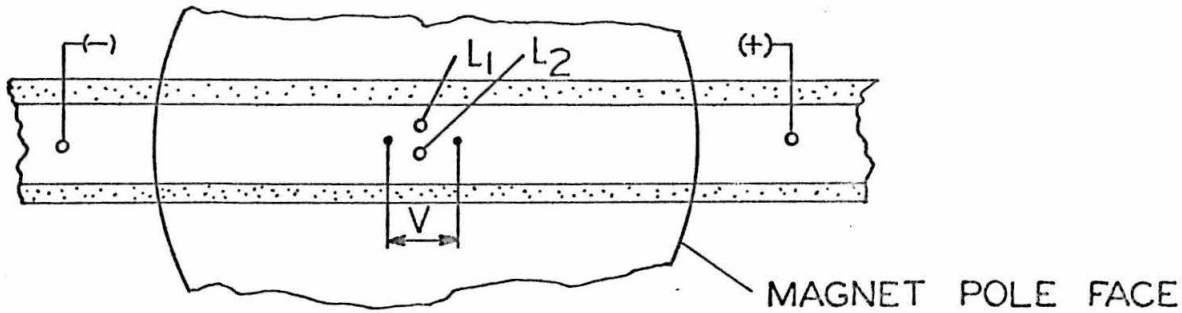

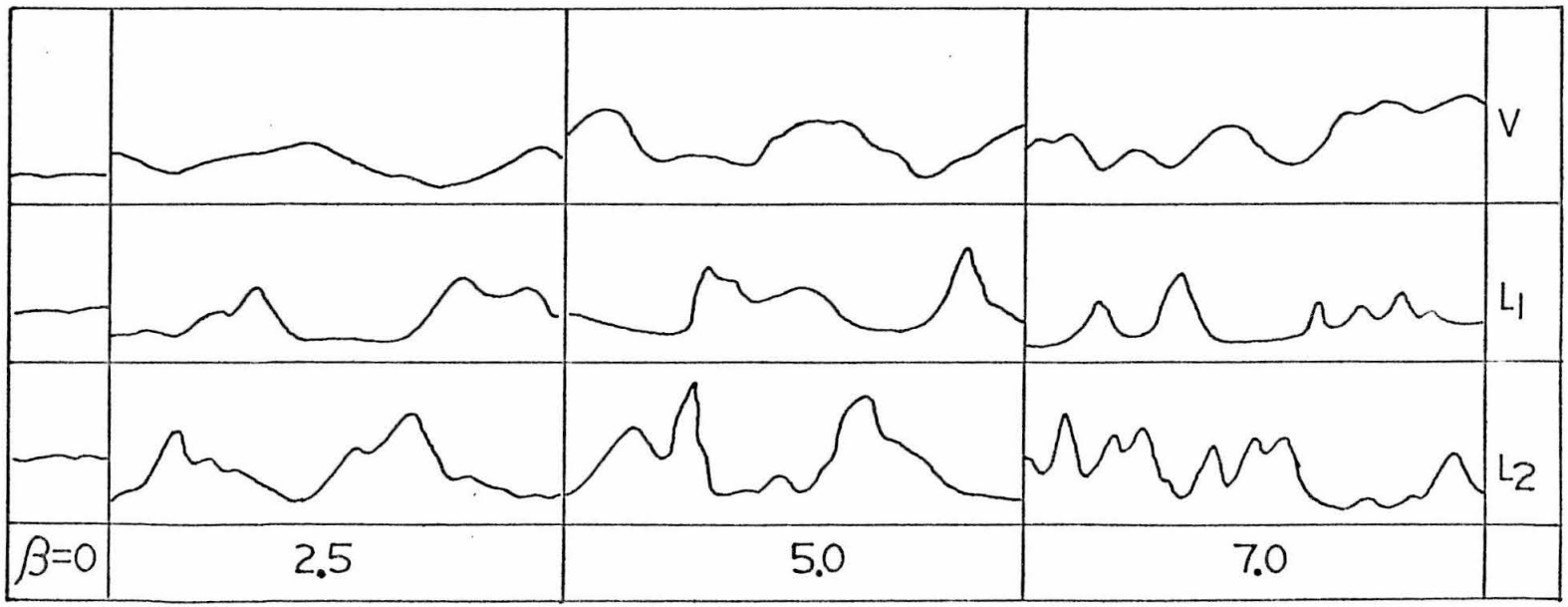

FIG. 19 STREAMERS IN A LONG TEST SECTION

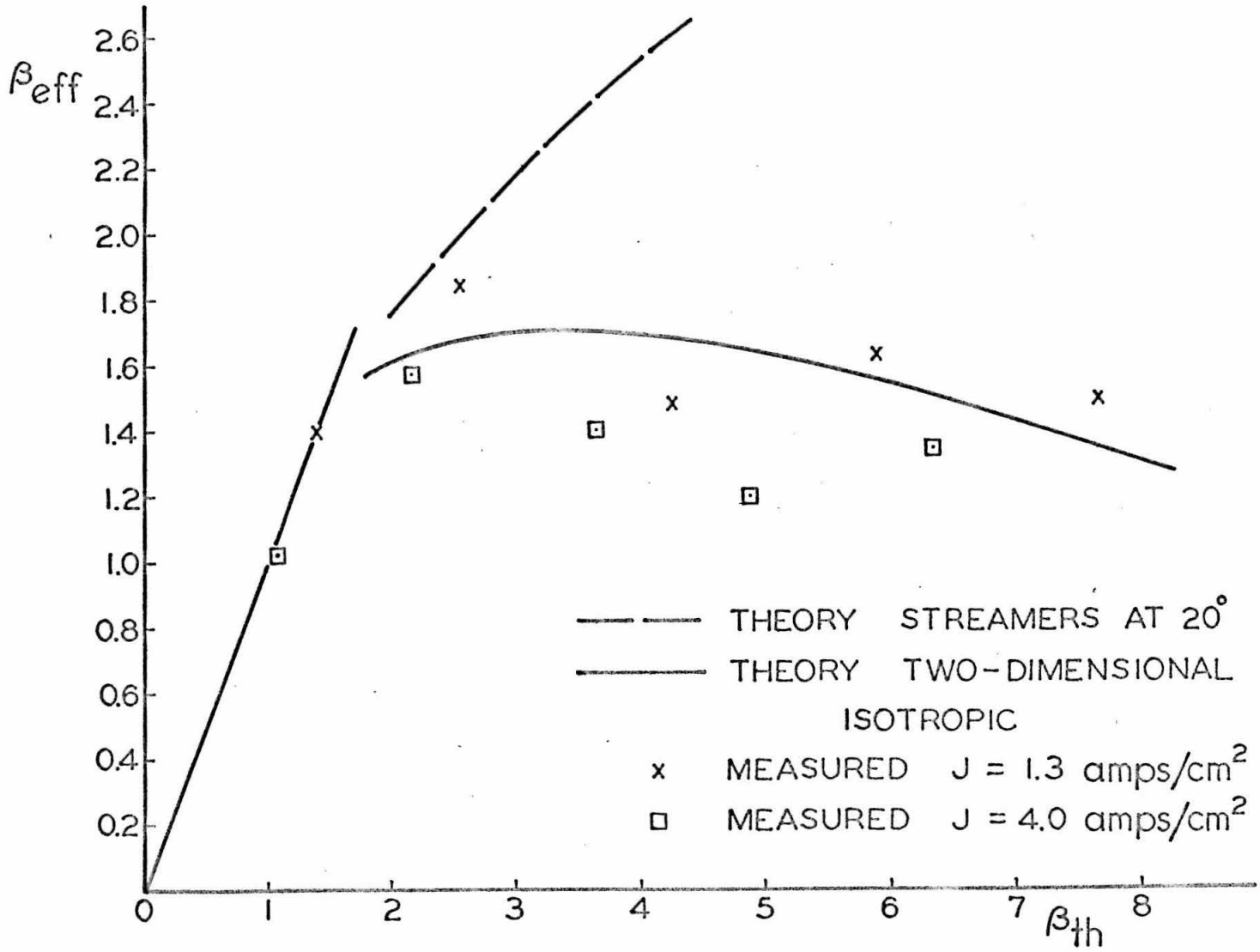

FIG. 20 EFFECTIVE HALL PARAMETER IN LONG TEST SECTION

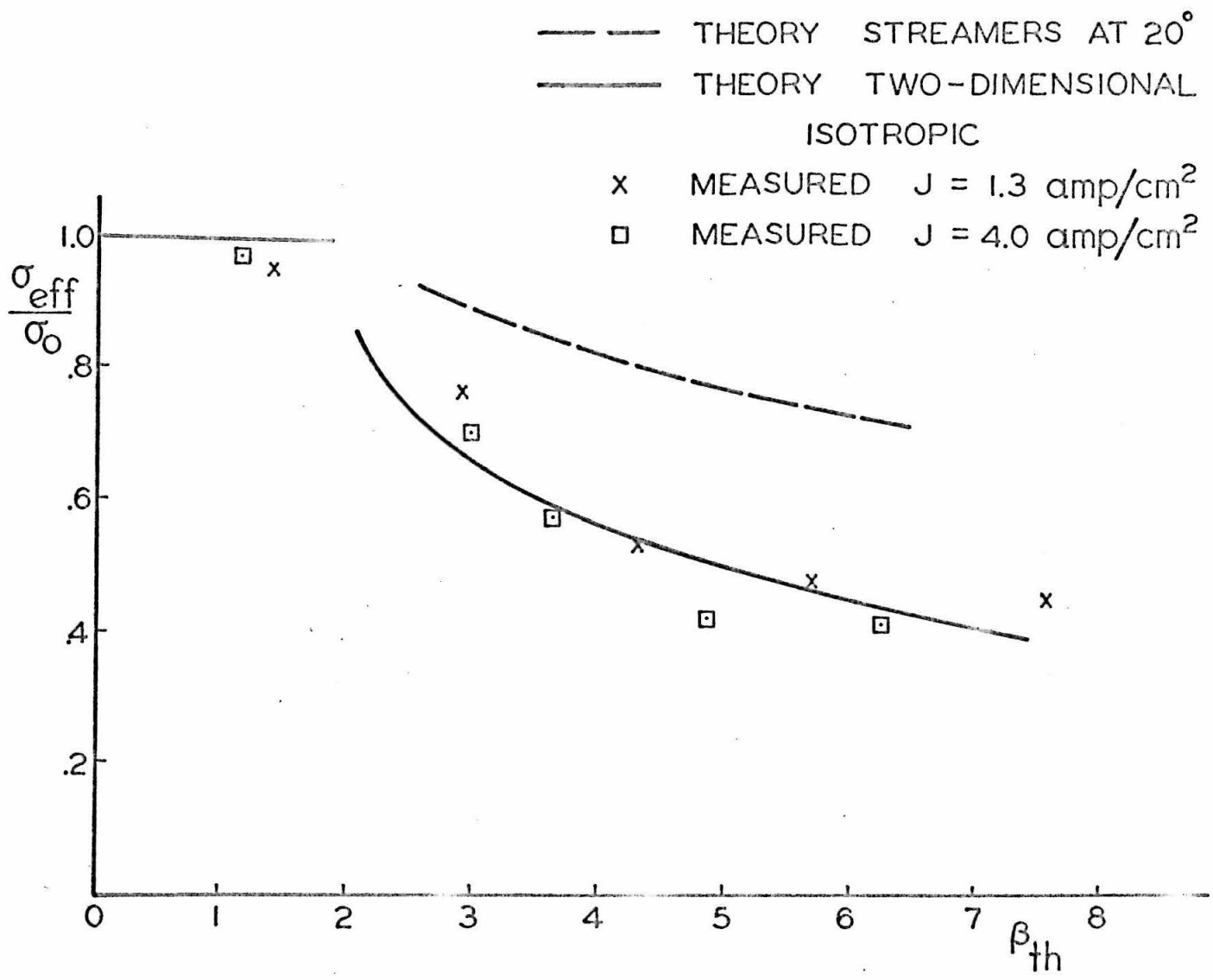

FIG. 21 EFFECTIVE CONDUCTIVITY IN THE LONG TEST SECTION

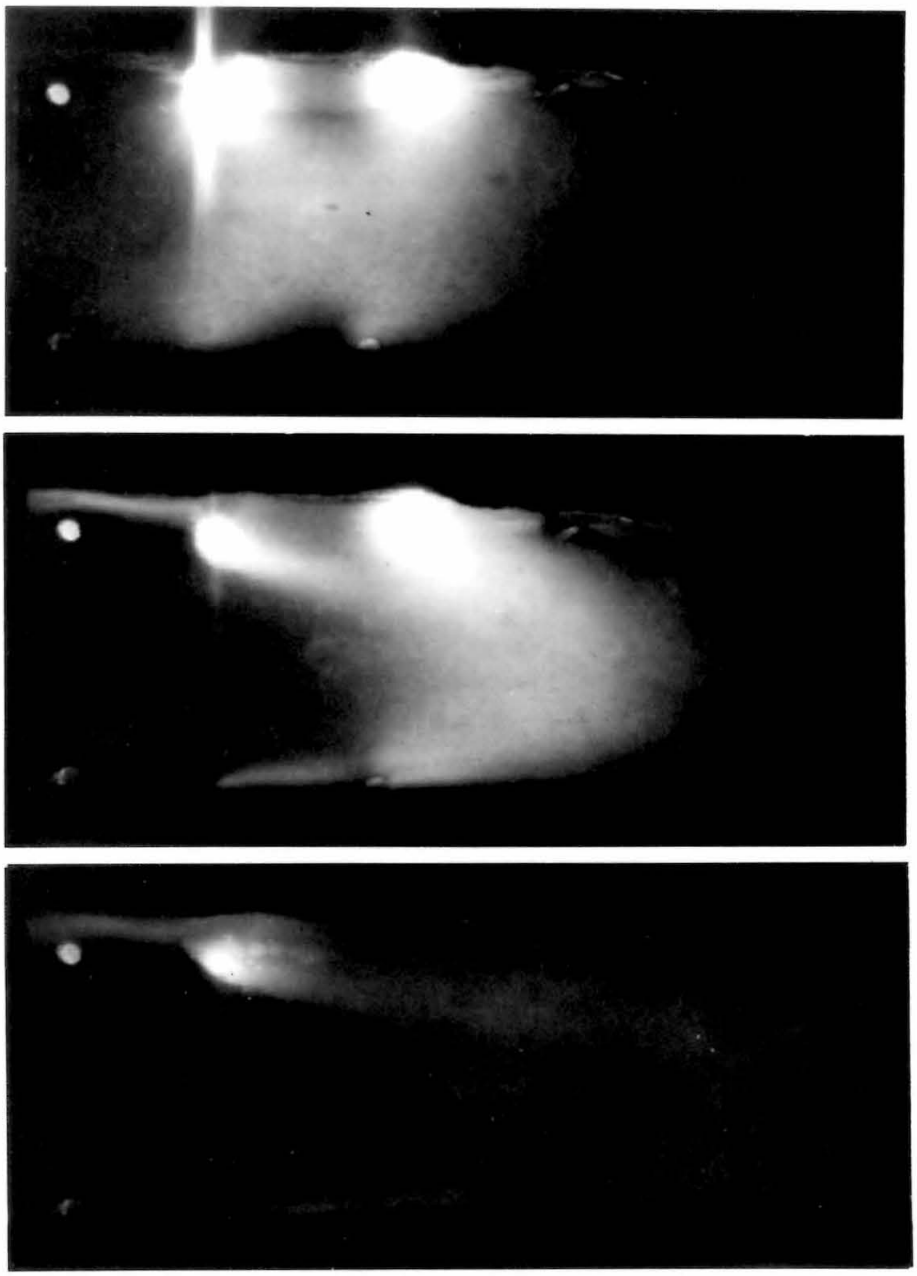

(a)

(b)

(c)

Fig. 22 Effect of magnetic field on the inlet to a discharge region
(a) B=0, I=1.5 amps per electrode pair.
(b) B=3Kg, I=1.0 amps per electrode pair.
(c) B=6Kg, I=0.8 amps per electrode pair.

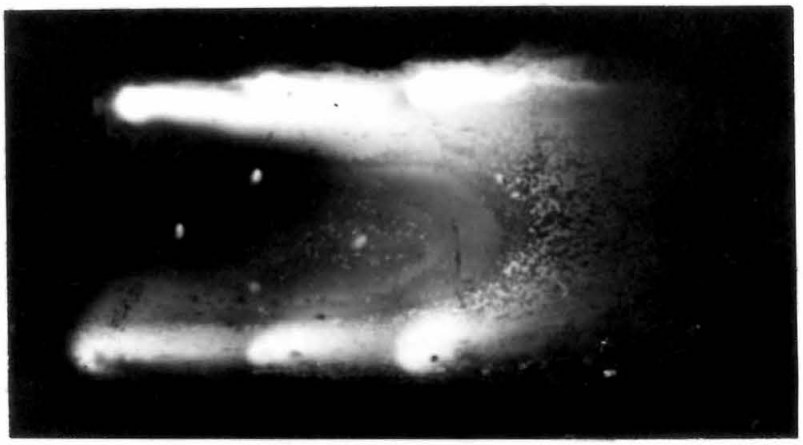

(a)

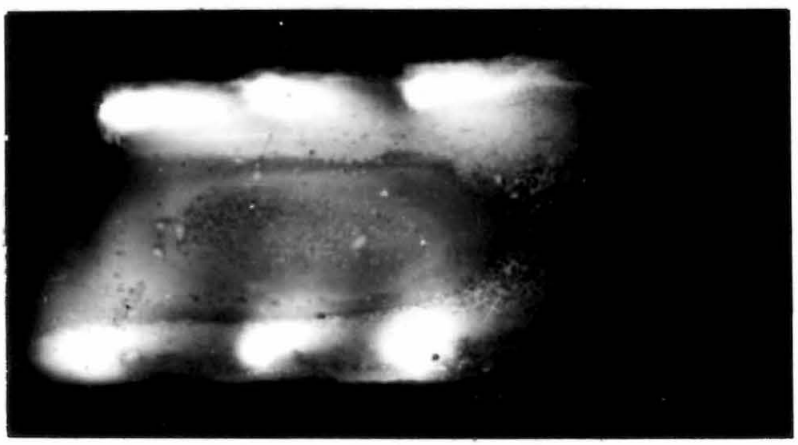

(b)

Fig. 23 Effect of electric field strength on the inlet to a discharge region. (a) I=1.5 amps per electrode pair, B=6Kg.
(b) I=3.0 amps per electrode pair, B=6Kg.

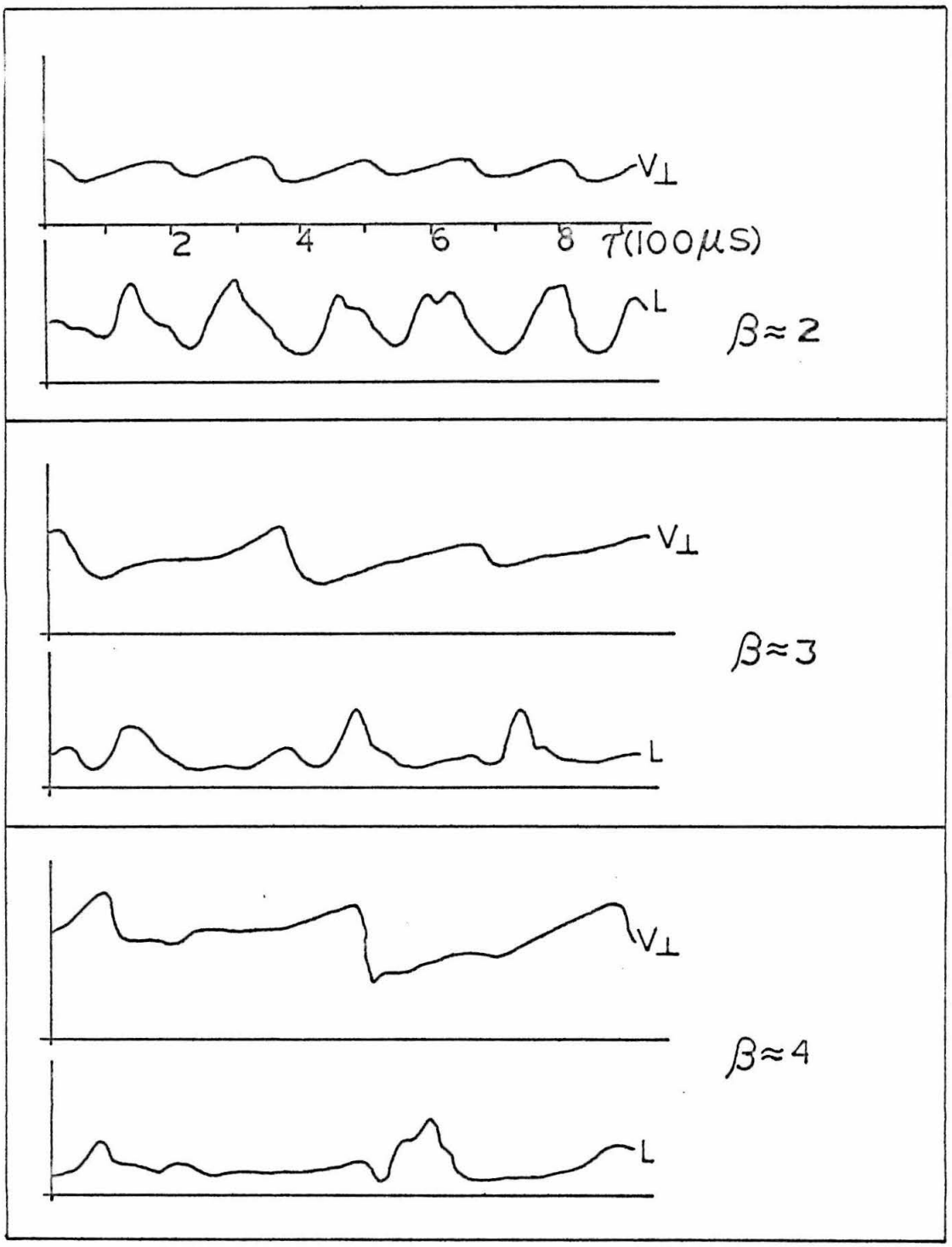

FIG.24 SINGLE DISCHARGE IN CROSS FLOW

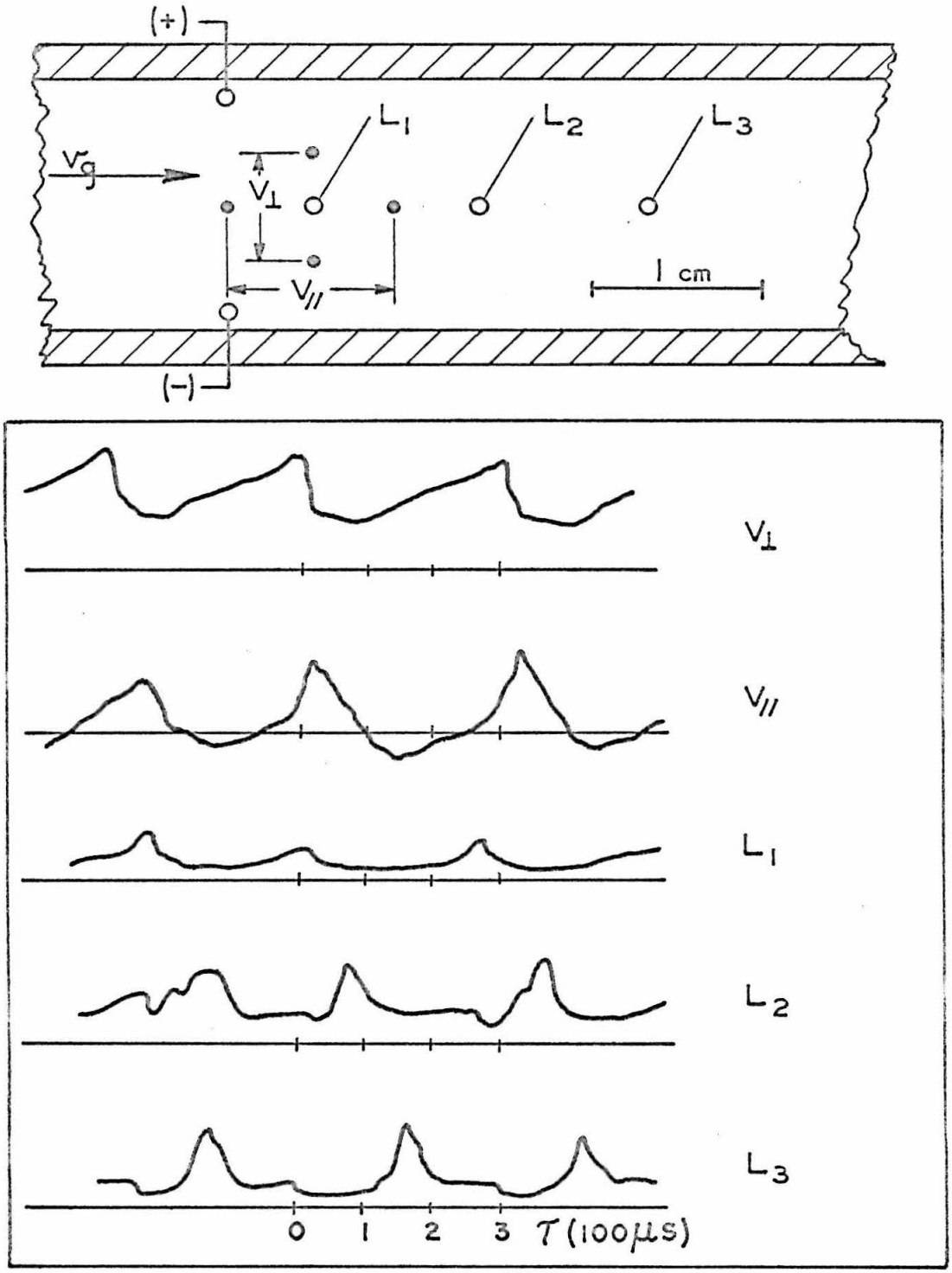

FIG. 25 LIGHT AND VOLTAGE MEASUREMENTS IN INLET TEST SECTION

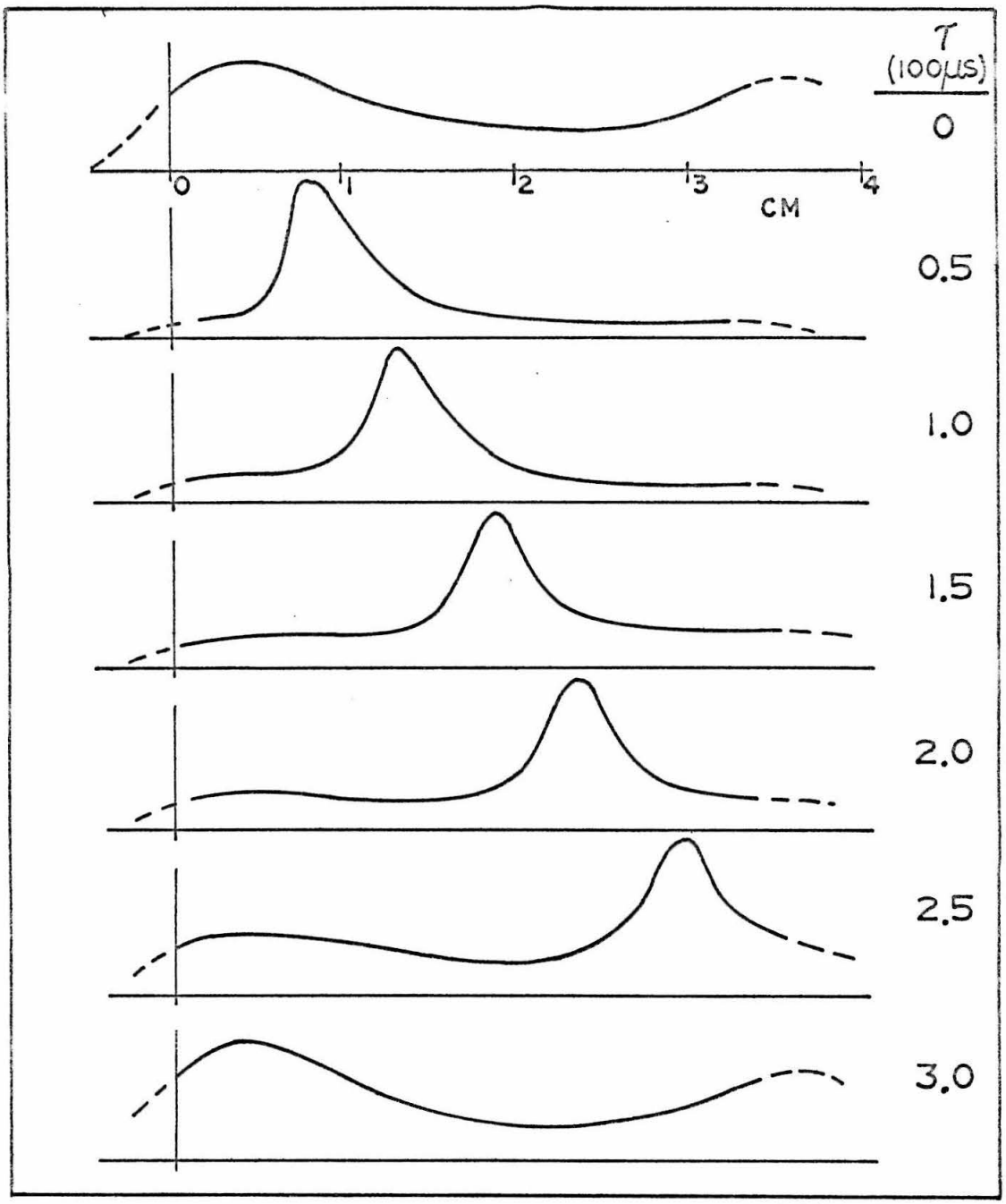

FIG. 26 CENTER LINE LIGHT INTENSITY PROFILES

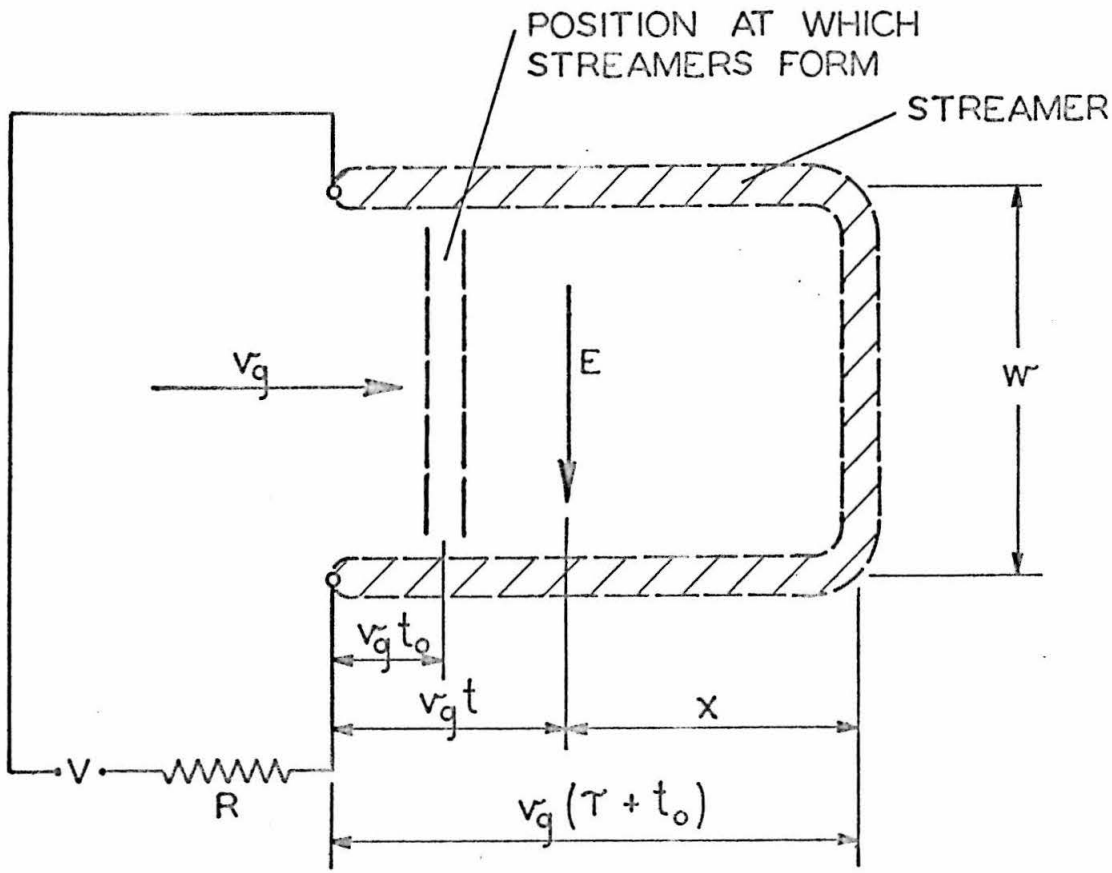

FIG. 27 IDEALIZED INLET CIRCUIT

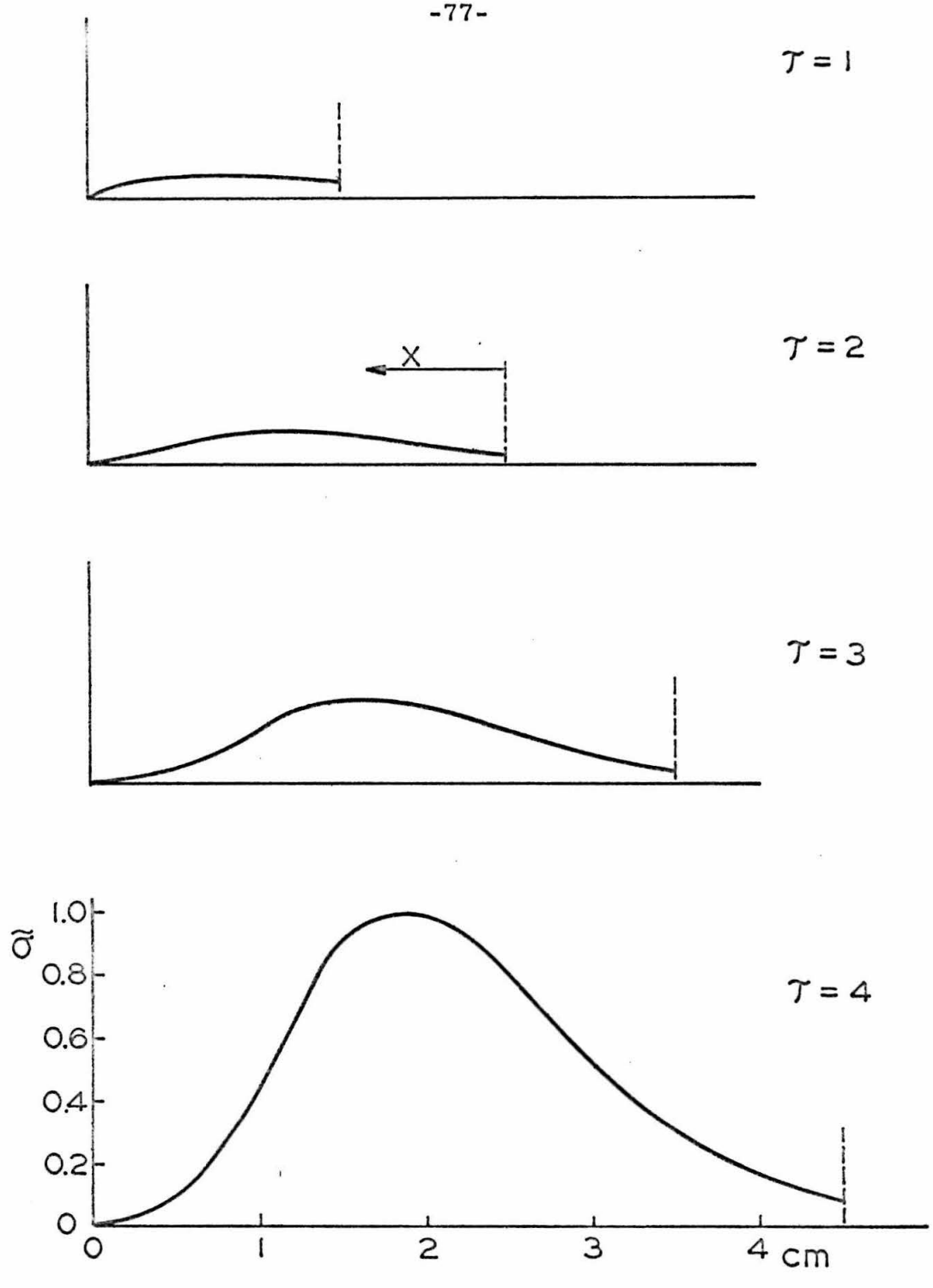

FIG. 28 CALCULATED INLET CONDUCTIVITY PROFILES

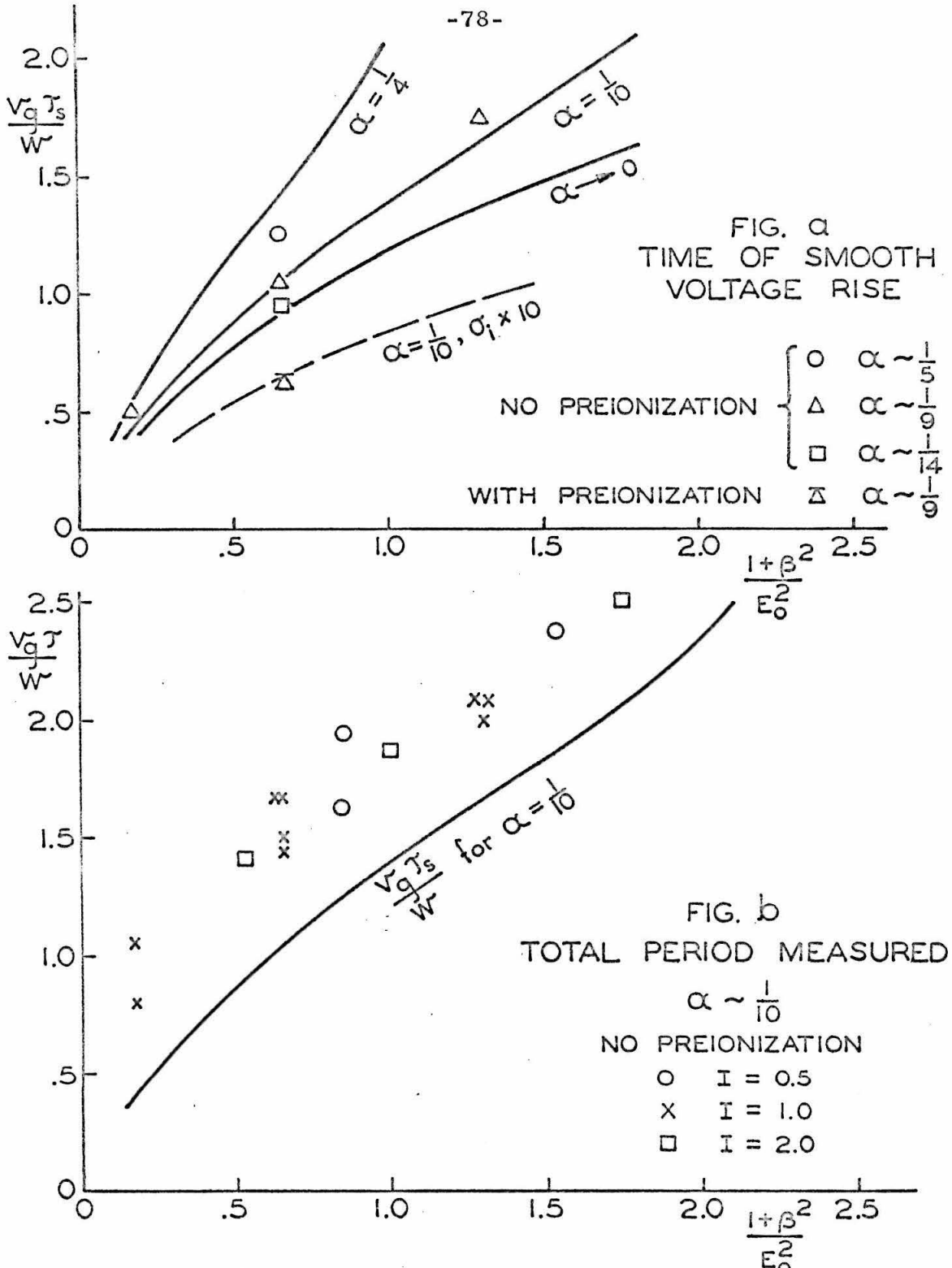

FIG. a
TIME OF SMOOTH VOLTAGE RISE

FIG. b
TOTAL PERIOD MEASURED
$\alpha \sim \frac{1}{10}$

FIG.29 a & b PERIOD OF STREAMER FORMATION IN INLET REGION

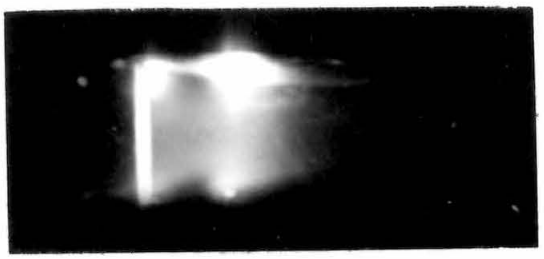

(a)

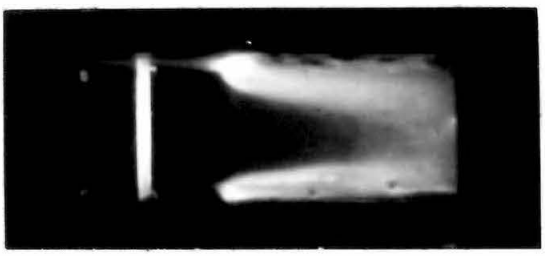

(b)

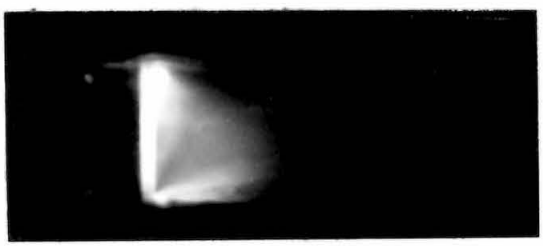

(c)

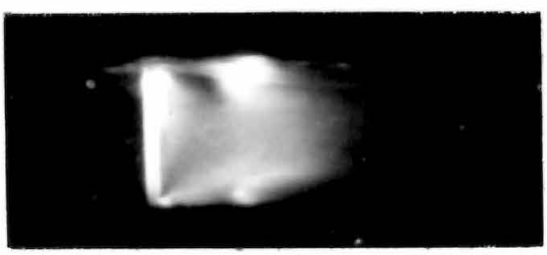

(d)

Fig. 30 Effect of preionization on a transverse discharge.
(a) Preionizor on, test discharge on, B=0.
(b) Preionizor off, test discharge on, B=8Kg.
(c) Preionizor on, test discharge off, B=8Kg.
(d) Preionizor on, test discharge on, B=8Kg.

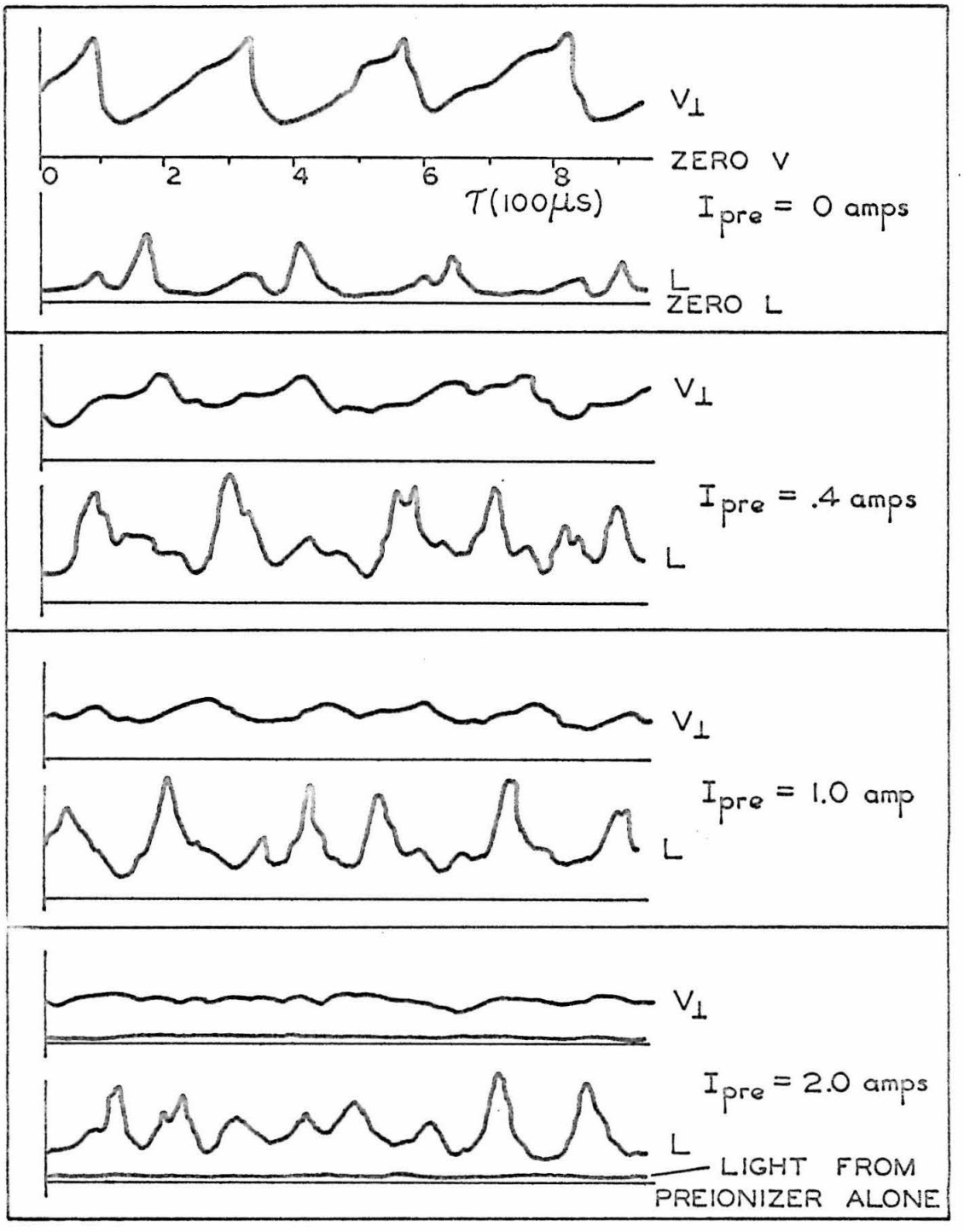

FIG. 31 EFFECT OF PREIONIZATION ON A SINGLE DISCHARGE

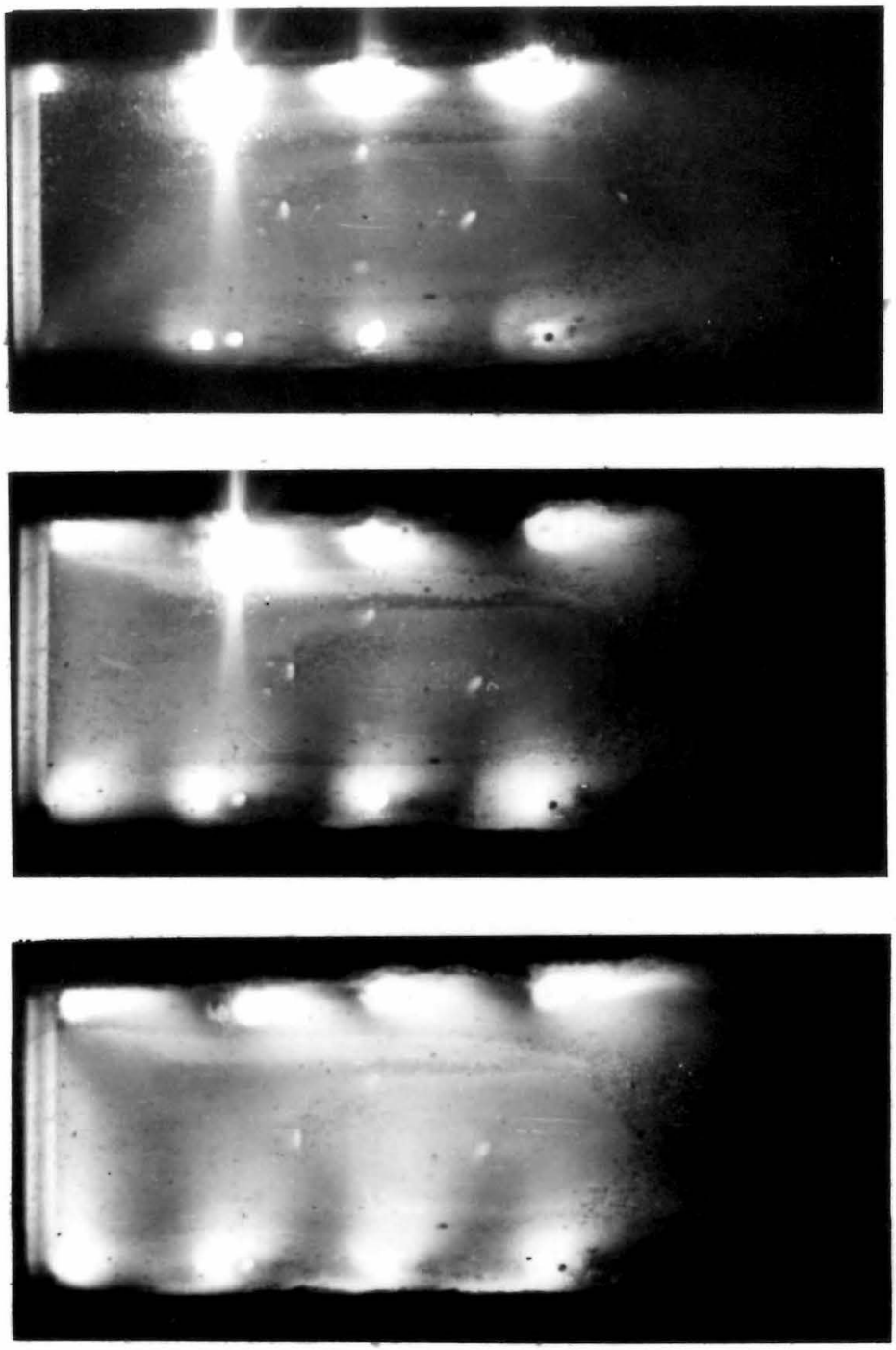

(a)

(b)

(c)

Fig. 32 Test section with multiple transverse discharges.
(a) B=0, (b) B=3Kg, (c) B=8Kg.

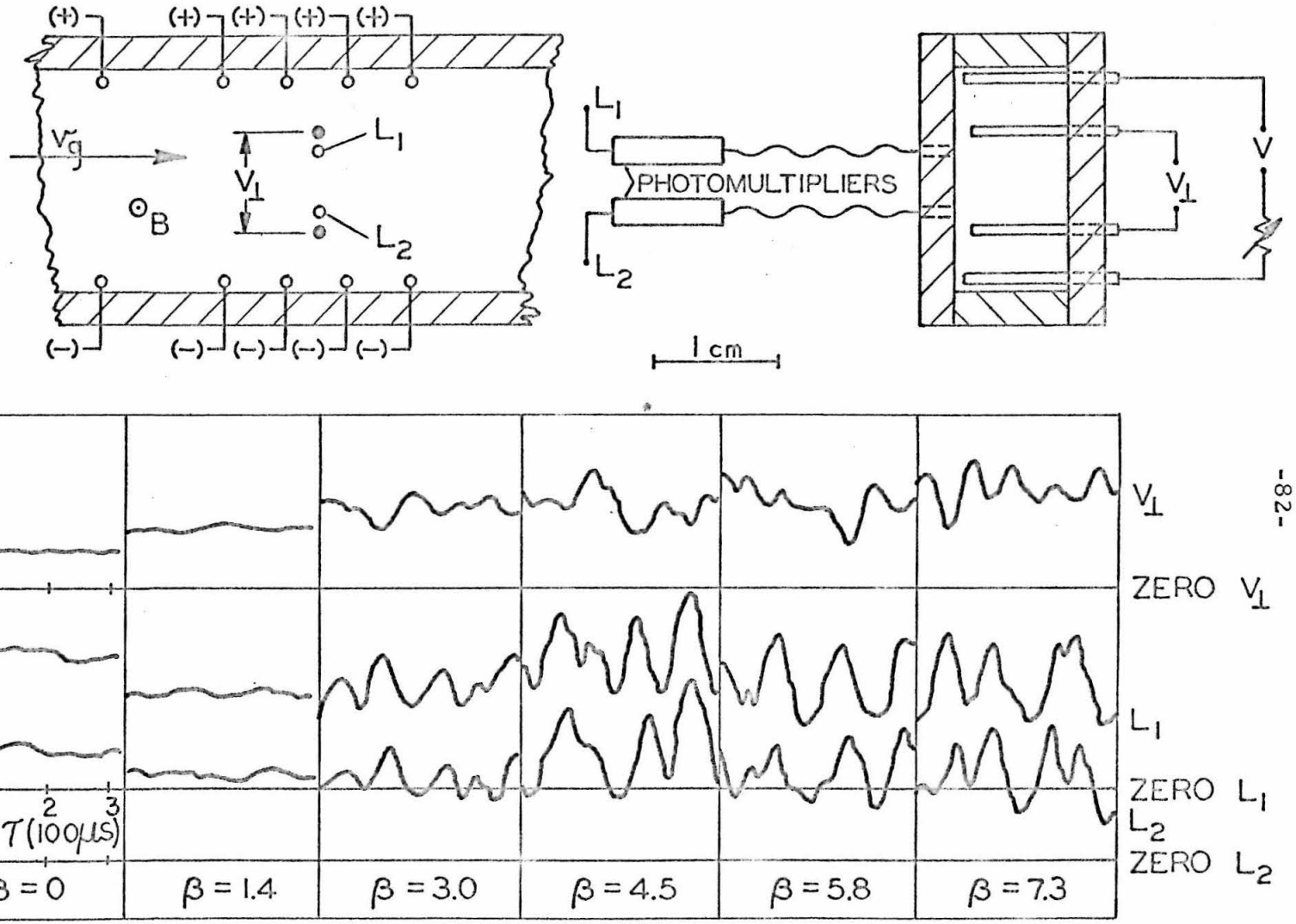

FIG. 33 MULTIPLE TRANSVERSE DISCHARGES

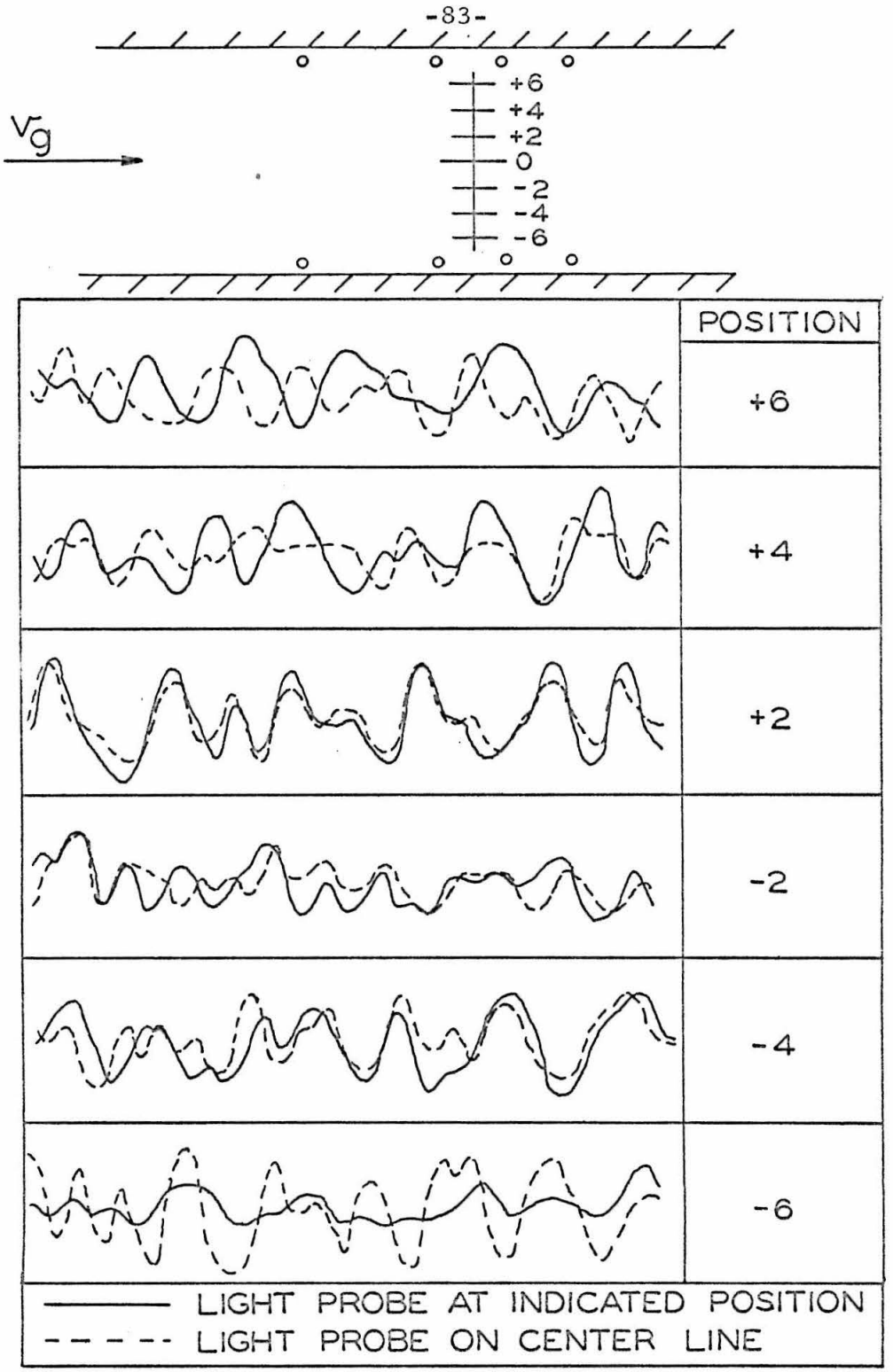

FIG. 34 LIGHT PROBES PERPENDICULAR TO FLOW

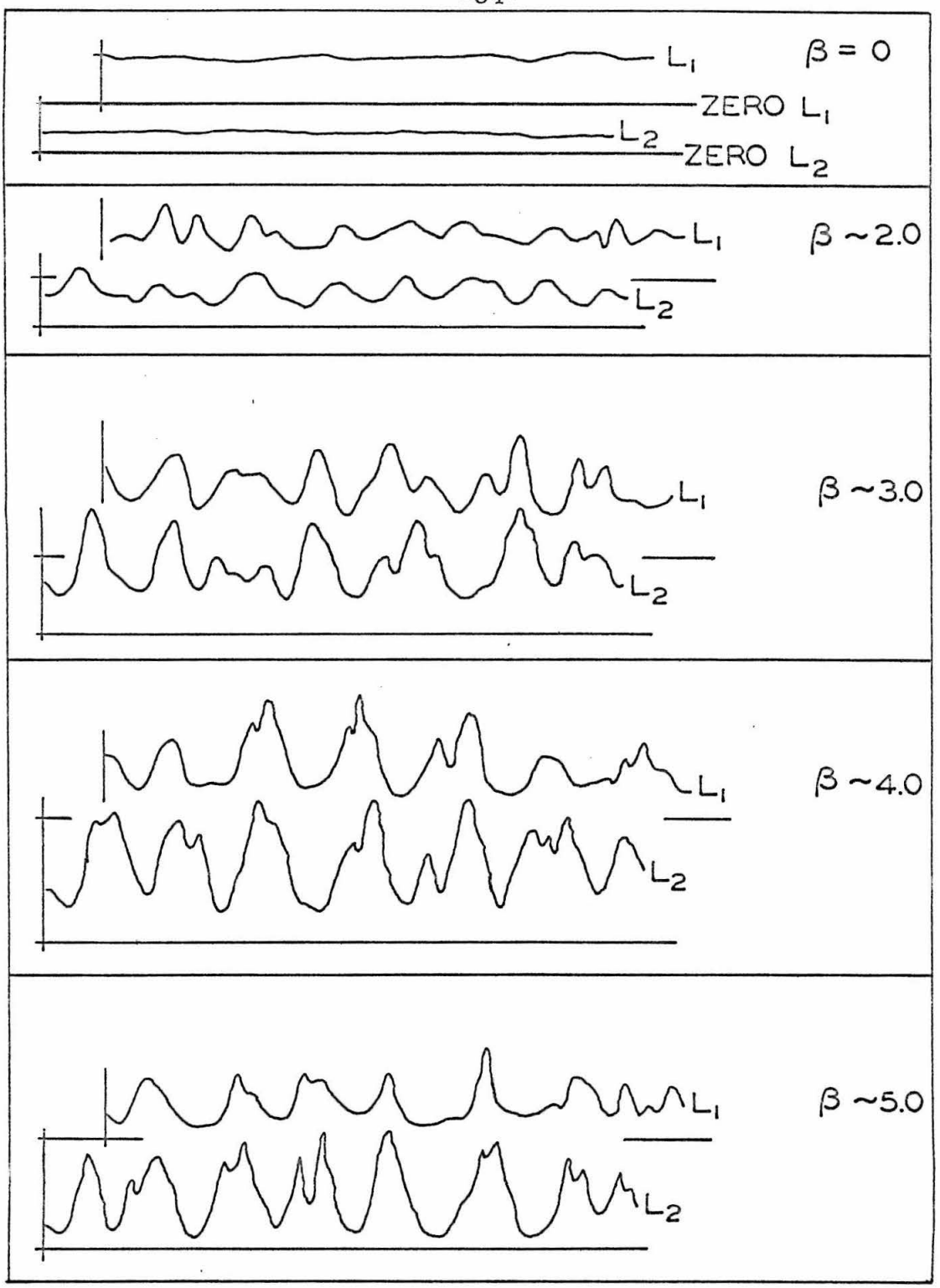

FIG. 35 LIGHT PROBES PARALLEL TO FLOW

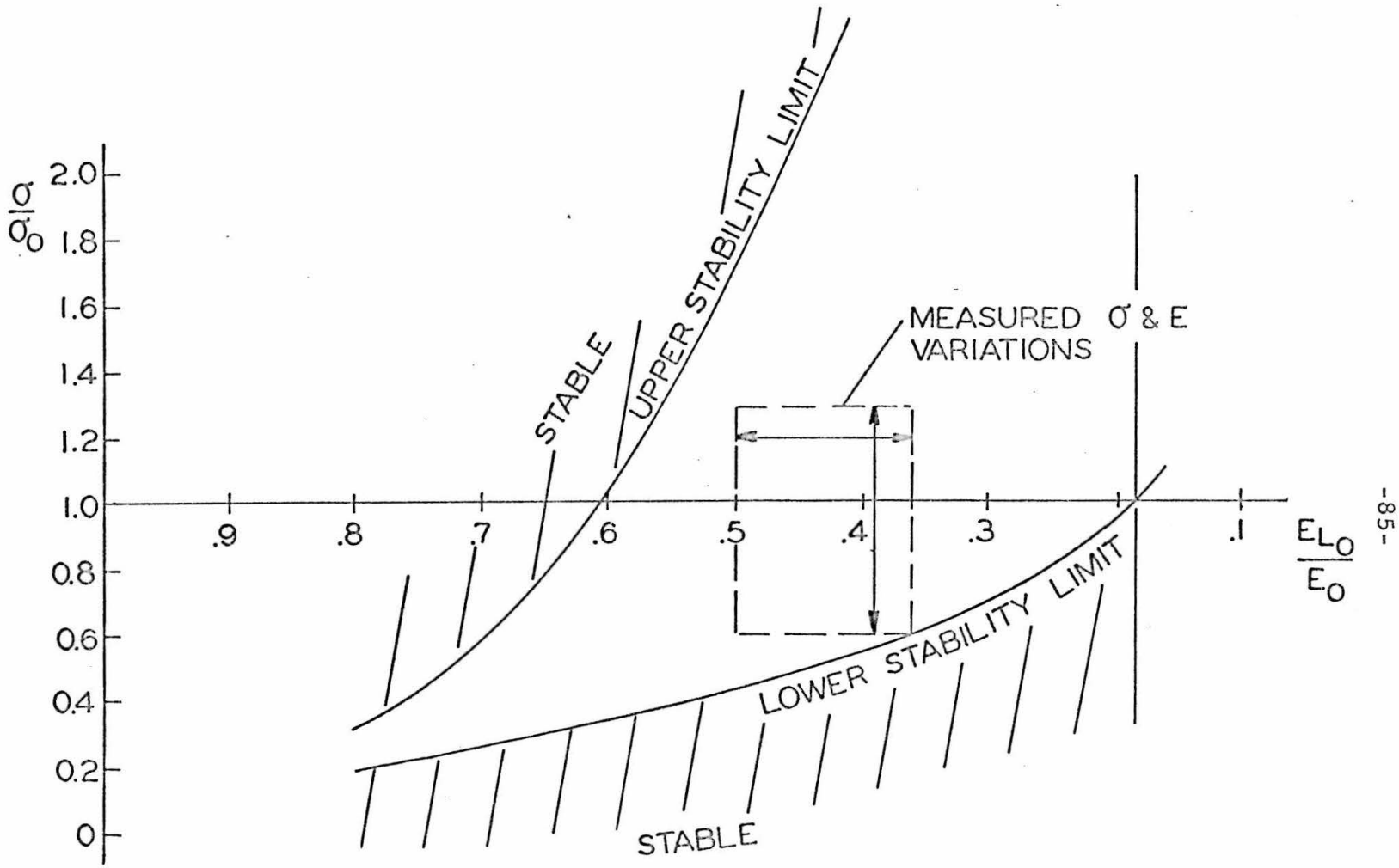

FIG. 36 σ & E VARIATIONS MEASURED IN STREAMERS

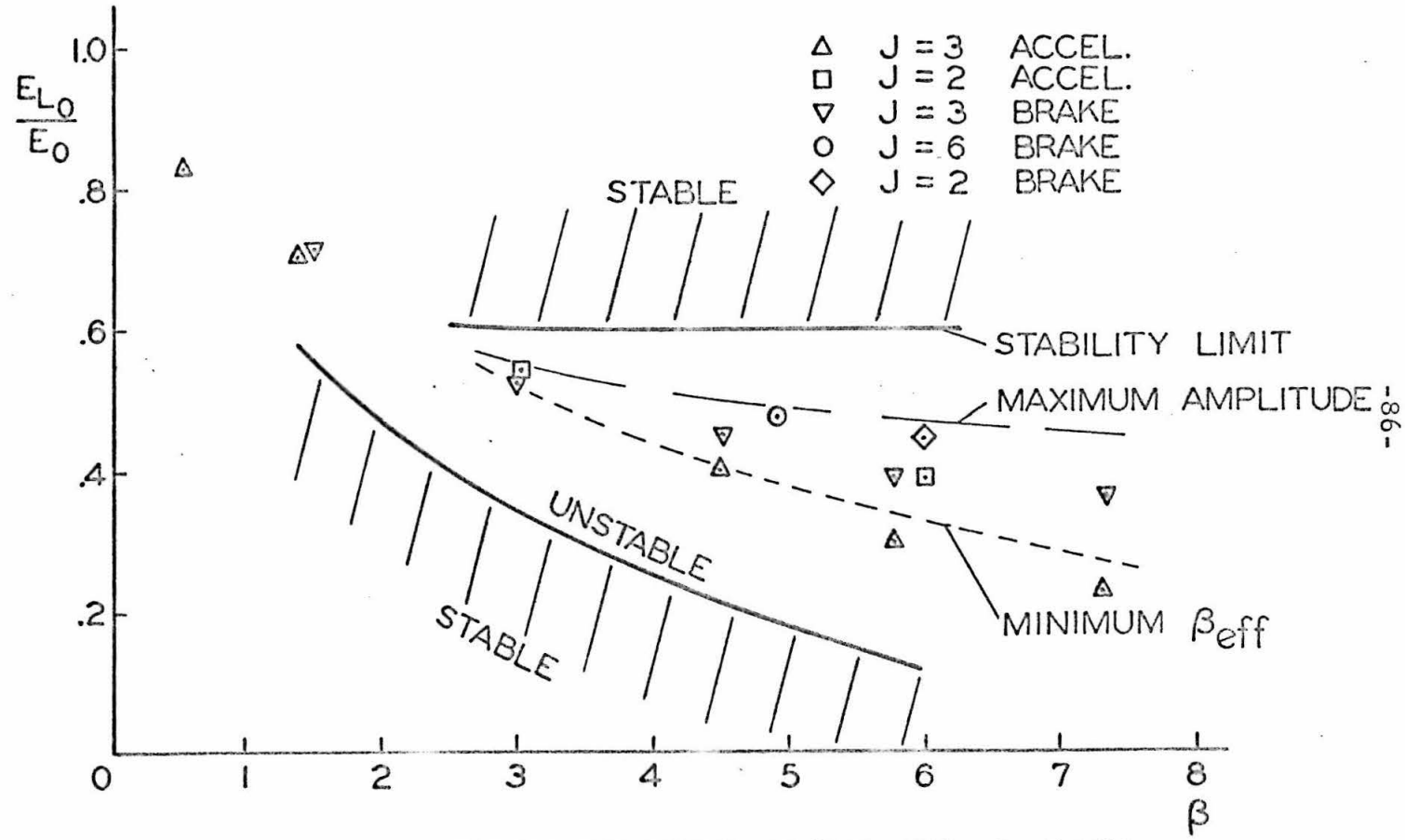

FIG. 37 COMPARISON OF FIELD ALONG WAVES WITH FIELDS FOR UNSTABLE REGIME

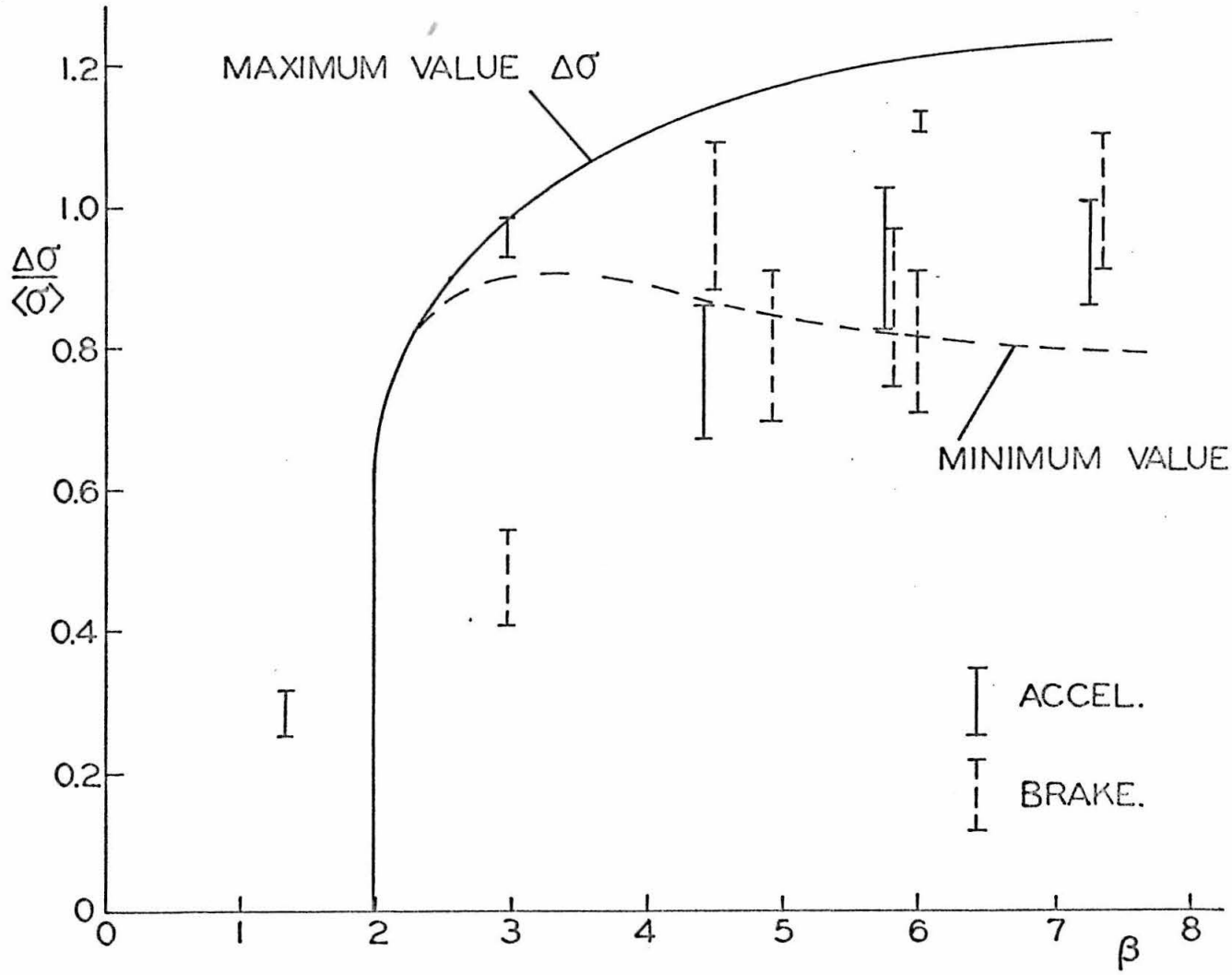

FIG. 38 COMPARISON OF $\frac{\Delta\sigma}{\langle\sigma\rangle}$ WITH THEORY

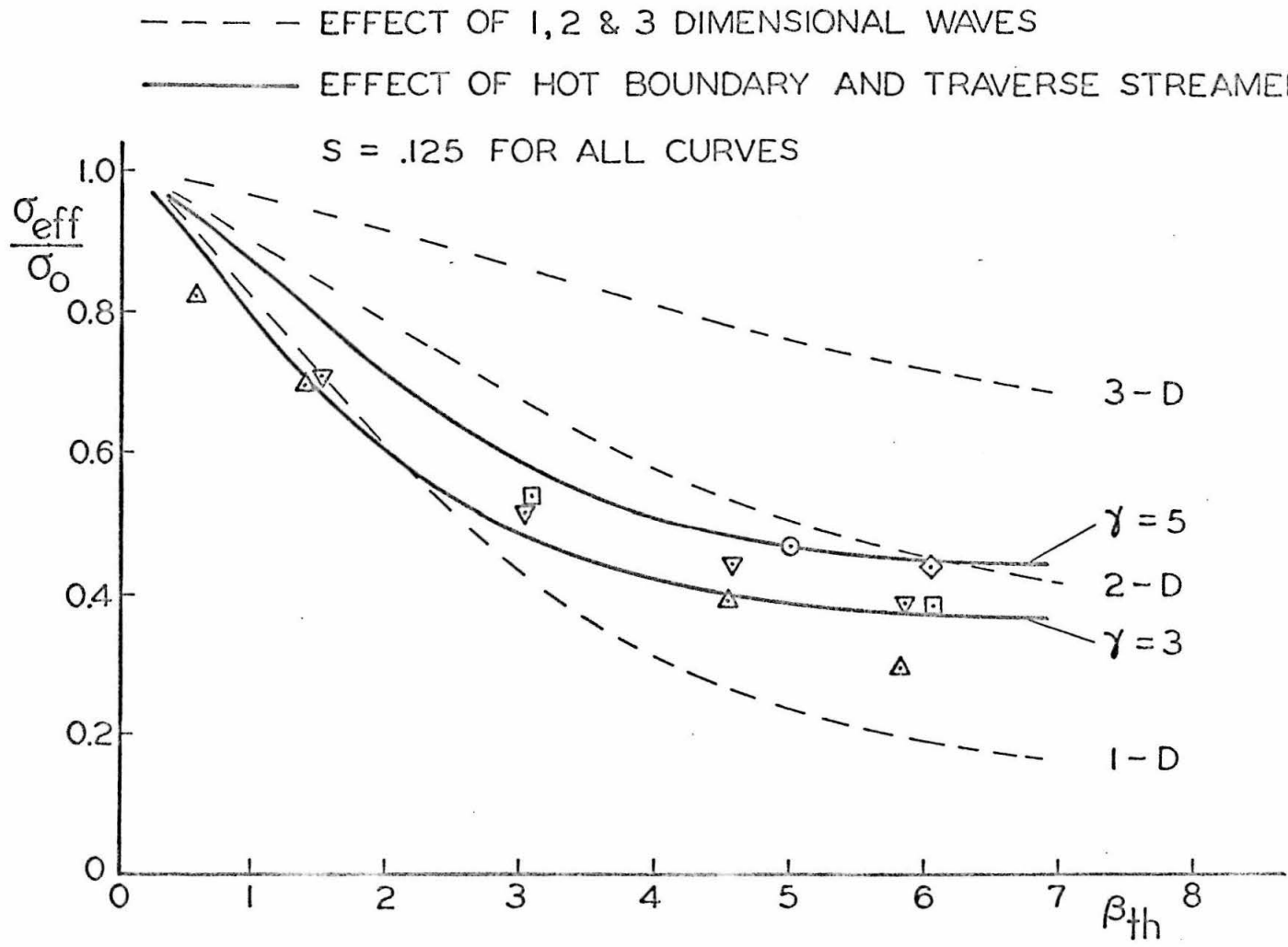

FIG. 39 COMPARISON OF DATA WITH VARIOUS PATTERNS OF NON-UNIFORMITIES

NOMENCLATURE

α	load factor of inlet circuit
β	Hall parameter
β_{crit}	minimum Hall parameter at which instability occurs
β_{eff}	effective Hall parameter
γ	hot boundary region parameter
δ	thickness of hot boundary region
ε_e	electron energy
$\varkappa_e$	electronic diffusion coefficient
$\varkappa_R$	radiative diffusion coefficient
λ	wavelength of steady disturbances
λ_o	wavelength of light at resonant lines of seed
$\underline{\underline{\mu}}$	conductivity tensor
ν_{ee}	electron-electron collision frequency
$\Delta\nu$	width of resonant line
σ	electrical conductivity
σ_s	Spitzer conductivity
σ_c	close encounter conductivity
σ_u	upper zero of heating term
σ_L	lower zero of heating term
$\Delta\sigma$	peak-to-peak conductivity variation
$\langle\sigma\rangle$	average conductivity
σ_o	conductivity of undisturbed state
σ_i	initial conductivity
$\tilde{\sigma}$	normalized conductivity , σ/σ_o

σ_{BL}	boundary region conductivity
σ_{eff}	effective conductivity
τ	time since formation of last streamer
τ_s	time of smooth rise in voltage
ϕ	angle between current streamers and average current
ω_e	damping due to electronic heat diffusion
ω_R	damping due to radiative diffusion
$\dot{\Omega}$	elastic collision loss
c	electron thermal speed
k	Boltzmann constant
m_a	mass of argon atom
m_e	mass of an electron
m_o	reciprocal photon mean free path at line center
n	exponent of J in $\sigma(J)$ formula
n_e	electron density
n_{e_o}	undisturbed electron density
p	exponent of n_e in $\sigma(n_e)$ formula
r	resistance per unit length of a streamer
t_o	distance streamers form behind electrodes divided by v_g
v_g	gas velocity
w	duct width
B_o	blackbody radiation intensity
E_o	electric field along a streamer
E_L	total electric field in undisturbed plasma
E_{L_o}	electric field along J in undisturbed plasma

H	radiative heat transfer term
I	effective conductivity parameter (Appendix B)
I_i	ionization potential of seed
I_{pre}	pre-ionizing current
J_o	current density normal to streamer
J_L	current density in undisturbed plasma
Q	electronic heating term
Q_n	collision cross section of n^{th} species
R	resistance of external circuit
$\dot{R}$	radiation term
R_{ex}	escaping radiation
S	mean square conductivity variation
T_e	electron temperature
$V_\perp$	voltage perpendicular to gas flow
$V_{//}$	voltage parallel to gas flow

REFERENCES

1. Cool, T. A. and Zukoski, E. E., "Recombination, Ionization, and Nonequilibrium Electrical Conductivity in Seeded Plasmas," Phys. of Fluids, Vol. 9 (1966), pp. 780-796.

2. Kerrebrock, J. L., "Nonequilibrium Ionization Due to Electron Heating: Part I. Theory," AIAA Journal, Vol. 2 (1964), pp. 1072-1080.

3. Velikhov, E. P., Dykhne, A. M., and Shipuk, I. Y., "Ionization Instability of a Plasma with Hot Electrons," Proceedings of the VII International Conference on Phenomena in Ionized Gases, Belgrade (1965).

4. Brederlow, G., Feneberg, W., and Hodgson, R., "The Nonequilibrium Conductivity in an Argon-Potassium Plasma in Crossed Electric and Magnetic Fields," Proceedings of the International Symposium on MHD Electrical Power Generation, Paper SM-74/88, Salzburg (1966).

5. Nedospasov, A. V., "Speed of Ionization Waves in Low Temperature Plasmas," Proceedings of the International Symposium on MHD Electrical Power Generation, Paper SN-74/97, Salzburg (1966).

6. Solbes, A., "Nonlinear Plane Wave Study of Electrothermal Instabilities in Nonequilibrium Plasmas," Proceedings of the 8th Symposium on Engineering Aspects of MHD, Stanford (1967).

7. Feneberg, W., "The Electrical Conductivity of a Partially Ionized Argon-Potassium Plasma in a Magnetic Field," Z. f. Naturf., Vol. 21a (1966), p. 1468.

8. Lutz, M. A., "Radiation and Its Effect on the Nonequilibrium Properties of a Seeded Plasma," AIAA Journal, Vol. 5 (1967), pp. 1416-1423.

9. Dethlefson, R. and Kerrebrock, J. L., "Experimental Investigation of Fluctuations in Nonequilibrium MHD Plasmas," Proceedings of the 7th Symposium on Engineering Aspects of Magnetihydrodynamics, Princeton (1966).

10. Klepeis, J. and Rosa, R. J., "Experimental Studies of Strong Hall Effects and U×B Induced Ionization," AIAA Journal, Vol. 3 (1965), pp. 1659-1666.

11. Zauderer, B., "Discharge Structure and Stability of a Linear, Nonequilibrium Magnetohydrodynamic Channel," Proceedings of the AIAA Electric Propulsion and Plasmadynamics Conference, Colorado Springs (1967).

12. Cool, T. A., "Recombination, Ionization, and Nonequilibrium Electrical Conductivity in Seeded Plasmas," Ph. D. Thesis, California Institute of Technology (1965).

13. Kerrebrock, J. L., "Segmented Losses in MHD Generators with Nonequilibrium Electrical Conductivity in Seeded Plasmas," AIAA Journal, Vol. 4 (1966), pp. 1938-1947.

14. Evans, N. A., "Effect of Flow Velocity on a Single, Controlled Glow Discharge in Cesium-Seeded Argon," AIAA Journal, Vol. 5 (1967), pp. 1908-1913.

15. Rosa, R. J., "The Hall and Ion Slip Effects in a Nonuniform Gas," Avco Research Report No. 121 (1961).

16. Louis, J. F., "Effective Ohm's Law in a Partially Ionized Plasma with Electron Density Fluctuations," Phys. of Fluids, Vol. 10 (1967), pp. 2062 - 2065.

17. Yoshikawa, S. and Rose, D. J., "Anomalous Diffusion of a Plasma Across a Magnetic Field," Phys. of Fluids, Vol. 5 (1962), pp. 334-340.

APPENDIX A

Quantitative Interpretation of Photographs and Photomultiplier Output

A. Photographs

In some experiments, variations in electron temperature and thus electron density and conductivity, occurring when a magnetic field was applied to the plasma, were inferred from photographs of the discharge. Since the plasma was uniform and the conductivity was known when the magnetic field was zero, the film could be calibrated by photographing the discharge at various current levels with no magnetic field applied. From these photographs, the film density could be calibrated as a function of conductivity. Figure A-1 gives a typical calibration curve. Using curves such as this, the film density variations in photographs of the discharge with magnetic field could then be converted into conductivity variations.

One problem with using photographs was that the light intensity variations emitted from the discharge ranged over several orders of magnitude, and since photographic film generally has a linear response over only two or two and one-half orders of magnitude, photographs were often exposed in the nonlinear response regions of the film.

This problem was partially overcome by making calibration curves over a large range of intensities for each film and for each setting of shutter speed and f-number. However, the exposure was still quite often in the dark or light wings of the response curve where

the film is not very sensitive to intensity variations.

B. Photomultiplier Output

Photomultiplier data were much easier to interpret than the photographs because the source voltage to the photomultiplier could be varied so as to keep the tube operating in its linear range. Several calibration curves are shown in Figure A-2 and indicate that to the limit of accuracy of the measurement the response is linear. Also, the response curve passes through the origin in Figure A-2, which means the dark current was essentially zero. This condition was obtained by packing the photomultipliers in dry ice. Since the response curve was linear and passed through the origin, the parameter $\Delta\sigma/\langle\sigma\rangle$ was identical to $\Delta L/\langle L\rangle$ where L is the output signal of the photomultiplier.

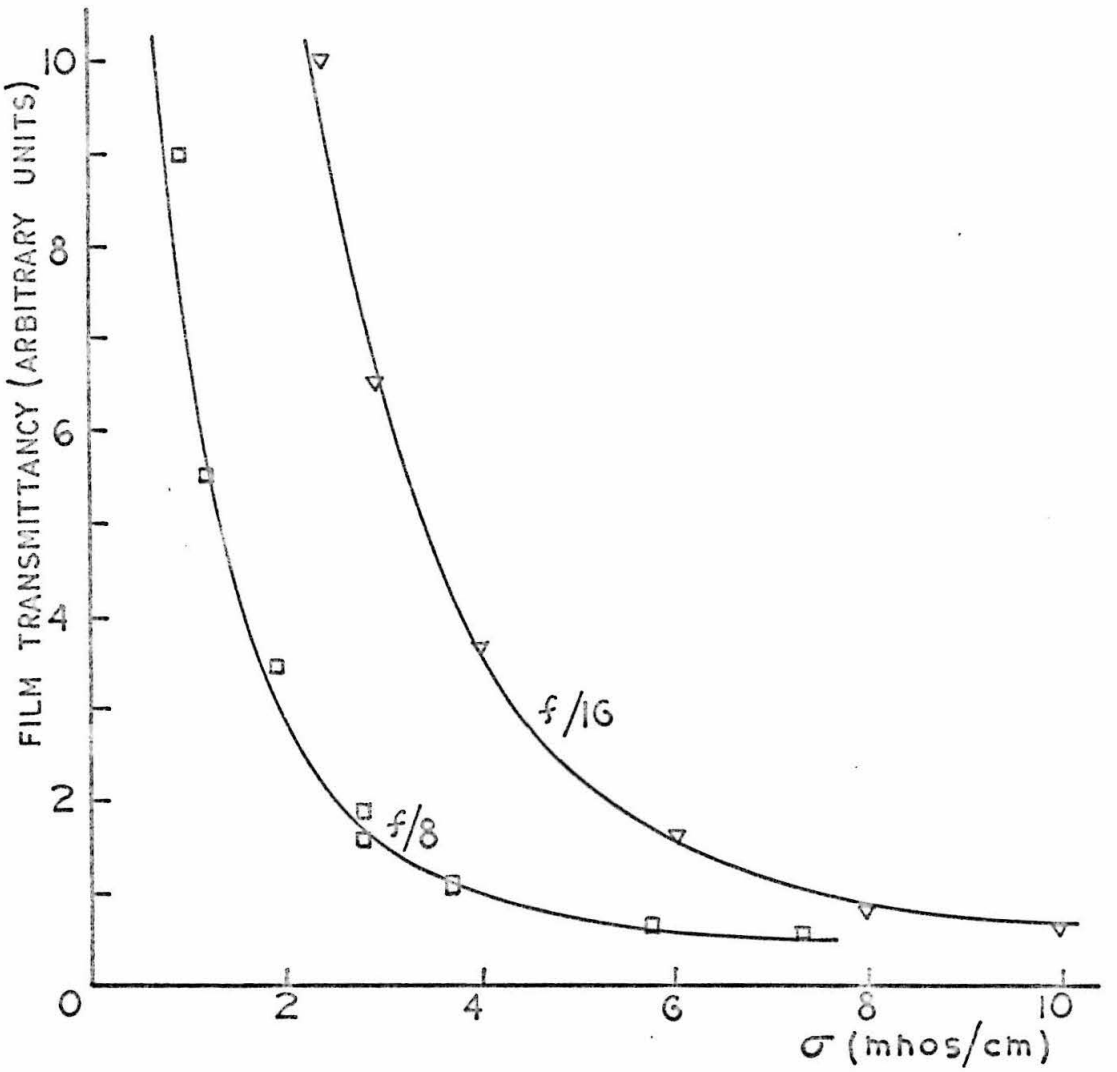

FIG. A.1 TYPICAL FILM CALIBRATION CURVES

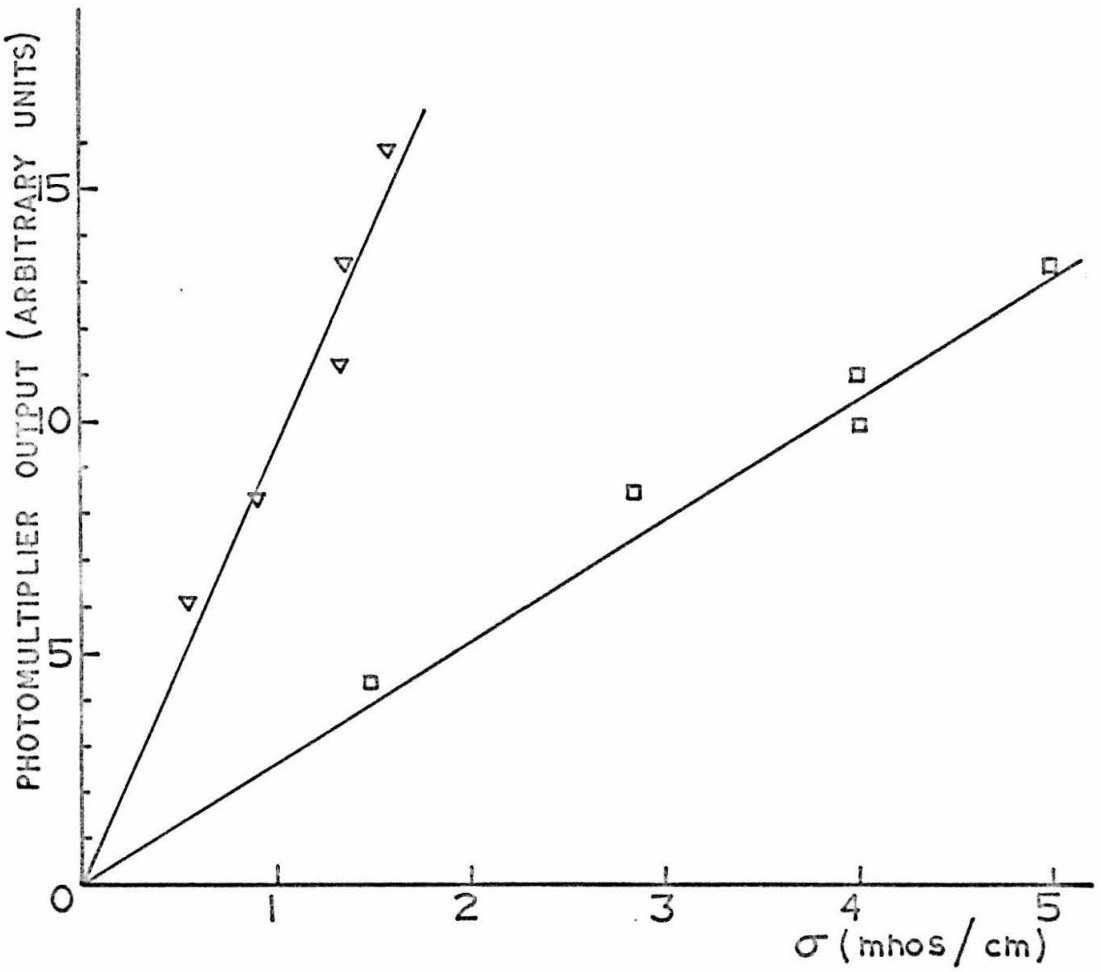

FIG. A.2 PHOTOMULTIPLIER CHECK

APPENDIX B

Calculation of the Effect of Nonuniformities on Effective Plasma Parameters

A. Waves at an Angle to the Average Current

In the theory of the electrothermal waves, it was found that these waves cause nonuniformities in the plasma which lie at an angle to the average current. The effective plasma properties with such a set of nonuniformities can be calculated following the scheme used by Rosa[15]. Here, the variation in Hall parameter β, is neglected in comparison with variations in σ. This is because variations in β are due only to variation in collision frequency which is essentially constant when the Spitzer term is small, whereas variations in σ are due to the variation in electron number density which is large.

We assume a distribution of nonuniformities as shown in Figure B-1 with the condition that the average current in the ζ-direction is zero. Then we have the condition:

$$0 = J_o \cos\phi + \sin\phi \langle J_y \rangle \tag{B.1}$$

$$\langle J_\eta \rangle = J_o \sin\phi - \cos\phi \langle J_y \rangle \tag{B.2}$$

$$\langle E_\eta \rangle = E_o \cos\phi + \sin\phi \langle E_x \rangle \tag{B.3}$$

$$\langle E_\zeta \rangle = -E_o \sin\phi + \cos\phi \langle E_x \rangle \tag{B.4}$$

Also, from the averaged Ohm's Law (eqns. 18),

$$\langle J_y \rangle = -\langle \sigma \rangle E_o + \beta J_o \tag{B.5}$$

$$\langle E_x \rangle = -\beta E_o + (1+\beta^2) J_o \langle 1/\sigma \rangle . \tag{B.6}$$

From (B. 1) and (B. 5)

$$J_o = \frac{\sin\phi\langle\sigma\rangle}{\cos\phi + \beta\sin\phi} E_o \quad . \tag{B.7}$$

Using eqn. (B.7), eqns. (B.2), (B.3), and (B.4) can be written in terms of E_o.

$$\langle J_\eta\rangle = \frac{\langle\sigma\rangle}{\cos\phi + \beta\sin\phi} E_o$$

$$\langle E_\eta\rangle = \frac{1 + (\langle 1/\sigma\rangle\langle\sigma\rangle - 1)(1+\beta^2)\sin^2\phi}{\cos\phi + \beta\sin\phi} E_o$$

$$\langle E_\zeta\rangle = \frac{-\beta + (\langle 1/\sigma\rangle\langle\sigma\rangle - 1)(1+\beta^2)\sin\phi\cos\phi}{\cos\phi + \beta\sin\phi} E_o$$

Then the effective values of σ and β are

$$\sigma_{eff} = \frac{\langle J_\eta\rangle}{\langle E_\eta\rangle} = \langle\sigma\rangle \frac{1}{1+(\langle 1/\sigma\rangle\langle\sigma\rangle - 1)(1+\beta^2)\sin^2\phi} \tag{B.8}$$

and

$$\beta_{eff} = \frac{-\langle E_\zeta\rangle}{\langle E_\eta\rangle} = \frac{\beta - (\langle 1/\sigma\rangle\langle\sigma\rangle - 1)(1+\beta^2)\sin\phi\cos\phi}{1+(\langle 1/\sigma\rangle\langle\sigma\rangle - 1)(1+\beta^2)\sin^2\phi} \quad . \tag{B.9}$$

If $\sigma = \langle\sigma\rangle + \frac{\Delta\sigma}{2}\sin\frac{2\pi x}{\lambda}$, then

$$\langle 1/\sigma\rangle = \frac{1}{\langle\sigma\rangle} \frac{1}{\sqrt{1 - \frac{1}{4}\left(\frac{\Delta\sigma}{\langle\sigma\rangle}\right)^2}} \approx \frac{1}{\langle\sigma\rangle}\left\{1 + \frac{1}{8}\left(\frac{\Delta\sigma}{\langle\sigma\rangle}\right)^2\right\} \quad .$$

Therefore,

$$\langle 1/\sigma\rangle\langle\sigma\rangle - 1 \approx \frac{1}{8}\left(\frac{\Delta\sigma}{\langle\sigma\rangle}\right)^2 = s \tag{B.10}$$

where $\Delta\sigma/\langle\sigma\rangle$ is the calculated peak to peak conductivity variation divided by the average and s is the mean square deviation.

B. Normal Mode

In a duct with a number of transverse discharges operating in the normal mode, it was found that the pattern of conductivity variations consisted of a boundary region of high conductivity on either side

of a central region in which transverse streamers existed. This pattern is shown in Figure B-2. The Ohms law in regions 1 and 2 will be:

$$(1)\quad J_{x_1} = \sigma_1 E_{x_1} + \beta J_{y_1} \tag{B.11}$$

$$E_{y_1} = \beta E_{x_1} + \frac{(1+\beta)^2}{\sigma_1} J_{y_1} \quad , \tag{B.12}$$

$$(2)\quad \langle J_{x_2} \rangle = \langle \sigma_2 \rangle E_{x_2} + \beta J_{y_2} \tag{B.13}$$

$$\langle E_{y_2} \rangle = \beta E_{x_2} + (1+\beta^2)\langle 1/\sigma_2 \rangle J_{y_2} \quad . \tag{B.14}$$

The matching conditions across the boundary between the two regions are:

$$J_{y_1} L_1 = -J_{y_2} L_2 \tag{B.15}$$

$$J_{x_1} = \langle J_{x_2} \rangle \tag{B.16}$$

$$E_{y_1} = \langle E_{y_2} \rangle \tag{B.17}$$

From equations B.11 through B. 17, the relationship between current and field in region 2 can be solved for. The result is:

$$\langle J_{x_2} \rangle = \frac{\frac{L_2}{\sigma_1 L_1} + \langle \frac{1}{\sigma_2} \rangle + \beta^2 \left(\langle \frac{1}{\sigma_2} \rangle - \frac{1}{\langle \sigma_2 \rangle} \right)}{\frac{L_2}{\sigma_1 L_1} + \langle \frac{1}{\sigma_2} \rangle + \beta^2 \left(\langle \frac{1}{\sigma_2} \rangle - \frac{1}{\sigma_1} \right)} \langle \sigma_2 \rangle E_{x_2} \quad .$$

Define

$$\gamma = \frac{\frac{L_2}{L_1} + \sigma_1 \langle \frac{1}{\sigma_2} \rangle}{\sigma_1 \langle \frac{1}{\sigma_2} \rangle - 1}$$

and

$$\alpha = \frac{\langle \frac{1}{\sigma_2} \rangle - \frac{1}{\langle \sigma_2 \rangle}}{\langle \frac{1}{\sigma_2} \rangle - \frac{1}{\sigma_1}}$$

and redefining $L_1+L_2 = w$, $L_1 = \delta$, $\sigma_1 = \sigma_{BL}$, and $\langle \sigma_2 \rangle = \langle \sigma \rangle$, and remembering that for a sine wave nonuniformity : $\langle 1/\sigma \rangle \approx \frac{1}{\langle \sigma \rangle}(1+S)$ we obtain:

$$\gamma = 1 + \frac{w}{\delta} \frac{1}{\sigma_{BL}/\langle \sigma \rangle - 1 + S}$$

and

$$\alpha = \left[\frac{1}{1+S - \sigma_{BL}/\langle \sigma \rangle}\right] S \quad .$$

Then

$$\frac{\sigma_{eff}}{\langle \sigma \rangle} = \frac{\gamma + \beta^2 \alpha}{\gamma + \beta^2} \quad . \qquad \text{(B. 18)}$$

C. Isotropic Distribution of Nonuniformities

To approximate the effective plasma properties of a plasma with an unknown distribution of nonuniformities, Louis[16] has suggested assuming a random distribution and calculating phasma properties by the isotropic theory developed by Yoshikawa and Rose[17]. The calculation of Yoshikawa and Rose was done for a gas in which Coulomb collisions dominate; thus, the collision frequency was proportional to the electron density. To more nearly approximate the conditions occurring in our plasma, the calculation was redone assuming a constant collision frequency. Also, the calculation was done for an isotropic distribution only in the two dimensions perpendicular to the magnetic field as well as the usual three-dimensional

distribution.

Ohm's law can be written as:

$$\sigma \underline{E} - \frac{\beta}{B} (\underline{J} \times \underline{B}) = \underline{J} \ . \qquad \text{(B. 19)}$$

The assumption that the collision frequency is constant means that σ is directly proportional to n_e ; thus:

$$\sigma = \langle \sigma \rangle \left(\frac{n}{\langle n \rangle} \right) \ . \qquad \text{(B. 20)}$$

Expanding the electron density, electric field, and current in harmonics;

$$n_e = \langle n \rangle + \Sigma' n_k e^{ikr} \qquad \text{(B. 21)}$$

$$\underline{E} = \langle \underline{E} \rangle + \Sigma' \underline{E}_k e^{ikr} \qquad \text{(B. 22)}$$

$$\underline{J} = \langle \underline{J} \rangle + \Sigma' \underline{J}_k e^{ikr} \qquad \text{(B. 23)}$$

where Σ' indicates a sum over all k except zero. Substitution eqns. (B. 20) to (B. 23) in (B. 19) and taking the zeroth harmonic gives:

$$\langle \sigma \rangle \langle \underline{E} \rangle + \frac{\langle \sigma \rangle}{\langle n \rangle} \Sigma' n_k \underline{E}_k - \frac{\beta}{B} (\langle \underline{J} \rangle \times \underline{B}) = \langle \underline{J} \rangle \ . \qquad \text{(B. 24)}$$

This is the average Ohm's law with the effect of nonuniformities included in the term $\Sigma' n_k E_k$. This term is calculated from the equation of the k^{th} harmonic in the Ohm's law

$$\langle \sigma \rangle \underline{E}_k + \frac{\langle \sigma \rangle}{\langle n \rangle} n_k \langle \underline{E} \rangle + [\ldots \text{cross terms} \ldots] - \frac{\beta}{B} (\underline{J}_k \times B) = \underline{J}_k \ . \qquad \text{(B. 25)}$$

To close this set of equations, the cross terms, terms of the type $\Sigma_\ell n_k E_{k-\ell}$, must be dropped. However, the effect of this approximation for waves of the amplitude observed could not adequately be predicted.

Since the curl of E is zero, $E_k \times \underline{k} = 0$, and writing $\underline{\gamma} = \underline{k}/|k|$, we get

$$E_{k_x} = E_k \gamma_x ,$$

$$E_{k_y} = E_k \gamma_y , \qquad \text{(B. 26)}$$

and

$$E_{k_z} = E_k \gamma_z .$$

Using eqn. (B. 26) and solving for the components of current from (B. 25) gives:

$$J_{k_x} = \frac{\langle\sigma\rangle}{1+\beta^2} \left[E_k(\gamma_x - \beta\gamma_y) + \frac{n_k}{\langle n\rangle} (\langle E\rangle_x - \beta\langle E\rangle_y)\right] , \qquad \text{(B. 27)}$$

$$J_{k_y} = \frac{\langle\sigma\rangle}{1+\beta^2} \left[E_k(\beta\gamma_x + \gamma_y) + \frac{n_k}{\langle n\rangle} (\beta\langle E\rangle_x + \langle E\rangle_y)\right] , \qquad \text{(B. 28)}$$

$$J_{k_z} = \langle\sigma\rangle E_k \gamma_z . \qquad \text{(B. 29)}$$

Here, it has been assumed that $\underline{B}$ is in the z-direction.

Also, the divergence of J is zero. This gives:

$$J_{k_x}\gamma_x + J_{k_y}\gamma_y + J_{k_z}\gamma_z = 0 . \qquad \text{(B. 30)}$$

Substituting (B. 27), (B. 28), and (B. 29) in (B. 30) and solving for E_k gives:

$$E_k = -\frac{1}{1+\beta^2\gamma_z^2} \frac{n_k}{\langle n\rangle} \left[\langle E\rangle_x(\gamma_x + \beta\gamma_y) + \langle E\rangle_y(-\beta\gamma_x + \gamma_y)\right] . \qquad \text{(B. 31)}$$

Since the waves are assumed isotropic, n_k is independent of γ ; thus:

$$\Sigma' n_k E_{-kx} = -\frac{1}{\beta} \left[\langle E\rangle_x - \beta\langle E\rangle_y\right]\langle n\rangle SI(\beta) \qquad \text{(B. 32)}$$

and

$$\Sigma' n_k E_{-ky} = -\left[\langle E\rangle_x + \frac{1}{\beta}\langle E\rangle_y\right]\langle n\rangle SI(\beta) \qquad \text{(B. 33)}$$

where

$$I(\beta) = \beta\langle \frac{\gamma_x^2}{1+\beta^2\gamma_z^2} \rangle = \beta\langle \frac{\gamma_y^2}{1+\beta^2\gamma_z^2} \rangle$$

and

$$S = \Sigma \frac{n_k\, n_{-k}}{\langle n \rangle^2} \quad .$$

Substituting (B. 32) and (B. 33) back into the equation for the zeroth harmonic, (B. 24) then gives:

$$\langle\sigma\rangle(1 - SI/\beta)\langle E\rangle_x + \langle\sigma\rangle SI\langle E\rangle_y = \langle J\rangle_x + \beta\langle J\rangle_y \quad , \tag{B. 34}$$

$$\langle\sigma\rangle SI\langle E\rangle_x - \langle\sigma\rangle(1 - SI/\beta)\langle E\rangle_y = \beta\langle J\rangle_x - \langle J\rangle_y \quad . \tag{B. 35}$$

Fixing the x-axis along the average current, that is, $\langle J\rangle_y = 0$, eqns. (B. 34) and (B. 35) can be solved for the ratios $\langle J\rangle_x/\langle E\rangle_x$ and $\langle E\rangle_y/\langle E\rangle_x$ which are defined as σ_{eff} and $-\beta_{eff}$, respectively. This gives:

$$\frac{\sigma_{eff}}{\langle\sigma\rangle} = \frac{1 + (SI)^2 - 2\frac{SI}{\beta} + (\frac{SI}{\beta})^2}{1 - \frac{SI}{\beta} + SI\beta} \tag{B. 36}$$

and

$$\beta_{eff} = \frac{\beta - 2SI}{1 - \frac{SI}{\beta} + \beta SI} \quad . \tag{B. 37}$$

For the three-dimensional case,

$$I = -\frac{\beta}{2} + (1 + \frac{1}{\beta^2})^{\frac{1}{2}} \tan^{-1}\beta \quad .$$

Note that as $\beta \to \infty$, $I(\beta) \to \pi/4$.

For the two-dimensional case,

$$I = \beta/2 \quad ,$$

which gives:

$$\frac{\sigma_{eff}}{\langle\sigma\rangle} = \frac{1 - S + \frac{S^2}{4} + \frac{S^2}{4}\beta^2}{1 - \frac{S}{2} + \frac{S}{2}\beta^2} \qquad \text{(B. 38)}$$

and

$$\beta_{eff} = \frac{(1-S)\beta}{1 - \frac{S}{2} + \frac{S}{2}\beta^2} \quad . \qquad \text{(B. 39)}$$

D. Changes in the Average Conductivity Caused by Nonuniformities

The formulas just derived, (B. 8), (B. 18), and (B. 36), relate the effective to the average conductivities, whereas experimentally the ratio of effective conductivity to the conductivity with no magnetic field was actually measured. The difference between these two ratios is the amount that the average conductivity changes when nonuniformities appear in the plasma. This can be calculated from the average energy equation as follows.

In a uniform plasma, time and space derivatives are zero; thus, using eqn. (20), eqn. (19) gives:

$$\underline{J}\cdot\underline{E} = \frac{J_L^2}{\sigma_o}\left(\frac{\sigma}{\sigma_o}\right)^{\frac{2}{n}-1} \quad . \qquad \text{(B. 40)}$$

If the reference current, J_L, is taken to be the current at σ_o, then

$$\underline{J}\cdot\underline{E} = \frac{J_L^2}{\sigma_o} \quad .$$

For a nonuniform plasma, we average the energy equation; thus, time and space derivatives will again disappear, giving:

$$\langle\underline{J}\cdot\underline{E}\rangle = \frac{J_L^2}{\sigma_o}\left\langle\left(\frac{\sigma}{\sigma_o}\right)^{\frac{2}{n}-1}\right\rangle \quad .$$

For plane waves, the perturbations in $\underline{J}$ and $\underline{E}$ are mutually perpen-

dicular; therefore,

$$\langle \underline{J} \cdot \underline{E} \rangle = \langle J \rangle \cdot \langle E \rangle ,$$

and since σ_{eff} was defined as the ratio of the average current to the average field along $\langle J \rangle$,

$$\langle J \rangle \cdot \langle E \rangle = \frac{\langle J \rangle^2}{\sigma_{eff}} .$$

Therefore, if the average current was kept fixed, as it was in the experiments,

$$\sigma_o/\sigma_{eff} = \langle (\sigma/\sigma_o)^{2/n - 1} \rangle .$$

Writing

$$\sigma/\sigma_o = (\langle\sigma\rangle/\sigma_o)(1 + \Delta\sigma/(2\langle\sigma\rangle))$$

where $\Delta\sigma$ is the peak-to-peak amplitude gives:

$$\sigma_o/\sigma_{eff} = (\langle\sigma\rangle/\sigma_o)^{2/n - 1} \langle (1 + \Delta\sigma/(2\langle\sigma\rangle))^{2/n - 1} \rangle .$$

Expanding gives

$$\langle (1 + \Delta\sigma/(2\langle\sigma\rangle))^{\frac{2}{n} - 1} \rangle \approx 1 + \frac{(\frac{2}{n} - 1)(\frac{2}{n} - 2)}{2} \langle (\frac{\Delta\sigma}{2\langle\sigma\rangle})^2 \rangle ,$$

which will be valid if the mean square deviation of σ is much less than one. In terms of S , the mean square deviation, this gives:

$$\langle\sigma\rangle/\sigma_o = [(\sigma_{eff}/\sigma_o)(1 + aS)]^{\frac{1}{1 - 2/n}} , \qquad (B.41)$$

where $a = \frac{1}{2}(\frac{2}{n} - 1)(\frac{2}{n} - 2)$. Then eqns. (B.8), (B.18), and (B.36), which are of the form $\sigma_{eff} = f(S)\langle\sigma\rangle$, can be rewritten in terms of σ_o as

$$\sigma_{eff}/\sigma_o = (f(S))^{1 - \frac{n}{2}} (1 + aS)^{-n/2} . \qquad (B.42)$$

For our experiments, $n \approx 2/3$, which gives

$$\sigma_{eff}/\sigma_o = (f(S))^{2/3} (1+S)^{-1/3} . \qquad (B.43)$$

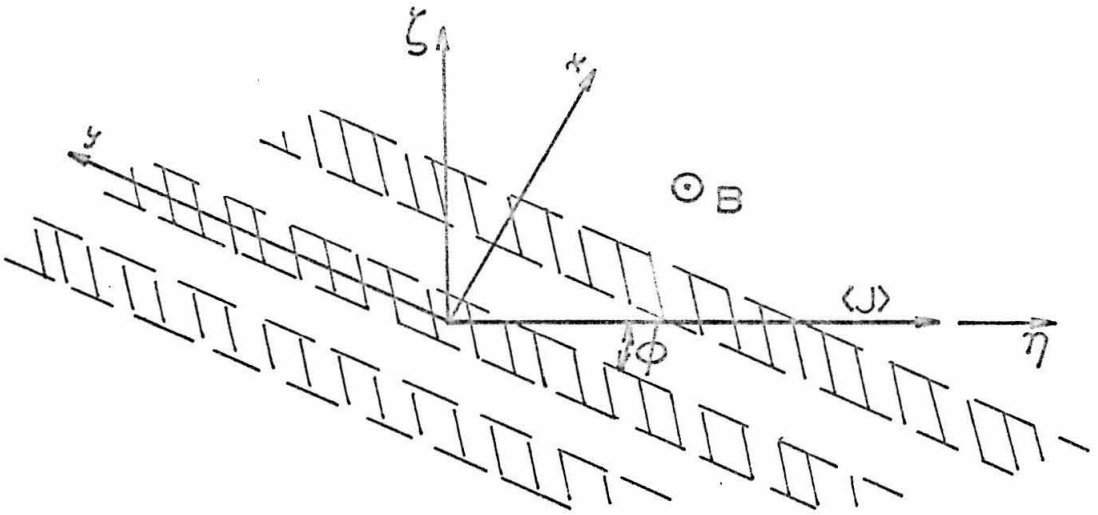

FIG. B.1 WAVES AT AN ANGLE TO THE AVERAGE CURRENT

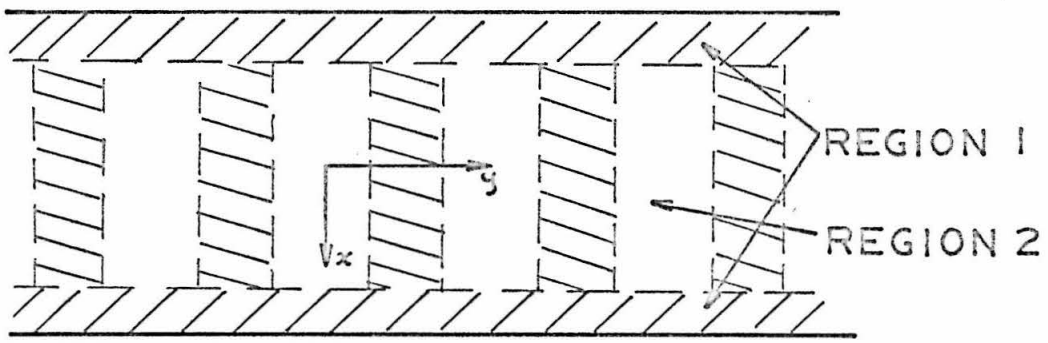

FIG. B.2 CONDUCTIVITY PATTERN IN THE NORMAL MODE

APPENDIX C

The Averaged Energy Equation

To determine the stability of a plasma with a uniform set of waves, the energy equation is averaged over these waves and the stability of the plasma with respect to perturbations of the average conductivity studied. Using the results of Appendix B, Part C:

$$\langle Q\rangle = \langle J\rangle \cdot \langle E\rangle - \frac{\langle J\rangle_L^2}{\sigma_o}(1+aS)\left(\frac{\langle\sigma\rangle}{\sigma_o}\right)^{\frac{2}{n}-1} . \qquad (C.1)$$

Also using $\sigma_{eff} = f(S)\langle\sigma\rangle$ and eqn. (B.41) for a plasma with a uniform average conductivity, $\langle\sigma\rangle_o$, we get:

$$\left(\frac{\langle\sigma\rangle_o}{\sigma_o}\right)^{-2/n} = (1+aS)f(S) .$$

This, in eqn. (C.1), gives:

$$\langle Q\rangle = \langle J\rangle \cdot \langle E\rangle - \frac{\langle J\rangle_L^2}{\langle\sigma\rangle_o}\frac{1}{f(S)}\left(\frac{\langle\sigma\rangle}{\langle\sigma\rangle_o}\right)^{2/n} .$$

Now, writing $\langle J\rangle \cdot \langle E\rangle$ in the form used in eqn. (19) gives:

$$\sigma_{eff}\langle E\rangle_o^2 + 2\beta_{eff}\langle E\rangle_o\langle J\rangle_o + \frac{1+\beta_{eff}}{\sigma_{eff}}\langle J\rangle_o^2$$

where $\langle E\rangle_o$ and $\langle J\rangle_o$ are analogous to E_o and J_o of the uniform plasma and σ_{eff} and β_{eff} are the effective values of conductivity and Hall parameter. Normalizing the equation by $\langle\sigma\rangle_o f(S)\langle E\rangle_{L_o}^2$ and using $\sigma_{eff} = f(S)\langle\sigma\rangle$, we obtain:

$$\frac{\langle Q\rangle}{\langle\sigma\rangle_o f(S)\langle E\rangle_{L_o}^2} = \frac{\langle\sigma\rangle}{\langle\sigma\rangle_o}\left(\frac{\langle E\rangle_o}{\langle E\rangle_{L_o}}\right)^2 + 2\beta_{eff}\left(\frac{\langle J\rangle_o}{f(S)\langle\sigma\rangle_o\langle E\rangle_{L_o}}\right)\left(\frac{\langle E\rangle_o}{\langle E\rangle_{L_o}}\right)$$
$$+\frac{1+\beta_{eff}}{\langle\sigma\rangle/\langle\sigma\rangle_o}\left(\frac{\langle J\rangle_o}{f(S)\langle\sigma\rangle_o\langle E\rangle_{L_o}}\right) - \left(\frac{\langle\sigma\rangle}{\langle\sigma\rangle_o}\right)^{2/n-1} . \qquad (C.2)$$

From the theory of the steady waves, S is a function only of β and n , and therefore f(S) can be considered a constant with respect to changes of $\langle\sigma\rangle$. Now using the fact that $\langle Q\rangle = 0$ at $\langle\sigma\rangle = \langle\sigma\rangle_o$ gives

$$\frac{\langle J\rangle_o}{f(S)\langle\sigma\rangle_o\langle E\rangle_{L_o}} = \frac{-\beta_{eff} \pm \sqrt{(1+\beta_{eff}^2)\left(\frac{\langle E\rangle_{L_o}}{\langle E\rangle_o}\right)^2 - 1}}{1+\beta_{eff}^2}\left(\frac{\langle E\rangle_o}{\langle E\rangle_{L_o}}\right). \quad \text{(C. 3)}$$

Equations (C. 2) and (C. 3) are identical to eqns. (22) and (23) when averaged fields and conductivities replace constant ones and the effective Hall parameter replaces the theoretical one. We can therefore conclude that if the plasma described by eqns. (22) and (23) will be unstable for values of $\beta > \beta_{crit}$, then the plasma described by (C. 2) and (C. 3) will be unstable for $\beta_{eff} > \beta_{crit}$.